

MASTER THESIS

Thesis submitted in partial fulfillment of the requirements for the degree of Master of Science in Engineering at the University of Applied Sciences Technikum Wien - Degree Program Tissue Engineering and Regenerative Medicine

Modeling lung tumorigenesis using CRISPR/Cas9-based genome editing in *ex vivo* 3D organoids

By: Pia Weidinger, BSc
Student Number: 1510692023

Supervisor 1: FH-Prof. MMag. Dr. Veronika Jesenberger
Supervisor 2: Dr. Purushothama Rao Tata

Grafenwörth, 01.09.2017



Declaration of Authenticity

“As author and creator of this work to hand, I confirm with my signature knowledge of the relevant copyright regulations governed by higher education acts (for example see §§ 21, 42f and 57 UrhG (Austrian copyright law) as amended as well as § 14 of the Statute on Studies Act Provisions / Examination Regulations of the UAS Technikum Wien).

In particular I declare that I have made use of third-party content correctly, regardless what form it may have, and I am aware of any consequences I may face on the part of the degree program director if there should be evidence of missing autonomy and independence or evidence of any intent to fraudulently achieve a pass mark for this work (see § 14 para. 1 Statute on Studies Act Provisions / Examination Regulations of the UAS Technikum Wien).

I further declare that up to this date I have not published the work to hand nor have I presented it to another examination board in the same or similar form. I affirm that the version submitted matches the version in the upload tool.”

Grafenwörth, 01.09.2017

Place, Date

Anna Gerding

Signature

Kurzfassung

Bisher waren Tiermodelle das primäre präklinische Testsystem, um neue Wirkstoffe zu evaluieren. Diese erlauben jedoch nur einen geringen Durchsatz, und sind enorm zeit-, arbeits- und kostenintensiv. Darüber hinaus stellen bestimmte Tumore in Tiermodellen nicht das volle Spektrum der Pathogenese beim Menschen dar. Daher sind Alternativen zu Tierversuchen, die vorzugsweise auf menschlichen Zellen basieren, dringend gesucht. Die neuartige "Organ-on-a-Chip"-Technologie ist ein vielversprechender Ansatz, da sie ein Humanzell-basiertes Miniaturesystem darstellt, das die schnelle Generierung von verlässlichen und reproduzierbaren wissenschaftlichen Daten ermöglicht. Bislang konnte jedoch kein "Lung-on-a-Chip"-System entwickelt werden, um den Effekt von Wirkstoffkandidaten auf Lungenkrebs zu untersuchen.

Ziel dieser Arbeit war die Erzeugung solcher 3-dimensionaler, Organoid-basierter Systeme aus gesunden Lungen-Epithelstammzellen, und das Modellieren der häufigsten Lungenkrebsarten, durch Einführung spezifischer *EGFR*-Mutationen mittels CRISPR/Cas9. Die zu diesem Zweck entworfenen Konstrukte wurden durch die NEPA21-Elektroporation eingeschleust. Um die Selektion von Klonen mit einer speziellen Mutation zu ermöglichen, wurden Atemwegs-Basalstammzellen (BCs) in niedrigen Dichten kultiviert, und ein PCR-System wurde entworfen, um positive Klone zu identifizieren. Des Weiteren wurden Organoide aus anderen Zelltypen etabliert, wie alveoläre Typ-2-Epithel-Stammzellen (AEC2s), und verschiedene histologische Marker wurden eingefärbt, um spezifische Organoid-Charakteristika zu untersuchen.

Obwohl die Transfektion von murinen BCs in einigen Fällen Wirkungsgrade von über 70% aufwies, konnte nur eine sehr geringe Anzahl von menschlichen BCs erfolgreich transfiziert werden. Die Mehrheit der Einzelzell-Kulturmethoden führte zu hohen Mortalitätsraten. Der vielversprechendste Ansatz war, einzelne BCs auf Transwells zu säen und andere BCs unterhalb der Membran zu kultivieren, um wesentliche Überlebenssignale bereitzustellen. Organoide, die aus BCs entstanden, entwickelten definierte Trachea-ähnliche Strukturen, im Gegensatz zu AEC2-abgeleiteten Organoiden, die meist Alveolen ähnelten. Der Vergleich von normalen und *NKX2-1* BC-Organoiden zeigte, dass BCs in Richtung intestinaler Zellen differenzieren können, in einem Prozess, der als zelluläre Plastizität bezeichnet wird.

Das übergeordnete Ziel dieses Projektes war es, ein *ex vivo* Kultursystem zu etablieren, um die Tumorentstehung in der Lunge zu untersuchen. Sobald diese Organoide die physiologische Entstehung von Lungenkrebs ausreichend nachbilden, werden sie in "Lung-on-a-Chip"-Systemen platziert, um die Prüfung potentieller Wirkstoffkandidaten zu ermöglichen. Mit diesem Projekt wurde der Grundstein für weiterführende Studien gelegt, um das Potenzial neuartiger therapeutischer Ansätze gegen Lungenkrebs zu erforschen.

Schlagwörter: "Organ-on-a-chip", Organoide, CRISPR/Cas9, Plastizität, Tumorentstehung

Abstract

Hitherto, animal models have been the primary preclinical test system used to assess novel therapeutic options. However, these experiments are of low throughput, enormously time-consuming, laborious, and expensive. In addition, certain tumors in animal models do not recapitulate the full spectrum of pathogenesis in humans. Therefore, superior alternatives to animal testing, preferentially based on human cells, are urgently needed. The novel 'organ-on-a-chip' technology is a very promising approach, as it provides a human cell-based miniature system, enabling the fast achievement of sound and reproducible scientific data. However, no 'lung-on-a-chip' system could have been established yet, to evaluate the effects of potential drug candidates on lung cancer.

The aim of this thesis was the generation of such 3-dimensional, organoid-based systems from healthy lung epithelial stem cells, and modeling the most frequent types of lung cancer by introducing specific *EGFR* mutations using CRISPR/Cas9. The constructs designed for this purpose were introduced by NEPA21 electroporation. In order to enable the selection of single cell-derived clones harboring a specific mutation, airway basal stem cells (BCs) were cultured at low densities, and a PCR system was designed to screen for positive clones. In addition, organoids were established from other cell types, such as alveolar type 2 epithelial stem cells (AEC2s), cryosectioned, and stained for distinct histological markers to evaluate specific organoid characteristics.

Although transfection of murine BCs showed efficiencies of over 70% in some cases, only very small numbers of human BCs could be transfected successfully. The majority of single cell culture methods resulted in high mortality rates. However, the most promising approach was seeding single BCs on transwells, and co-culturing other BCs underneath the membrane to provide essential survival signals. Organoids established from BCs developed well-defined trachea-like architectures, whereas AEC2-derived organoids resembled that of alveoli. Comparison of normal and *NKX2-1* BC organoids demonstrated that BCs can differentiate towards the intestinal lineage, in a process termed cellular plasticity.

The overarching goal of this project was to establish an *ex vivo* culture system to study lung tumorigenesis. Once these organoids sufficiently emulate physiological lung tumorigenesis, they will be placed on microfluidic 'lung-on-a-chip' devices, to enable testing of potential drug candidates. With this project, the foundation has been laid for prospective studies, to explore the potential of novel therapeutic approaches to treat lung cancer.

Keywords: 'organ-on-a-chip', organoids, CRISPR/Cas9, cellular plasticity, tumorigenesis

Acknowledgements

First of all, I want to thank my colleague Huifang Dai, who introduced me to all the methods and procedures that were new to me. Moreover, I want to thank my colleague Yoshihiko Kobayashi for assistance with my cell cultures, and Ruben Gerrit Scheuring for stimulating discussions. Furthermore, I thank my FH Technikum Wien supervisor Veronika Jesenberger for her valuable feedback on my written work, and my Duke supervisor Purushothama Rao Tata for giving me the opportunity to come here and learn so much. I also want to thank the Austrian Marshall Plan Foundation for their financial support, which made my stay in the USA possible. Last but not least I am grateful for my family and friends who have always supported me in everything I do.

Table of Contents

1	Introduction	6
1.1	Lung cancer	6
1.2	Research problem and significance of the project	7
1.3	'Organ-on-a-chip' technology.....	8
1.4	Gene editing technologies	10
1.4.1	The CRISPR/Cas system	11
1.5	Structure and cellular composition of the lung	13
1.6	Cell types applied in organoid culture	15
1.6.1	Airway basal stem cells	15
1.6.2	Alveolar type 2 epithelial cells.....	18
1.7	Formation of organoids.....	19
1.7.1	Application of organoids to microfluidic devices.....	21
2	Materials and Methods	21
2.1	Basic cell culture	21
2.2	Generation of plasmids.....	25
2.2.1	sgRNA design	25
2.2.2	Cloning of vectors.....	26
2.2.3	Plasmid purification	28
2.3	Transfection methods.....	29
2.3.1	Electroporation	30
2.4	Screening for positive clones.....	32
2.4.1	Single cell culture	33
2.5	Culturing organoids	34
2.5.1	Comparative studies.....	36
3	Results	39
3.1	Electroporation	39
3.1.1	Electroporation of human BCs.....	46
3.2	Single cell culture	49
3.3	Organoid culture.....	51
3.3.1	Growth kinetics.....	59

4	Discussion.....	61
4.1	Availability and other limitations of cells.....	61
4.2	Electroporation with px458 plasmid.....	62
4.3	Single cell culture.....	63
4.4	Characteristics of organoid cultures.....	64
4.4.1	Growth kinetics of organoid cultures.....	65
4.5	Outlook.....	65
	Bibliography.....	67
	List of Figures.....	74
	List of Tables.....	76
	List of Abbreviations.....	77

1 Introduction

The overarching goal of this project was to establish an *ex vivo* culture system to study lung tumorigenesis. Therefore, 3-dimensional organoids were generated from healthy lung epithelial stem cells, and the most frequent types of lung cancer were modeled by introducing mutations into specific genomic sequences using clustered regularly interspaced short palindromic repeat (CRISPR)/CRISPR-associated protein 9 (Cas9)-based genome editing (see Figure 1). The arising histological alterations were to be investigated and compared to healthy organoids. Once these tumor organoids sufficiently emulate lung tumorigenesis *in vivo*, they will be placed on microfluidic ‘organ-on-a-chip’ devices, to enable testing of potential drug candidates. With this project, the foundation for prospective studies has been laid, to explore the potential of novel therapeutic approaches to treat lung cancer.

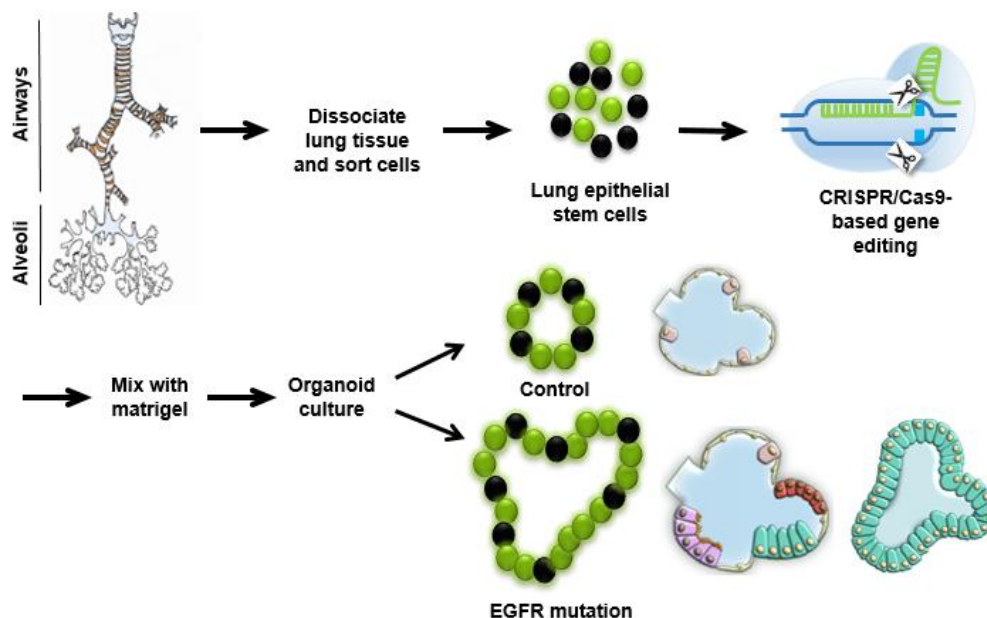


Figure 1: Scheme depicting the generation of *ex vivo* organoids to recapitulate *in vivo* tumor phenotypes. Healthy lung tissue was dissociated, and lung epithelial stem cells were isolated according to specific markers. CRISPR/Cas9-based genome editing was used to introduce specific mutations in the *EGFR* gene, and cells were mixed with matrigel for organoid culture. In addition, control organoids without mutations were established, in order to identify histological differences between healthy and tumorigenic organoids.

1.1 Lung cancer

The most frequent cause of cancer-related mortality is lung cancer [1]–[4], leading to approximately 1.4 million deaths globally each year [2]. Lung cancers comprise a broad range of diseases with diverse etiologies, but are generally divided into two main classes: small-cell lung cancers (SCLC), which represent 20% of all cases, and non-small-cell lung cancers (NSCLC), which constitute the vast majority with 80% of all cases [5]. Among NSCLC, adenocarcinomas are the most frequent histological subtype, followed by squamous cell carcinomas [1], [2]. Due to their abundance, the focus was placed on lung

adenocarcinomas. Comprehensive genome-wide association studies coupled with exome sequencing have identified many mutations associated with human lung adenocarcinomas. Genes encoding *KRAS*, *EGFR* and *TP53* harbor the most common genomic alterations in these cancers [1]. Among the most prevalent epidermal growth factor receptor (*EGFR*) mutations in NSCLC are deletions in exon 19, such as $\Delta E746-A750$, representing 45% of all *EGFR* mutations, and substitutions in exon 21, whereby L858R alone accounts for 40-45% of all mutations in *EGFR* [5]. Although mutations in the tyrosine kinase domain of *EGFR* are usually activating mutations, as they increase the receptor's kinase activity, these mutated receptors are not necessarily rendered fully active. However, they can become entirely ligand-independent by second site mutations, such as T790M substitution in exon 20 [5], which is found in 50% of all cases of acquired drug resistance [5], [6]. The most frequent mutations in the *EGFR* gene are depicted in Figure 2.

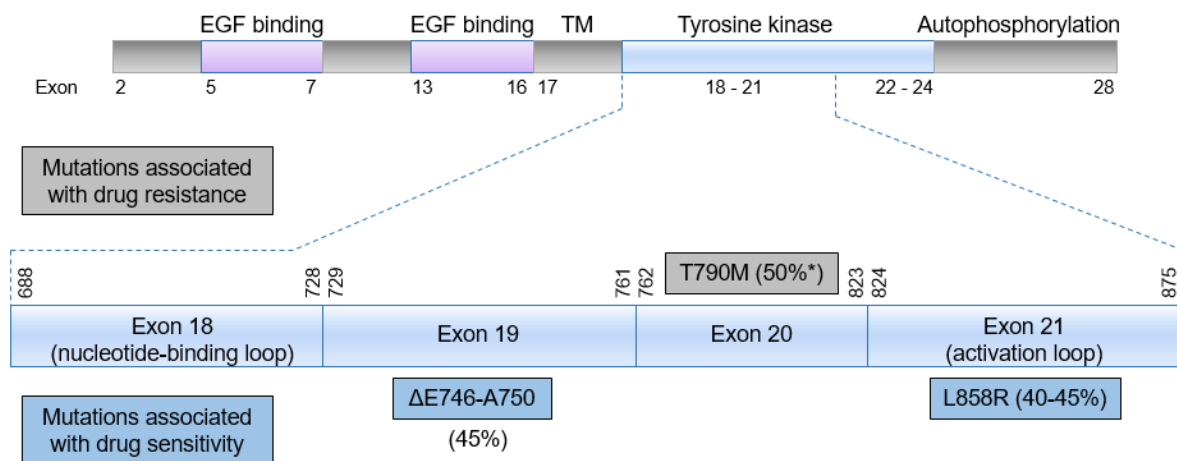


Figure 2: Most frequent mutations in the *EGFR* gene. A scheme of *EGFR* indicating the EGF-binding (extracellular) domain, transmembrane (TM), and intracellular domain (tyrosine kinase and autophosphorylation regions). Exons 18-21 are expanded, showing the most relevant mutations and their association with drug resistance (gray boxes) or sensitivity (blue boxes). Among the recurrent mutations in NSCLC are deletions in exon 19, representing 45% of all *EGFR* mutations, and substitutions in exon 21, whereby L858R alone accounts for 40-45% of all *EGFR* mutations [5]. In exon 20, the most relevant mutation is T790M, which is found in 50% of all cases as second site mutation, leading to drug resistance [5], [6]. Scheme redrawn from Sharma *et al.* 2007.

1.2 Research problem and significance of the project

Unfortunately, conventional cancer therapies, such as chemotherapy and irradiation, cause enormous side effects due to their inability to target cancer cells specifically. Therefore, new approaches and therapies are urgently needed to avoid this additional suffering of patients. Recently, novel therapies that molecularly target specific features of tumors, have tremendously improved the treatment options for patients with adenocarcinomas containing activated oncogenes, such as mutated *EGFR*, or translocated *RET*, *ALK*, or *ROS1* [3], [7]–[9]. For instance, phase 3 clinical trials have shown superior effectiveness of gefitinib, an *EGFR* inhibitor, on *EGFR*-mutant tumors as compared to chemotherapy [7]. However, most adenocarcinomas are lacking a determinable driver oncogene, and therefore still require

conventional chemotherapy [1]. Also mutations in *KRAS* are difficult to target, as the efficacy of agents inhibiting *KRAS* effectors is averted by activated compensatory pathways [10]. Moreover, abnormalities in tumor suppressor genes, such as *TP53*, *KEAP1*, *STK11*, *SMARCA4*, and *CDKN2A* [11]–[15], which are also very common, are not clinically targetable at present [1]. Similarly, for the treatment of lung squamous cell carcinomas, no specific molecularly targeted agents could have been developed yet [2].

Currently, many studies are being performed in order to identify new potential therapeutic targets in diverse tumors, seeking new pathways for the treatment of cancer. However, once these targets are determined, *in vitro* as well as *in vivo* studies need to be performed to assess potential treatment options. Hitherto, the process of preclinical testing has been enormously time-consuming, increasingly expensive [16], and required the use of countless laboratory animals. Moreover, many studies have indicated that the data obtained from animal testing cannot be easily translated to human patients [17]–[21], sometimes even leading to fatal reactions during subsequent clinical trials. In addition, the failure to determine toxicity and efficacy in preclinical trials causes serious delays in developing new drugs, and may lead to very expensive, but unsuccessful clinical trials [22]. Therefore, superior alternatives to animal testing, preferentially based on human cells, are urgently needed. Thus, the 3R principle for the replacement, refinement and reduction of animals in research has been established to find solutions to 1) replace the use of animals with innovative alternatives, 2) reduce the number of animals used, and 3) minimize their suffering by refining experimental procedures and husbandry. Meanwhile, it is generally recognized that implementing the 3Rs in experiments is concordant with good scientific practice [20].

1.3 ‘Organ-on-a-chip’ technology

The novel ‘organ-on-a-chip’ technology is an extremely promising approach to replace outdated animal testing, as it provides a human cell-based miniature system, enabling the fast achievement of sound and reproducible scientific data. Moreover, many potential therapeutic candidates may be tested in parallel, thereby tremendously accelerating the progress of medical research. Meanwhile, microfluidic devices are basically found in every research facility and hospital, where they are deployed for drug delivery, diagnostics, and monitoring of analytes, due to their superior accuracy [23]. However, the most important feature of these devices may arise upon the integration of cellular constructs, which allows researchers to model physiological as well as pathological conditions of highly complex tissues, and even whole organs [24]–[26]. In this way, microfluidic test systems may be used to model various stages of diseases, to predict absorption, distribution, metabolism, and excretion (ADME) profiles, toxicity, immunogenicity, and even treatment efficacy, before entering clinical trials. Therefore, biology-inspired microphysiological systems may be a cornerstone, not only to bridge the increasingly evident translational gap between different species, but also to enhance the productivity of drug development [21].

An overview of the diverse, currently available, microphysiological systems is depicted in Figure 3. Basically, microfluidic systems are subdivided in single-organ systems, including plates and chips, multi-organ systems, emulating interactions of several organs, and whole 'body-on-a-chip' devices, which are simulating an entire organism by integrating all relevant single-organ modules [21].

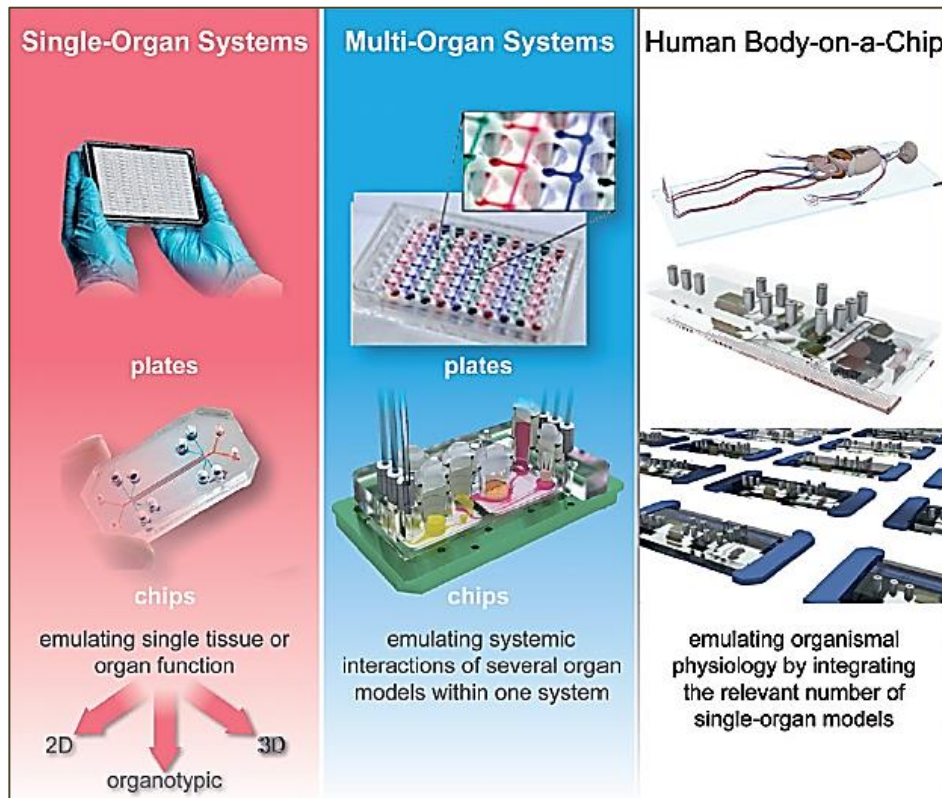


Figure 3: Different biology-inspired microphysiological *in vitro* systems used to simulate the human biology. An OrganoPlate for perfused 3D cell cultures in a microtiter form (top left), a lung-on-a-chip (middle left), a microtiter plate for hanging drops with microfluidic channels connecting several spheroids (top center), a four-organ-chip (center bottom), and a whole human body-on-a-chip system (right) [21].

Several laboratories have established microphysiological test systems, such as cerebral organoids developed by Lancaster *et al.* at the Institute of Molecular Biotechnology in Vienna. These cerebral organoids are used to study microcephaly, a disease difficult to explore in mice. The obtained data have shown that 3-dimensional organoids are indeed capable of mimicking development and disease of the brain, which constitutes the most complex tissue in the human body [27]. Another example is the microsystem established by Huh *et al.*, which mimics the alveolar-capillary interface within the human lung. These organoids have been used in nanotoxicology studies, revealing the importance of cyclic mechanical strain to enhance inflammatory responses to nanoparticles. Thus, mechanically stimulated 'organ-on-a-chip' devices may even extend the opportunities of these systems and constitute low-cost alternatives to both, animal and clinical studies [28]. Hitherto, no 'lung-on-a-chip' system has been established to study the effect of potential drug candidates

on lung cancer. Therefore, the host laboratory of Dr. Tata is working on establishing such organoid-based systems, and already gained expertise in developing healthy organoids (see Figure 4) [29].

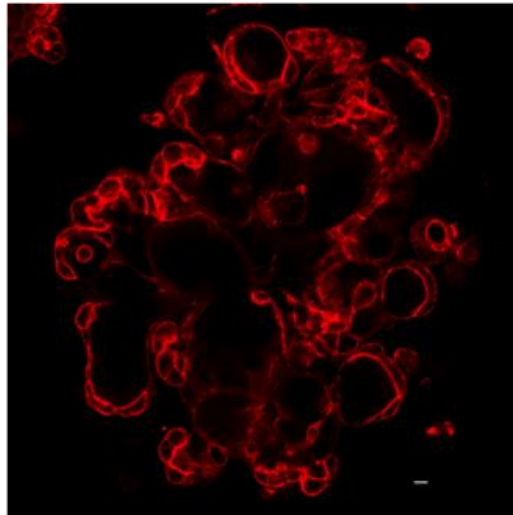


Figure 4: An example of a cross-sectional view of a murine lung organoid generated in *ex vivo* cultures. Sorted alveolar type 2 cells were cultured in matrigel and stained for surfactant protein C (SFTPC; in red), a marker for alveolar type 2 cells. Image provided by Dr. Tata. Scale bar: 20 μ m

1.4 Gene editing technologies

Several genome editing systems have been developed utilizing artificial nucleases [30]. The first methods to target nucleases that induce double strand breaks (DSBs) at specific genomic sites were based on protein systems with modifiable DNA-binding characteristics, such as meganucleases, transcription activator-like effector nucleases (TALENs), and zinc finger nucleases (ZFNs) [31]. Meganucleases are artificially altered versions of natural restriction enzymes with extended DNA recognition domains. TALENs and ZFNs are engineered proteins generated by fusing a specifically designed DNA binding sequence to the non-specific nuclease of *FokI* restriction enzyme [31]. While the DNA-binding domain of ZFNs harbors a common cys_2 - his_2 sequence [32], the DNA recognition domain of TALENs consists of 33-35 repeated amino acid motifs, each targeting a specific nucleotide (nt). By remodeling these recognition motifs, specific DNA sequences can be targeted with engineered TALENs [30]. Although these techniques have enabled major advances in gene editing, and have been used extensively to induce genomic modifications in many different organisms and cell types, certain challenges have been revealed to be associated with each method [31]. The difficulty in modifying meganucleases has been due to the intertwined nature of their DNA recognition and cleavage sites, which are found within the same domain of these enzymes [33], [34]. By contrast, in TALENs and ZFNs, the *FokI* cleavage site is spatially separated from the DNA binding sequence [35], which facilitates easier modification of their DNA-binding domains. In addition, customized TALENs and ZFNs can be combined in arrays to enable binding of extended DNA sequences [31]. However, sound construction

of zinc finger arrays has been impeded by the need to prevent unintended effects between the individual zinc finger domains [36]. Therefore, ZFNs have not been widely applied, although various methods are available to simplify their creation [37]–[40]. In contrast, TALE domains have shown to be less impaired by context-dependent effects, and can be modularly combined to target essentially any DNA sequence [41]. Despite their simple design, the assembly of large numbers of TALE repeats may require non-standard cloning techniques, and their repetitive nature precludes delivery by certain viral vectors, including lentiviruses [42]. Nevertheless, the simplicity of TALENs compared to ZFNs and meganucleases has resulted in their widespread application [31].

1.4.1 The CRISPR/Cas system

More recently, a new platform has been developed, based on the bacterial CRISPR-Cas system, which provides a versatile alternative to TALENs and ZFNs [31], [43]. In contrast to protein-guided cleavage methods, CRISPR/Cas relies on short RNA strands, which guide the nuclease to a specific DNA sequence [31], [44]. This system is unique and highly flexible, as it depends merely on designed RNA sequences to achieve sequence specificity [30], [31]. Moreover, the CRISPR/Cas system relies on simple base pairing between the target DNA sequence and the engineered RNA [31], which makes it easily applicable, and has led to its rapid development over the past years [30].

The CRISPR/Cas system originally represents the adaptive immune response of bacteria and archaea to fight invading nucleic acids, such as plasmids or viruses [44]–[47]. It is based on the insertion of short ‘protospacer’ sequences of foreign DNA into the CRISPR locus of the bacterial genome, thereby creating a cellular memory. These incorporated sequences are transcribed into CRISPR RNA (crRNA), which recognizes complementary sequences in case of repeated infection by the same intruder. To exert its function, crRNA hybridizes with trans-activating crRNA (tracrRNA), and this complex guides Cas nuclease to cleave the foreign DNA, thereby disarming it [30], [31], [48]. Based on the broad variety of Cas proteins, three main types of CRISPR/Cas systems have been identified [49], among which type II is most widely used, as it requires only one Cas protein, Cas9 [44]. This system from *Streptococcus pyogenes* can be used to generate a DSB in a genomic target sequence [44], which is then repaired by the host cell’s repair machinery. At least two different repair mechanisms are possible, non-homologous end joining (NHEJ), which rapidly joins the DNA ends, but likely produces small insertions or deletions (indels), and homology-directed repair (HDR), which is far less error-prone, but requires a homologous template to repair the damage adequately [30], [50]. Thus, by providing a specifically designed template, CRISPR/Cas9 allows to introduce a defined change at a specific locus of a cell’s genome [30], [31]. In such gene editing applications, three components need to be introduced into the target cells: the Cas9 nuclease, a single guide RNA (sgRNA), which is generated by fusing the designed crRNA and tracrRNA [44], and a single-stranded oligodeoxynucleotide

(ssODN) template (see Figure 5) [30], [31]. Instead of using one fused sgRNA, crRNA and tracrRNA have been applied separately in earlier studies [31]. However, it has been shown that using a sgRNA results in substantially higher efficiencies [51]–[53], presumably due to the fact that two components, namely sgRNA and Cas9, can associate and function more easily, as compared to three components [31]. Once the required components have entered a cell, the 20 nt sgRNA sequence binds to its complementary DNA target in the genome, and Cas9 cuts precisely 3 base pairs (bp) upstream of a protospacer adjacent motif (PAM) site [50]. Because Cas9 only cleaves DNA adjacent to a PAM sequence, the available target loci are limited [30], [31]. However, web-based programs are available to identify these potential target sites, such as CRISPR Design Tool [31].

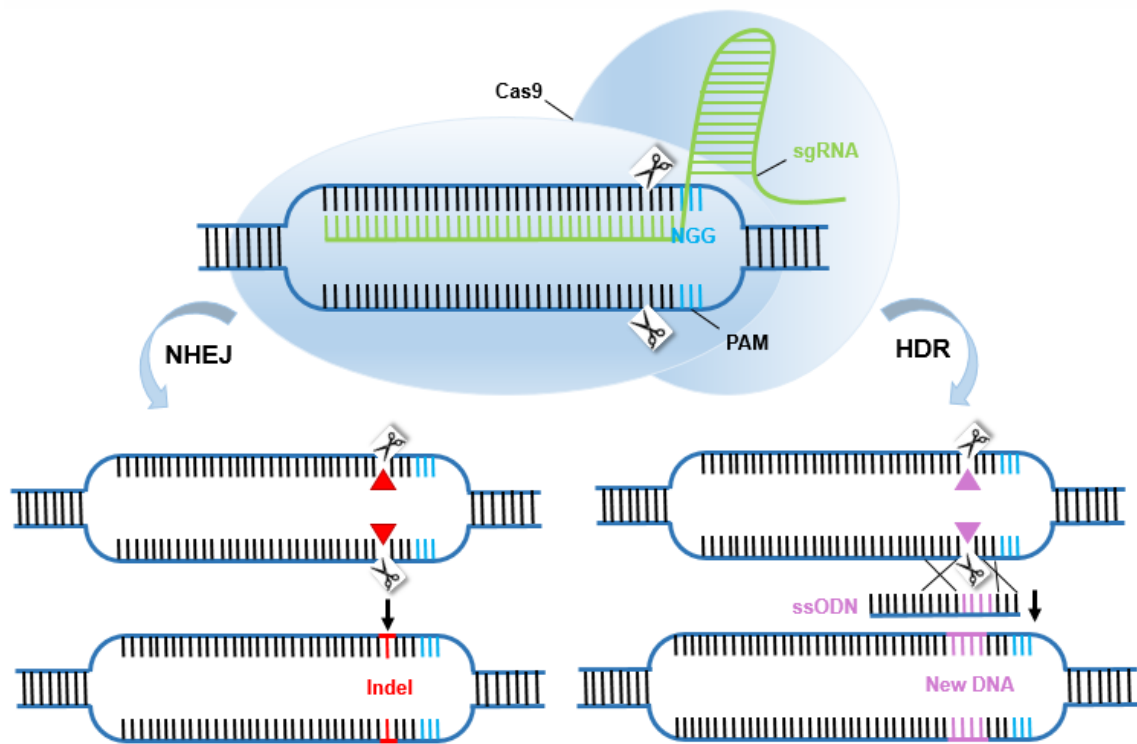


Figure 5: Cellular repair mechanisms of CRISPR/Cas9-induced DSBs. Cas9 nuclease generates a DSB in the host genome, which can be repaired by NHEJ or HDR. While NHEJ is highly error-prone, frequently leading to small indels, HDR requires a homologous DNA template, with which the damage can be repaired properly. By providing a specifically designed template ssODN together with Cas9 and the sgRNA, a defined change can be introduced at a specific locus in a DNA sequence [30], [31].

The CRISPR/Cas9 technology represents a long awaited system to manipulate genomes at will. Successful applications in a multitude of organisms, including yeasts, worms, plants, insects, and mammals, led to its rise as the most widespread genome editing tool in history [54]–[59]. Remarkably, through integration of Cas9 together with several guide RNAs (gRNAs) in a CRISPR/Cas9 array, even multiple modifications can be induced at distinct target sites at once [53]. In addition, the inactive variant, referred to as dead Cas9 (dCas9), has been proven useful in manipulating gene expression profiles and performing genome wide genetic screens [60]–[62]. Moreover, the broad applicability of CRISPR/Cas9 in human

tissues, including somatic cells, stem cells, as well as induced pluripotent stem cells, demonstrates its vast potential for medicine [63]–[65]. Most importantly, CRISPR/Cas9 represents a promising tool to cure genetic diseases. Moreover, preclinical trials have already been conducted to evaluate its potential to treat HIV, cancers and other conditions [64]–[67]. CRISPR/Cas9 has also been applied to develop high throughput systems to screen for genes and drugs in an attempt to discover novel treatment options for ovary cancer [68], which may facilitate discoveries in other cancer types as well [50].

However, CRISPR/Cas9 applications are also facing certain challenges. The major concerns are off-target effects, limitations of target loci due to the restriction of PAM sites, and variations in efficacy [67], [69]. Especially off-target activities, leading to the cleavage of DNA sequences that are not entirely matching the corresponding gRNA, are of substantial concern in medicine, as they could potentially result in pathologic conditions [50]. To address this issue, crystallization of the Cas9-gRNA-DNA complex has been performed at different stages of the binding process, in order to examine its mechanistic details, and to facilitate the design of improved versions of CRISPR/Cas9 [70]–[72]. Advances have also been made regarding the development of improved bioinformatics tools for the design and selection of gRNAs [69], [73], the application of different gRNA lengths [74], [75], and inducible CRISPR/Cas9 variations [61], [76], the direct application of the Cas9-gRNA complex [76], and PAM alterations to broaden the availability of genomic target sites [77]. Another tool to increase efficiency and specificity that has been successfully used, is pre-screening of gRNAs via fluorescent reporters, or performing sensitivity tests, such as T-7 endonuclease assay [78]–[80]. Furthermore, the application of ‘paired nickases’ has been proposed, which generates two nicks at the target site, one in each strand, by using two gRNAs [81], [82]. Since nickases create single strand breaks only, the probability that off-target DSBs are induced can be minimized with this method. Moreover, off-target activities can be considerably reduced by using truncated gRNAs, which have shortened 5’ ends, and consist of only 17 or 18 nt complementary to the target sequence. While they show the same efficiency as full-length gRNAs in guiding on-target cleavage, they seem to be more sensitive to mismatches at the DNA/gRNA interface, and therefore generate less mutagenic off-target effects [83]. The generation of a CRISPR/Cas9 variant with optimal efficiency and specificity, independent of the genomic target site, is clearly desirable, but not likely to be achieved, due to the great diversity of genomic compositions and target sites. Therefore, novel strategies need to be developed to fully obtain these desired advancements [50].

1.5 Structure and cellular composition of the lung

The basic structure of the respiratory system is conserved among most vertebrate species [84]. A single trachea splits into tree-like branches of airway tubes, which terminate in millions of highly delicate alveolar units performing gas exchange [84], [85]. Due to the lung’s function in gas exchange between inhaled air and the circulating blood, it has a remarkably

large surface area lined by continuous, highly vascularized epithelium [85], [86]. However, there are significant differences in epithelium lining the proximal and distal regions of the lung, regarding structural organization as well as cellular composition, including stem cell populations [85]. Basically, the proximal conducting airways are lined by pseudostratified epithelium, which consists of secretory cells (goblet cells and club cells, originally known as Clara cells), ciliated cells, basal cells (BCs), and neuroendocrine cells [84], [87]. Whereas the distal alveolar regions consist of flat and elongated alveolar type 1 epithelial cells (AEC1s), forming the alveolar boundaries that mediate gas exchange, and cuboidal alveolar type 2 epithelial cells (AEC2s) producing surfactant protein C (SFTPC), which prevents the alveoli from collapsing [86]–[88]. The structures of pseudostratified epithelia and alveoli in the lung are shown in Figure 6.

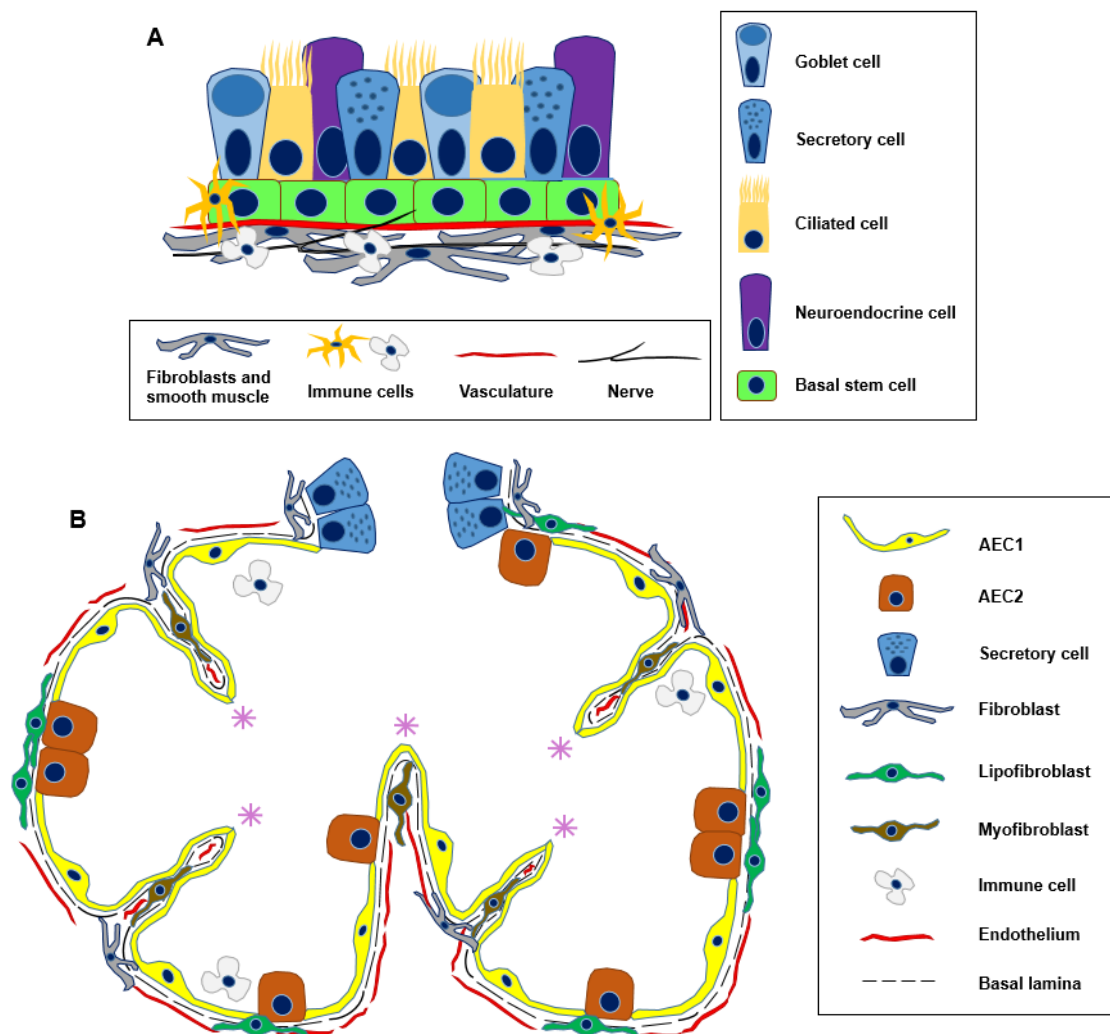


Figure 6: Structure of pseudostratified epithelia and alveoli in the lung. A) The pseudostratified epithelium of human airways consists of goblet, secretory, ciliated, and neuroendocrine cells, resting on a layer of basal stem cells. Underlying tissue contains fibroblasts, smooth muscle cells, immune cells, vasculature and nerves. B) Alveoli of the adult murine lung are made of AEC1 and AEC2 cells. The external tissue adjacent to the basal lamina consists of fibroblasts, lipofibroblasts, myofibroblasts, and endothelium. Alveoli are subdivided by septa (asterisks) that harbor myofibroblasts producing elastin, thereby forming a fibroelastic network. Immune cells are scattered within the alveoli to fight airborne germs [85]. Images were redrawn from Hogan *et al.* 2014.

There are also notable differences between human and mouse lungs, presumably due to the enormous body size difference. Naturally, this discrepancy poses differential requirements to their respective airway architectures. For instance, the diameter of a mouse trachea resembles the diameter of small human peripheral airways. Hence, while cartilage is present along several bronchial levels in the human lung, cartilage rings in murine lungs are restricted to the extrapulmonary airways [84]. Moreover, submucosal glands are only found in the proximal trachea in mice, but extend deep into the lungs of humans. Furthermore, goblet cells, which secrete mucin, are relatively abundant in human lungs but rare in adult mice [84]. Importantly, pseudostratified epithelium containing BCs is present in all human bronchioles of a diameter larger than 0.5 mm, and only smaller bronchioles are missing BCs in their simple cuboidal epithelium. By contrast, pseudostratified epithelium is restricted to the trachea in mice, and all bronchioles distal to the mainstem bronchi are lined by simple columnar epithelium lacking BCs. Thus, the organization and cellular composition of the small bronchioles in mice are only comparable to the most distal branches of human airways, suggesting that studies of the airway epithelium in mice should ideally focus on the trachea and mainstem bronchi, which resemble most of the human bronchiolar levels [84].

1.6 Cell types applied in organoid culture

NSCLC mostly originates from mutations in epithelial cells [5], more specifically lung stem cells, such as airway BCs and AEC2s [89]. Therefore, these two cell types were used, derived from murine as well as human tissues, to generate lung organoids.

1.6.1 Airway basal stem cells

BCs are found in all stratified and pseudostratified epithelia of the body. They are named after their close proximity to the underlying basement membrane [84], to which they are firmly attached via hemidesmosomes [90], [91] as well as other adhesion molecules [84]. Both, in human and mouse lungs, BCs also form desmosomal contacts with their neighboring cells [84], [91]. Their abundant adhesive, junctional and cytoskeletal proteins anchor the epithelium to the extracellular matrix and segregate the underlying stroma from external tissues [84]. BCs form a continuous monolayer in both, the mouse trachea and in larger human airways, while more distally, they present as clusters or as single cells [92]. Evidence suggests that BCs are long-lived, multipotent stem cells, responsible for homeostasis in normal epithelium as well as regeneration after injury [84], [93]. While BCs are relatively quiescent in normal tissue, they become rapidly active after injury, presumably regulated by signaling with their niche [93]. This behavior is characteristic for stem cells of diverse tissues undergoing repeated cycles of regeneration, such as hair follicles and mammary glands [94], [95]. Therefore, these cells also express several genes similarly, such as transcription factors and intercellular signaling receptors and ligands, which likely regulate interactions between stem cells and their niches [93]–[95]. BCs are able to quickly regenerate the entire epithelium after injury, due to self-renewal and differentiation into ciliated and secretory cells. Whereby,

it has been found that the ratio of club cells versus ciliated cells that arise depends on the local conditions [93].

Several genes are commonly expressed in both, human and murine BCs, such as high levels of transformation-related protein 63 (*TRP63*), which is a transcription factor required for the development of BCs [96], and the cytoskeletal proteins cytokeratin 5 (*KRT5*) and cytokeratin 14 (*KRT14*) [84], [93]. At steady state, *KRT5* is expressed by most BCs, whereas *KRT14* is more restricted, and usually upregulated after injury [97], [98]. Another gene expressed in murine as well as human BCs is *NGFR*, which belongs to the TNF receptor superfamily [93].

1.6.1.1 Culture of airway basal stem cells

The standard method to culture epithelial stem cells relies on the co-culture with irradiated stromal cells, such as fibroblasts [99]. However, these feeder cells represent a contamination of the culture and may distort the interpretation of experimental results [100]. Moreover, previous studies using air-liquid interface (ALI) cultures to investigate the potential of BCs to regenerate airway epithelium have been difficult to reproduce [93]. Therefore, Rock *et al.* have adapted a protocol established to form 3-dimensional spheres from prostate stem cells [93], [101]. With this assay, they have demonstrated that single tracheal BCs are able to form 'tracheospheres' within one week, even in the absence of stromal cells. After 9 days in culture, a pseudostratified epithelium has been observed with TRP63⁺ KRT14⁺ BCs surrounding luminal KRT8⁺ cells. After 20 days, the spheres had increased luminal diameters, thinner epithelia, and beating cilia. On day 26, approximately 50% were ciliated KRT8⁺ cells, which equals the percentage in adult mouse trachea. Similar results have been achieved using TRP63⁺ NGFR⁺ ITGA6⁺ cells isolated from human bronchi, which formed 'bronchospheres' after 10 days, indicating that human BCs (hBCs) are equally capable of regenerating the entire pseudostratified epithelium. Interestingly, when BCs from mice constitutively expressing either green fluorescent protein (GFP) or red fluorescent protein (RFP) were mixed, the arising spheres fluoresced only green or red, indicating that each sphere was derived from a single cell [93].

By contrast, long-term culture of epithelial cells while simultaneously maintaining their stem cell characteristics has been even more challenging [100]. Despite achievements in improving culture conditions, such as organoid models, which do not rely on stromal co-cultures [93], [102], [103], or using Rho-associated protein kinase (ROCK) inhibitor [104], the ability to maintain pure epithelial stem cell cultures has been limited [100]. Recently, Mou *et al.* have been able to establish culture conditions to address this problem. They have demonstrated that by the addition of BMP as well as TGF β signaling antagonists to the culture medium, differentiation of human as well as murine BCs can be prevented for up to 25 passages (approximately 80 population doublings). Moreover, the cells proliferated faster, were highly homogeneous in size, and maintained expression of stem cell markers and

transcription factors that indicate epithelial stem cell identity. This effect is due to BMP and TGF β signaling through the SMAD pathway, which is associated with differentiation. It has been shown that early expression of KRT8 in differentiating luminal cells coincides with beginning SMAD phosphorylation, and p-SMAD expression even increases in mature luminal cells. Mou *et al.* have found that blocking SMAD signaling through BMP and TGF β antagonists compromised differentiation efficiently. Moreover, BMP antagonist (DMH-1, 1 μ M) as well as TGF β antagonist (A8301, 1 μ M) alone substantially increased cell proliferation. By contrast, ROCK inhibitor (Y-27632, 10 μ M), which was also investigated, only moderately enhanced proliferation. However, all three inhibitors combined had the strongest effect, resulting in small, homogeneous, tightly packed cells, expressing TRP63 and KRT5, and more than 85% were positive for Ki67, which indicates mitotic activity [100]. The results of Mou *et al.* are shown in Figure 7. Due to these findings, the culture medium for the expansion of airway basal stem cells was constantly supplemented with all three inhibitors during this project.

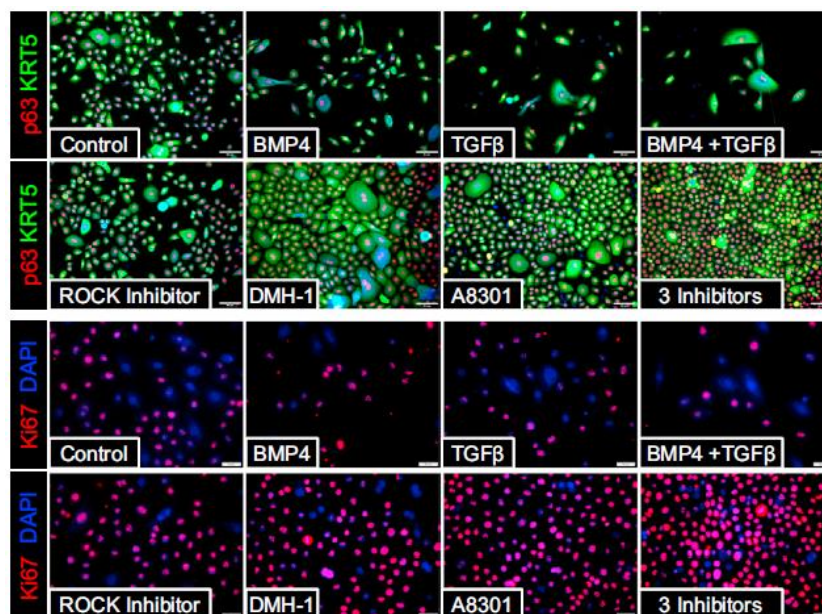


Figure 7: Effects of ROCK inhibitor, TGF β and BMP antagonists on human airway stem cells. BCs were cultured for 4 days under several conditions. TGF β (10 ng/ml) and BMP4 (50 ng/ml) strongly suppressed proliferation, while A8301 (1 μ M) and DMH-1 (1 μ M) substantially increased cell expansion, and ROCK inhibitor (10 μ M) moderately enhanced it. All three inhibitors combined had the strongest effect. After fixation, cells were stained for KRT5, TRP63, and Ki67. Scale bars: upper panel 50 μ m, lower panel 20 μ m [100]

In addition, a fourth substance was added to the basal cell medium, according to findings of Fujii *et al.*, who used this glycogen synthase kinase 3 (GSK-3) inhibitor (CHIR99021, 1 μ M) to increase recovery of single intestinal cells [105].

1.6.2 Alveolar type 2 epithelial cells

Two main epithelial cell types are found in the alveolar regions of the lung, AEC1 and AEC2 (see Figure 6B). While AEC1s are flat and elongated squamous cells, constituting most of the alveolar boundaries and mediating gas exchange, AEC2s are cuboidal cells secreting surfactant [86]–[88]. Barkauskas *et al.* have shown that AEC2s are able to self-renew for several months, thereby meeting the criteria for being long-term adult stem cells [86]. In addition, it has been demonstrated that AEC2s are progenitors of AEC1s, and therefore have an important role in tissue maintenance [86], [106]. However, many questions remain regarding their identity and behavior, for instance, whether the AEC2 population is a heterogeneous mixture of cells with distinct capacities for differentiation, or what the precise composition of their niche is [86].

1.6.2.1 Culture of alveolar type 2 epithelial cells

AEC2s are progenitors of AEC1s [86], [106], and exert a great tendency to differentiate under most conditions, which has made it difficult to maintain AEC2s in culture [107]. To address this issue, Yu *et al.* have established a 3-dimensional culture system by seeding freshly isolated and purified human AEC2s on a thin layer of matrigel, and covering them with Minimum Essential Medium (MEM) containing 2% matrigel [107]. With this system, they could observe the formation of hollow structures, termed cysts, lined by a monolayer of cuboidal, polarized AEC2s. Moreover, the cells were found to retain their specific properties, secreting surfactant and remaining well differentiated. Interestingly, in contrast to cysts formed by other cell types, these structures emerged solely by cell aggregation and rearrangement, not by proliferation and apoptosis. Evidence for their AEC2 identity has been provided by staining for prosurfactant C and using LysoTracker Green DND-26 to label lamellar bodies. In addition, multivesicular bodies, another characteristic of AEC2s, were observed. Within the lumens of the cysts, surfactant proteins secreted from lamellar bodies were identified, arranged in the distinctive form of tubular myelin, which has a unique grid pattern. Cell polarity was examined by staining for β -catenin, which is a marker for the basolateral cell membrane, as well as zonula occludens (ZO)-1, which is a marker for tight junctions and was found only at apical cell-cell contacts sealing the lumen. Moreover, microvilli were observed solely facing the lumen, and β 1 integrins only at the basolateral surfaces [107]. However, although this culture system has enabled the establishment of well-defined cyst-like structures from AEC2s, cultures have been terminated after 5 days, leaving open the question as to whether AEC2s can be cultured for longer time periods.

In a more recent study, a system has been established involving the culture of AEC2s with PDGFRA⁺ mesenchymal cells, including LipidTOX⁺ lipofibroblasts, which are naturally found in close proximity to AEC2s in the lung [86]. In this 3D system, 5,000 lineage-labeled AEC2s were seeded together with 100,000 PDGFRA⁺ cells in 50% matrigel on transwell membranes. Four to six days after plating, single AEC2s self-renewed and differentiated into

'alveolospheres', which are alveolar-like structures containing both, AEC2s and AEC1s. During the first ten days, these spheres enlarged and developed a single lumen, later they became denser and cells could be observed in the center. Histological analysis showed that peripheral cells were proliferating, SFTPC⁺ cuboidal cells, while most interior, elongated cells expressed AEC1 markers podoplanin (PDPN), aquaporin 5 (AQP5), and homeodomain only protein x (HOPX). Two weeks after plating, many cuboidal cells contained abundant lamellar bodies and secreted SFTPC in large amounts into the lumen, whereas the elongated cells had developed dense microvilli. However, the precise identity of cells, matrix components and signals that are required for clonal expansion of AEC2s, is still unknown [86].

1.7 Formation of organoids

A variety of culture systems has been developed to study the differentiation of lung stem cells [29], [86], [93], [108], [109]. The simplest method is to grow cells in 2-dimensional monolayers, however, this form does not recapitulate physiological conditions. It has been shown that lung epithelial stem cells lose their lung lineage markers under these conditions, which are therefore not suitable for long-term culture and differentiation studies [89], [110]. ALI cultures are 2-dimensional as well, but are more appropriate to mimic the *in vivo* environment of the lung [111], [112]. Hereby, cells are seeded on the membrane of a transwell insert and medium is applied above as well as below the permeable membrane, until cells reach confluency. Thereafter, the medium from the upper chamber is removed to create an ALI and induce differentiation. Despite the development of secretory, ciliated and basal cells, also these cultures are not sufficiently emulating the architecture of pseudostratified epithelia *in vivo*. In addition, it has been found that stem cell behavior is highly regulated by complex signaling with their microenvironment, or niche. Therefore, 3-dimensional culture systems have been established using matrigel to mimic this niche [89]. Matrigel is a basement membrane extract produced by mouse tumor cells, consisting of collagen, fibronectin and laminin. At 4°C, matrigel is liquid and cells can easily be incorporated, by exposing this mixture to 37°C in the incubator, matrigel solidifies quickly and provides the cells with a matrix similar to their *in vivo* environment [113], [114]. Due to the gel-like properties of matrigel, droplets of cell-matrigel-suspension can easily be placed on regular multiwell plates. After a short incubation time to let the matrigel solidify, medium can be added to the wells to supply the cells with nutrients, without disrupting the droplets. Recent studies have successfully established a combination of these two culture systems, 3-dimensional matrigel and ALI, which has shown even better colony-forming efficiency [86], [115]. In this system, the cell solution is again mixed with matrigel at a 1:1 ratio, but then transferred to a transwell membrane, and medium is added to the lower chamber. This system is especially useful when different components are to be added or removed after some time, such as soluble factors or stromal cells, which can easily be confined to the lower chamber, spatially separated from the actual organoid culture [89]. An overview of the different culture techniques is given in Figure 8.

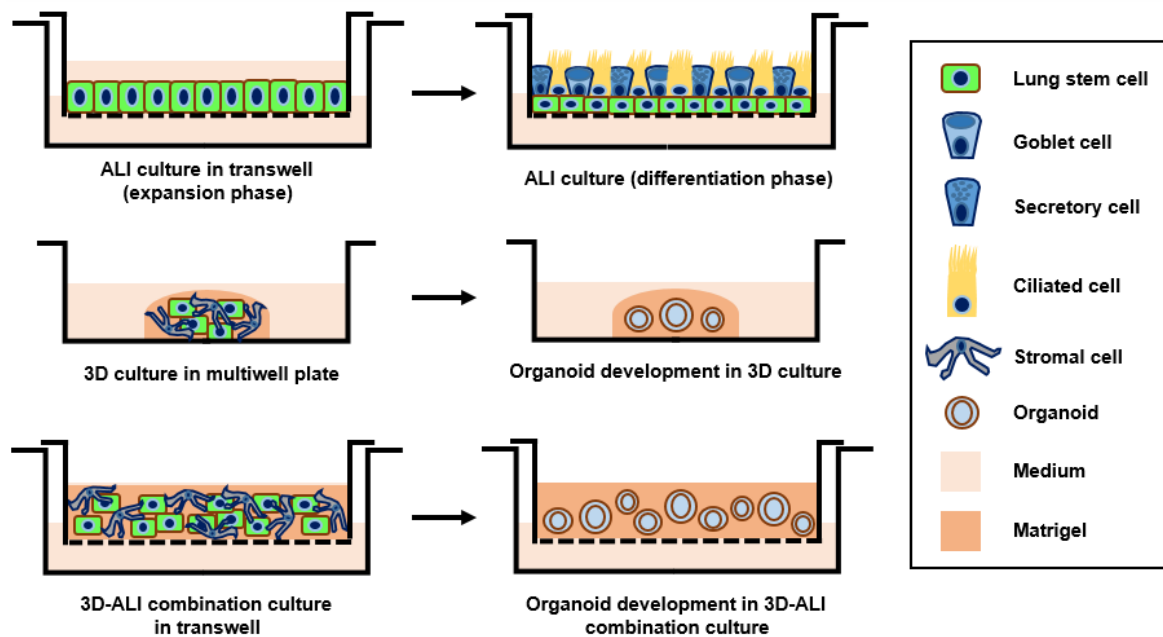


Figure 8: Culture systems to study the differentiation of lung stem cells. The upper panel shows an ALI culture, in which lung stem cells are seeded in a transwell insert, and medium is applied above as well as below the membrane, until cells reach confluency. Thereafter, the medium from the upper chamber is removed to create an ALI and induce differentiation. The middle panel shows a 3D culture of cell-matrigel-droplets placed in a multiwell. The lower panel represents the combination of 3D matrigel culture and ALI, in which the cell-matrigel-suspension is plated on a transwell membrane, and medium is added to the lower chamber only [89]. Images were redrawn from Choi *et al.* 2016.

Depending on the tissue, specific modifications to the culture system are required to adequately emulate the niche of the respective cell type and allow for long-term growth and appropriate differentiation [89]. Therefore, the protocols found in literature were slightly adapted to establish the best conditions for organoids from murine and human lung epithelial stem cells. Initially, organoids were generated from healthy murine lung stem cells, more precisely BCs and AEC2s, in co-culture with fibroblasts, such as MLGs (murine lung fibroblasts) or MRC5 cells (human lung fibroblasts). In addition, cultures were set up from *KRAS*-mutant murine lung cells. Eventually, human lung tissue was obtained, dissociated and enriched for BCs, which were then used to generate healthy human lung organoids. Most importantly, it was attempted to introduce *EGFR* mutations into hBCs using CRISPR/Cas9-based genome editing, in order to establish human lung tumor organoids. Moreover, a human lung adenocarcinoma cell line was used to set up *KRAS/p53*-mutant cancer organoids. Finally, murine and human, healthy and cancerous organoids were evaluated based on histological markers and growth kinetics.

Dr. Tata's laboratory had already used the CRISPR/Cas9 system to generate *KRAS*^{G12D} mutations as well as *NKX2-1* knock out cell lines as a proof of principle. As expected, these mutant cells generated tumor-like organoids that expressed markers of certain adenocarcinomas of the lung (Figure 9).

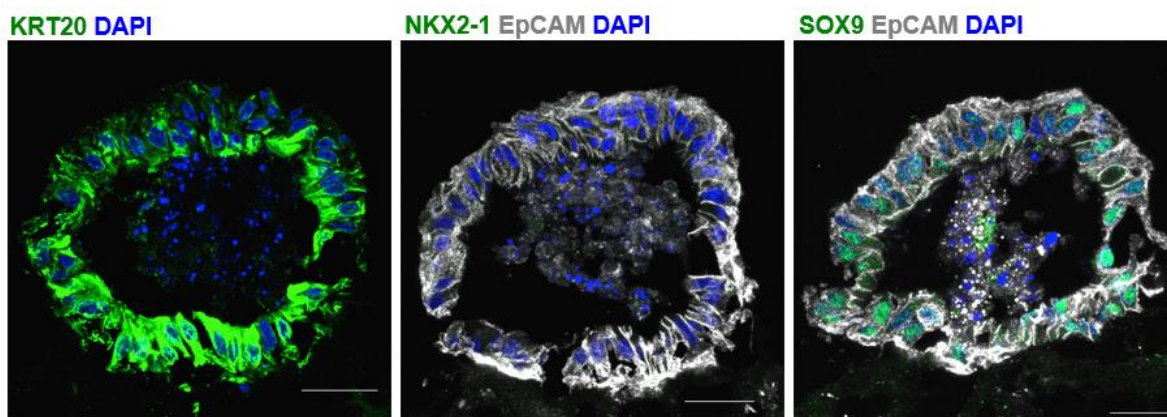


Figure 9: Murine tumor-like lung organoids generated by *KRAS*^{G12D} and *NKX2-1* knockout mutations in AEC2s. Immunofluorescence analysis of sections derived from tumor organoids indicating expression of KRT20 (in green; left), EpCAM (in gray; middle) and SOX9 (in green; right); DAPI marks nuclei.

1.7.1 Application of organoids to microfluidic devices

In a subsequent project, the established human lung tumor organoids will be combined with microfluidic devices to screen for small molecules as potential drugs against lung cancer. Therefore, single-cell RNA sequencing will be applied to investigate the response of distinct forms of lung tumors to certain chemicals. The Duke University has a library of about 300,000 different chemicals that may be used for this purpose. The effects of promising chemicals will be observed, as well as the emergence of resistances. Ultimately, clinically-relevant therapeutic substances will hopefully be discovered, in order to create novel, tailored treatment options for patients suffering from lung cancer.

2 Materials and Methods

2.1 Basic cell culture

Table 1: Materials and reagents used for basic cell culture. Company names and order numbers/models are provided for materials and reagents used in basic cell culture.

Material/Reagent	Company	Order number/Model
Petri dishes <ul style="list-style-type: none"> • 10 cm dishes • 6 cm dishes 	Denville Scientific Denville Scientific	T1110 T1106
Multiwell Plates <ul style="list-style-type: none"> • 96-well-plates • 24-well-plates • 12-well-plates • 6-well-plates 	Denville Scientific Denville Scientific Denville Scientific Denville Scientific	T1096 T1024 T1012 T1006
24-well 0.4 µm transwell inserts	Corning	353095
Waterbath	Intertek	WB10
CO ₂ Incubator	Thermo Fisher Scientific	HERAcell VIOS 160i
Laminar flow hood	Labconco	Purifier Class II Biosafety Cabinet

Centrifuges	Kendo	Legend RT
	Thermo Scientific	Heraeus Megafuge 8R
1x Phosphate buffered saline (PBS)	Sigma-Aldrich	D8537-500ML
1x Trypsin/EDTA 0.25% (T/E)	Gibco (Life Technologies)	25200-072
1x Dulbecco's Modified Eagle Medium (DMEM)	Corning	10-013-CV
Fetal bovine serum (FBS)	Gibco (Invitrogen)	16141-079
Sterile syringe filters, 0.22 µm	Olympus plastics	25-244
SAGM BulletKit	Lonza	CC-3118
• Small Airway Epithelial Cell Basal Medium (SABM)	Lonza	CC-3119
• Small Airway Epithelial Cell Growth Medium (SAGM) SingleQuot Kit	Lonza	CC-4124
TGFβ antagonist A8301	Fisher Scientific	50-176-036
BMP antagonist DMH-1	Fisher Scientific	41-261-0
GSK-3 inhibitor CHIR99021	Fisher Scientific	NC0226336
ROCK inhibitor Y27632	Selleck Chemicals	S1049
1x DMEM-F12	Thermo Fisher Scientific	11330-057
4-(2-hydroxyethyl)-1-piperazineethanesulfonic acid (HEPES)	GE Healthcare Life Science	SH30237.01
Sodium bicarbonate	Grainger	144-55-8
L-glutamine (Glutamax 100x)	Gibco (Life Technologies)	35050-061
Penicillin/streptomycin (pen/strep)	Gibco (Life Technologies)	15070-063
Antibiotic-Antimycotic 100x	Gibco (Life Technologies)	15240062
Insulin	Gibco (Life Technologies)	12585-014
Transferrin	Gibco (Life Technologies)	11107-018
Cholera toxin	Sigma-Aldrich	C8052
Epidermal growth factor (EGF)	Invitrogen	PHG0313
Bovine pituitary extract (BPE)	Invitrogen	13028-014
Retinoic acid	Sigma-Aldrich	R2625
1x Minimum Essential Medium (MEM)	Sigma-Aldrich	M8167-6X500ML
Sodium Pyruvate	Thermo Fisher Scientific	11360070
100x MEM Non-Essential Amino Acids (NEAA) solution	Thermo Fisher Scientific	11140-050
Vacuum filtration system	Millipore Sigma	SCGPU05RE
Ward's Economy Improved Neubauer Hemocytometer	VWR	470019-796
Trypan blue	Sigma Life Science	T8154-100ML
Dimethyl sulfoxide (DMSO)	Sigma-Aldrich	D8418-500ML
Light microscope	VWR	89404-462
Fluorescence microscopes	Carl Zeiss	Axiovert 200 Camera: AxioCam MRm
	Carl Zeiss	Axio Imager.D2 Camera: AxioCam MRm

In order to maintain undifferentiated BCs in culture, they were grown in SAGM plus medium supplemented with the appropriate growth factors as described previously. The full medium

was prepared by supplementing Small Airway Epithelial Cell Basal Medium (SABM) with all components of the Small Airway Epithelial Cell Growth Medium (SAGM) kit and the four inhibitors mentioned earlier (A8301, DMH-1, CHIR99021 and Y27632). Therefore, the SAGM kit and inhibitor aliquots were thawed at room temperature (RT). Then approximately half of the SABM medium was poured in the upper chamber of a 500-ml filtration unit. During preparation of the medium, the light in the laminar flow hood was turned off to protect light sensitive ingredients. Next, all reagents from the SAGM kit and the four inhibitors were transferred to the medium. Whereby, each vial was rinsed to assure that nothing was lost and the correct concentration was achieved. Thereafter, the remaining SABM medium was added, and the outlet of the filtration unit was connected to the suction pump to speed up filtration. Finally, the bottle was covered with aluminum foil to protect it from light, and stored at 4°C. All components are listed in detail in Table 2. Before the full SAGM plus medium was applied to BCs, it was pre-warmed at RT for at least 1 h. Warming in the waterbath was avoided, as some media components are sensitive to repeated 37°C / 4°C cycles.

Table 2: Components of full SAGM plus medium. Table showing the media components, provided volumes, stock and final concentrations.

Media component	Stock concentration	Volume	Final concentration
SABM	1x	500 ml	
SAGM kit			
• BPE (low protein – nonspecific)	-	2 ml	0.4%
• Recombinant human insulin	0.5%	0.5 ml	0.1%
• Hydrocortisone solution	-	0.5 ml	0.1%
• GA-1000	-	0.5 ml	0.1%
• Retinoic acid	10 mM	0.5 ml	10 µM
• Bovine Serum Albumin (BSA-FAF)	50 mg/ml	5 ml	250 mg
• Transferrin	-	0.5 ml	0.1%
• Triiodothyronine (T3)	-	0.5 ml	0.1%
• Epinephrine	-	0.5 ml	0.1%
• Recombinant human EGF	0.5 µg/ml	0.5 ml	0.25 µg
TGFβ antagonist A8301	10 mM	50 µl	1 µM
BMP antagonist DMH-1	10 mM	50 µl	1 µM
GSK-3 inhibitor CHIR99021	10 mM	50 µl	1 µM
ROCK inhibitor Y27632	10 mM	500 µl	10 µM

It has been shown that BCs require additional coating of culture vessels to attach. Therefore, plates used to grow BCs were coated with 804G-conditioned medium, which is the supernatant of 804G cells, an epithelial cell line derived from rat bladder carcinoma. These cells are special, as they are able to form hemidesmosomes when grown on plastic or glass, due to extracellular components they produce, such as laminin. It has been shown that this 804G-derived matrix can support the maintenance of other epithelial cells, which are not able to form hemidesmosomes themselves [116]. Therefore, 804G cells were cultured in 15-cm dishes with Dulbecco's Modified Eagle Medium (DMEM) supplemented with 10% fetal

bovine serum (FBS) until reaching confluency. The supernatant was collected every other day in a glass bottle kept at 4°C. After three collections, the cells were discarded and the combined supernatants were sterile-filtered. To coat a 10-cm dish, 4 ml of this conditioned medium were transferred to the dish and incubated at 37°C for at least 5 hours. After this period of time, the laminins and other matrix components essential for cell attachment have settled and bound to the surface. Hence, the remaining solution was aspirated, and the plate was washed once with phosphate buffered saline (PBS) before BCs were seeded in the dish. BCs as well as other cell types were passaged at a confluency of about 95%, frequency was depending on cell type-specific growth rates.

Medium for MLg mouse fibroblasts was prepared from 500 ml MEM, 50 ml FBS (10%), 5 ml penicillin/streptomycin (pen/strep, 100x, 1%), 5 ml Non-Essential Amino Acids solution (NEAA, 100x), and 5 ml sodium pyruvate (100x, 1%). Human MRC5 fibroblast medium was generated by supplementing 500 ml DMEM-F12 with 50 ml FBS (10%), and 5 ml pen/strep (100x, 1%). All media were sterile filtered at the end of the preparation. In addition, a medium to stop the trypsinization reaction was generated by the addition of 5 ml sterile-filtered FBS (10%) to 45 ml DMEM.

Organoids generated from mouse trachea epithelia contained mainly BCs, and were therefore grown in SAGM plus medium supplemented with 1% pen/strep. Organoids from cell mixtures were cultured in MTEC basic medium, as the co-cultured cells, such as fibroblasts, produce the essential growth factors required by epithelial cells. Organoids established from epithelial cells alone were grown in MTEC plus medium. MTEC basic medium was generated from DMEM and DMEM-F12, HEPES, sodium bicarbonate, L-glutamine, penicillin, streptomycin, and antibiotic-antimycotic. MTEC plus medium was produced by adding several components to the MTEC basic medium, i.e. insulin, transferrin, cholera toxin, epidermal growth factor (EGF), bovine pituitary extract (BPE), FBS, and after sterile-filtration, retinoic acid (see Table 3). In case ROCK inhibitor was required, 10 mM stock solution was added at a dilution of 1:1,000 or 1:3,000.

Table 3: Components of MTEC basic and MTEC plus media. Table showing the media components, stock concentrations, used volumes and final concentrations.

Medium	Medium component	Stock conc.	Volume	Final concentration
	DMEM	1x	450 ml	
	DMEM-F12	1x	450 ml	
MTEC basic	HEPES	1 M	15 ml	15 mM
	Sodium bicarbonate	0.9 M	4 ml	3.6 mM
	L-glutamine (Glutamax stock)	200 mM	20 ml	4 mM
	Penicillin	1x10 ⁴ U/ml	10 ml	100 U/ml
	Streptomycin	1x10 ⁴ µg/ml	10 ml	100 µg/ml
	Antibiotic-antimycotic	100x	10 ml	1x
MTEC plus	Insulin	4 mg/ml	2.5 ml	10 µg/ml
	Transferrin	-	5 mg	5 µg/ml
	Cholera toxin	1 µg/µl	100 µl	0.1 µg/ml
	Epidermal growth factor (EGF)	0.1 µg/µl	250 µl	25 ng/ml
	Bovine pituitary extract (BPE)	14 mg/ml	2.14 ml	30 µg/ml
	Fetal bovine serum (FBS)	-	50 ml	5%
	Retinoic acid	10 mM	1 µl	0.01 µM

2.2 Generation of plasmids

2.2.1 sgRNA design

In order to create different types of tumors, specific mutations were introduced into human lung BCs using CRISPR/Cas9. Due to their abundance, the focus was placed on the most prevalent *EGFR* mutations in NSCLC. Therefore, three mutations were introduced, Δ E746-A750, T790M, and L858R. The required plasmids were generated using protocols that had already been established by the host laboratory.

The sgRNAs were designed by inserting a 400 bp region flanking the mutation site into the CRISPR Design Tool (<http://crispr.mit.edu/>). The most suitable guides were selected according to the closest proximity to the target mutation, and the highest score - indicating the lowest number of off-target sites. For each target mutation, a set of one forward and one reverse guide was ordered from Eurofins Genomics. After receiving the sgRNAs, each set of guides was cloned separately into px458 plasmids, which encode Cas9 nuclease, and enhanced green fluorescent protein (EGFP) to facilitate the detection of positive clones. Moreover, these plasmids harbor a *BbsI* restriction site for sgRNA insertion under U6 promoter, and an ampicillin resistance cassette, which enables selection of positive bacterial clones used for plasmid expansion. A scheme of the px458 plasmid used for transfection is depicted in Figure 10.

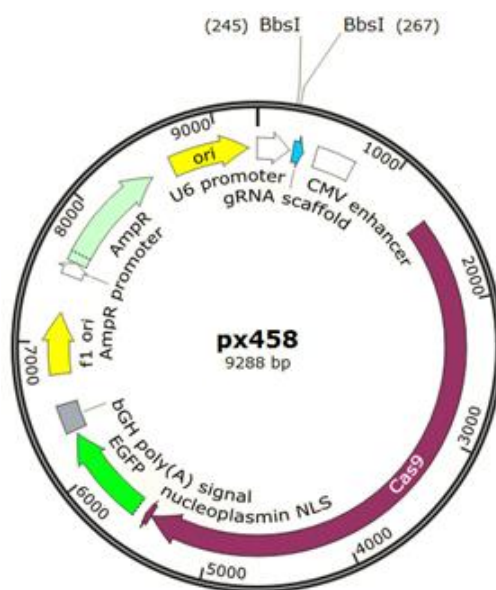


Figure 10: Scheme of the px458 plasmid used for transfection. The plasmid encodes Cas9 nuclease (purple), and EGFP to facilitate the detection of positive clones (green). It harbors a *BbsI* restriction site for sgRNA insertion (blue) under U6 promoter (white), and an ampicillin resistance cassette (light blue), which enables selection of positive bacterial clones used for plasmid expansion. The plasmid map was generated using SnapGene Viewer, version 3.3.3, by GSL Biotech LLC.

2.2.2 Cloning of vectors

Table 4: Materials and reagents used for cloning of vectors. Company names and order numbers/models are provided for materials and reagents used for cloning of vectors.

Material/Reagent	Company	Order number/Model
BbsI restriction enzyme	New England Bio Labs	R3539S
10x Fast Digest buffer	Thermo Scientific	B64
Ultrapure distilled water (DNase, RNase-free)	Invitrogen (Life Technologies)	10977-015
Agarose	Denville Scientific	GR140-500
Electrophoresis chamber	BioRad	Wide Mini-Sub Cell GT
TAE buffer <ul style="list-style-type: none"> • Tris base • Glacial acetic acid • Ethylenediaminetetraacetic acid (EDTA) 	Sigma-Aldrich Sigma-Aldrich Sigma-Aldrich	TRIS-RO A9967 E5513
20,000x GreenGlo Safe DNA dye	Denville Scientific	CA3600
6x DNA loading dye	Thermo Scientific	R0611
1x GeneRuler DNA ladder mix	Thermo Scientific	SM0333
UV illumination device	Accuris Instruments	Smart Blue Transilluminator E4000
Gel imaging device	BioRad	Universal Hood II
QIAquick gel extraction kit	Qiagen	28706
10x buffer for T4 DNA ligase with 10 mM ATP	New England Bio Labs	B0202S
T4 polynucleotide kinase (PNK)	New England Bio Labs	M0201L
Adenosine triphosphate (ATP) solution 25 mM	Epicentre	RA02825
Heating blocks	Denville Scientific	IncuBlock Plus

2x Quick ligase reaction buffer	New England Bio Labs	B2200S
Quick ligase	New England Bio Labs	M2200S
10x Plasmid Safe buffer	Epicentre	E3101K
Plasmid Safe exonuclease	New England Bio Labs	M0293L
Competent DH5 α <i>Escherichia coli</i>	Invitrogen	18265017
Waterbath	Thermo Scientific	Precision GP15D
2-YT bacterial broth	Teknova	Y0210
Platform shaker	New Brunswick Scientific	Innova 2300
Centrifuges	Kendro	Legend RT
	Beckman Coulter	Microfuge 20
Agar	Fisher BioReagents	BP1425-500
Bacteriological Petri dishes	Falcon	351029
Ampicillin sodium salt	Sigma-Aldrich	A0166-25G
EZ-10 Spin column plasmid DNA mini-prep kit	Bio Basic Canada	BS614-250
NanoDrop	NanoDrop Technologies	ND-1000 Spectrophotometer
Primer pLKO1	Eurofins Genomics	8287684

The target sequence cloning protocol from Zhang lab was followed for cloning of the vectors. First of all, the plasmids were digested by BbsI restriction enzyme (1 μ g px458, 1 μ l BbsI, 2 μ l 10x Fast Digest buffer, ultrapure distilled water [dH₂O] up to 20 μ l, incubation for 2 h at 37°C). Successful digestion was confirmed by agarose gel electrophoresis (70 ml 1% agarose in 1x TAE buffer with 5.6 μ l dye, 16 μ l sample and 4 μ l 6x loading dye per sample, run for 30 min at 150V). Next, each pair of sgRNAs was phosphorylated to generate a free 5' phosphate required for subsequent ligation, and annealed (1 μ l of each sgRNA [100 μ M], 1 μ l 10x buffer for T4 DNA ligase with 10 mM ATP, 0.5 μ l T4 PNK, dH₂O up to 10 μ l) using BioRad thermocycler (37°C for 30 min, 95°C for 5 min, ramped-down to RT at 0.1°C/sec), and then inserted into the plasmid via ligation reaction (5 μ l 2x Quick ligation buffer, 50 ng of digested plasmid, 1 μ l annealed oligo duplex [1:250 dilution in dH₂O], 1 μ l Quick ligase, dH₂O up to 11 μ l, incubation at RT for 10 min). Subsequently, the ligated sgRNAs were treated with Plasmid Safe exonuclease to prevent unwanted recombination products (1.5 μ l 10x Plasmid Safe buffer, 1.5 μ l 10 mM ATP, 1 μ l Plasmid Safe exonuclease, incubation at 37°C for 30 min). Finally, the constructs were introduced into competent DH5 α *Escherichia coli* for amplification of the plasmid (50 μ l DH5 α , 7.5 μ l sample, incubation on ice for 30 min, heat shock induced in the waterbath at 42°C for 45 sec, bacteria immediately kept on ice for 2 min). After transformation, 500 μ l 2-YT bacterial growth medium were added, and the cells were incubated at 37°C on a shaker for 1 h. Then, the tube was centrifuged at 13,000 rpm for 10 sec and the supernatant was removed keeping approximately 50 μ l. Finally, the pellet was resuspended, plated on an agar plate containing ampicillin and evenly distributed using small sterile glass beads.

The next day, five bacterial clones were selected. Therefore, 3 ml 2-YT medium were transferred to each of five 14 ml Falcons, and 3 μ l ampicillin were added to each. One colony

was transferred to each tube and incubated at 37°C on the shaker for 14 h. The next day, plasmids were purified from the bacterial cultures using EZ-10 spin column plasmid DNA miniprep kit, following the protocol for purification of plasmid DNA, and concentrations were measured with NanoDrop. Agarose gel electrophoresis was used to confirm successful purification by comparing the purified plasmids with the 'empty' px458 vector (70 ml 1% agarose in 1x TAE buffer with 5.6 µl dye, 1 µl sample [approximately 500 ng] and 5 µl 6x loading dye per sample, 8 µl 1x Gene Ruler Mix, run for 30 min at 150V). As all samples showed approximately the same size, indicating that all contained the same inserted sequence, the three highest concentrated samples were diluted in dH₂O to 150 ng/µl in 15 µl total volume, and sent for sequencing together with 5 µl 5 µM pLKO1 primer per sample.

2.2.3 Plasmid purification

Table 5: Materials and reagents used for purification of plasmids. Company names and order numbers/models are provided for materials and reagents used for purification of plasmids.

Material/Reagent	Company	Order number/Model
2-YT bacterial broth	Teknova	Y0210
Ampicillin sodium salt	Sigma-Aldrich	A0166-25G
Platform shaker	New Brunswick Scientific	Innova 2300
Centrifuges	Beckman Coulter	Microfuge 20
	Thermo Scientific	Heraeus Megafuge 8R
	Kendro	Legend RT
EZ-10 Spin column plasmid DNA mini-prep kit	Bio Basic Canada	BS614-250
E.Z.N.A. endo-free plasmid DNA maxi kit	Omega Bio-Tek	D6926-03
Sodium hydroxide (NaOH)	Sigma-Aldrich	795429-500G
Koptec pure ethanol (EtOH)	VWR	89125-188
Sodium acetate (NaOAc)	Sigma-Aldrich	58625-500G
Heating blocks	Denville Scientific	IncuBlock Plus
NanoDrop	NanoDrop Technologies	ND-1000
		Spectrophotometer

Through evaluation of the sequencing results, the clones harboring the correctly assembled plasmids were identified. For each mutation, one clone was selected and expanded in 150 ml 2-YT medium containing 150 µl ampicillin, in an autoclaved 500 ml Erlenmeyer flask at 37°C for 14 h on the shaker. 50 ml from each flask were transferred to a 50 ml Falcon, and centrifuged at 3,500 rpm for 30 min at RT. The supernatant was discarded, and 50 ml from each flask were transferred to the same Falcon, and centrifuged again. This step was performed a third time to eventually collect all bacteria, and the accumulated pellets were stored in the Falcons at -80°C until purification.

Initially, purification was performed using EZ-10 spin column plasmid DNA miniprep kit, following the protocol for purification of plasmid DNA. Later on, E.Z.N.A. endo-free plasmid DNA maxi kit was used, including the optional column equilibration step using 3 M sodium hydroxide (NaOH). The last steps of this protocol were adapted with time, due to low yields

in the first two purification attempts. Therefore, 750 μ l elution buffer (EB) were applied instead of 1.5 ml, distributed evenly across the filter surface, and incubated for 10 min instead of 5 min. After centrifugation, the filtrate was added to the column again, incubated for 10 min, centrifuged, and transferred to an Eppendorf tube. In addition, fresh 750 μ l EB were applied to the same column, incubated for 10 min, centrifuged, and collected additionally. Finally, concentration was measured with NanoDrop.

Because high concentrations of at least 1 μ g/ μ l could not be achieved, as required by the protocol for NEPA21 electroporation, ethanol (EtOH) precipitation was performed additionally. Therefore, the protocol included in the E.Z.N.A. kit was again adapted to achieve better results. The purified fractions were transferred to 15 ml Falcons, and 0.1 volumes 3 M sodium acetate (NaOAc) pH 5.2, as well as 3 volumes ice cold 100% EtOH were added. This mixture was shaken gently, until a small string of DNA was visible. To fully precipitate the DNA, the Falcons were kept at -80°C for 2-3 days. Then they were centrifuged at full speed (4,150 rpm in the Kendro centrifuge) for 30 min at 4°C, the pellet was washed twice with 0.5 ml ice cold 75% EtOH without disturbing the pellet, and centrifuged at 4°C for 10 min each time. EtOH was removed, the tubes were centrifuged (10 sec at top speed) and trace amounts of EtOH were removed. The pellet was then air-dried for max. 5-10 min, and EB was added according to the theoretical amount of DNA, in order to obtain a concentration of at least 1 μ g/ μ l, but min. 100 μ l to enable complete dissolving of the pellet. The samples were kept in a heating block at 37°C for 5-10 min, and then resuspended by pipetting. Finally, concentrations were measured with NanoDrop, and samples were stored at -20°C.

2.3 Transfection methods

A variety of available gene delivery methods was considered in this project. In general, transfection methods can be subdivided into three main groups: biological, i.e. virus-mediated, chemical, using e.g. cationic lipids, and physical, such as electroporation or direct injection. Viral transfection, also termed transduction, is easy to use and highly efficient. However, the size of DNA that can be packaged into a virus is limited [117]. Furthermore, this procedure requires some additional effort, such as transfection of cells for viral propagation, and titration of phages. Also, handling of viruses naturally implies a certain risk, and therefore requires compliance with specific biosafety regulations [105]. By contrast, chemical transfection methods have no package size limitation, and a variety of products are available that are also highly efficient and easy to use. However, certain cell types are difficult to transfect chemically, and some even show toxic reactions. On the contrary, physical transfections show less variability regarding cell types, are relatively simple and do not rely on a vector system [117]. For instance, electroporation is a convenient method, which is time-saving, has shown good efficiencies, and does not pose any risk to the researcher [105]. The major disadvantage of physical methods is the requirement for special devices, which usually involve high costs and require certain experimenter skills [117]. In this project,

liposomal transfection with Lipofectamine 3000 was first evaluated, but resulted in a very low efficiency. Therefore, two different electroporation devices were tested in the next step, Amaxa and NEPA21. Due to superior efficiency, NEPA21 was used for subsequent experiments. In addition, different buffers were assessed, BTXpress and Opti-MEM, as well as supplementation of the cell culture medium with dimethyl sulfoxide (DMSO) 24 h before and after electroporation, according to a report claiming that the addition of DMSO improves transfection efficiency [105]. Furthermore, different parameters were tested, including diverse voltages and pulse lengths as well as cell numbers per sample. Moreover, transfection with different plasmids, in terms of size and production methods, was evaluated.

2.3.1 Electroporation

Table 6: Materials and reagents used for electroporation. Company names and order numbers/models are provided for materials and reagents used for electroporation.

Material/Reagent	Company	Order number/Model
NEPA21 Electro-Kinetic Transfection System	Bulldog Bio	Super Electroporator NEPA21 type II
2 mm electroporation cuvettes for Nepa	Bulldog Bio	12358-346
Nepa Gene's plasmid DNA pCAG-EGFP	Nepa Gene	CAG-IL 1310-016
Amaxa electroporator	Lonza	Amaxa 4D-Nucleofector
2 mm electroporation cuvettes for Amaxa	Lonza	P3 Primary cell 4D-Nucleofector X kit L
Lonza pmax GFP vector	Lonza	P3 Primary cell solution box PBP3-00675
Nucleofector P3 solution		
Nucleofector supplement		
C29-52 ITPKA plasmid	-	-
SAGM plus	-	-
Dimethyl sulfoxide (DMSO)	Sigma-Aldrich	D8418-500ML
1x Phosphate buffered saline (PBS)	Sigma-Aldrich	D8537-500ML
1x Trypsin/EDTA 0.25% (T/E)	Gibco (Life Technologies)	25200-072
10 cm Petri dishes	Denville Scientific	T1110
Multiwell plates <ul style="list-style-type: none"> • 12-well-plates • 6-well-plates 	Denville Scientific Denville Scientific	T1012 T1006
Centrifuge	Thermo Scientific	Heracus Megafuge 8R
Ward's Economy Improved Neubauer Hemocytometer	VWR	470019-796
Trypan blue	Sigma Life Science	T8154-100ML
Light microscope	VWR	89404-462
Opti-MEM reduced serum medium	Gibco (Life Technologies)	31985-062
BTXpress solution	VWR	89130-538
Transfer pipets	VWR	14670-327
Fluorescence microscope	Carl Zeiss	Axiovert 200 Camera: AxioCam MRm
Paraformaldehyde (PFA)	Santa Cruz Biotechnology	sc-281692
4',6-Diamidino-2-phenylindole, dilactate (DAPI) staining solution	Invitrogen	D3571

Initially, two different electroporation devices were tested, Amaxa 4D-Nucleofector and NEPA21. Transfection with Amaxa was performed according to the protocol for normal human bronchial epithelial cells from Lonza. For NEPA21, the protocol provided by Nepa Gene Co. for transfection of cell suspensions using cuvettes, version 6, was followed. Due to superior efficiency, NEPA21 was used for subsequent transfections.

Before each trial, the appropriate number of multiwells had to be prepared for subsequent plating of transfected cells. Therefore, 804G-coated wells were washed once with PBS, SAGM plus was added to each well and the plates were pre-incubated at 37°C. Then, cells grown to a confluency of about 80-90% were harvested by trypsinization with 0.25% trypsin/EDTA (T/E). The reaction was neutralized with SAGM plus medium and cells were centrifuged at 400 g for 4 min at 4°C. Then the cell pellet was resuspended in Opti-MEM buffer to determine cell density in a hemocytometer. Next, one or two washing steps were performed to remove any medium and serum, which may severely reduce transfection efficiency and cell viability. Therefore, each time the pellet was resuspended in 5 ml Opti-MEM buffer and cells were centrifuged under the same conditions as before. Finally, the cell pellet was resuspended in the appropriate amount of Opti-MEM buffer by thorough pipetting to achieve a single cell suspension without cell clumps. The final cell density per sample was 1×10^5 to 1×10^6 cells, mixed with 10 μ g DNA in 100 μ l total volume.

According to the experimental set-up, the respective electroporation parameters were set at the NEPA21 device. Each sample was transferred separately to a cuvette, whereby one sample was processed at a time. To ensure that the sample covered the bottom of the vessel, the cuvette was gently tapped at the bottom. Then the vessel was placed in the cuvette chamber. Impedance was measured by pressing the Ω button to verify a value of 30-55 Ohms. Next, the start button was pressed to execute the electroporation. Subsequently, the cuvette was immediately taken out of the chamber and 400-900 μ l SAGM plus were added to the sample. Finally, the solution was mixed thoroughly using a transfer pipet to break up white clumps, and the sample was rapidly transferred to the prepared well and incubated at 37°C o/n.

The next day, the medium was replaced by fresh SAGM plus in order to remove dead cells. Cells were closely monitored for emerging fluorescence within 24-72 h after transfection. Depending on the signal intensity, cells were fixed 1-6 d after electroporation in 4% paraformaldehyde (PFA). Therefore, the medium was removed, cells were washed once with PBS and incubated in PFA for 15 min at RT. Then, the PFA was discarded, cells were washed twice with PBS, and stained with 100 ng/ml DAPI in PBS for 5 min. Thereafter, DAPI solution was removed and PBS was added to prevent cells from drying out. The samples were stored at 4°C covered with aluminum foil to prevent bleaching. Finally, transfection efficiency was determined by calculating the ratio of successfully transfected, hence GFP⁺ cells, in relation to DAPI-stained nuclei. In addition, viability was measured in some

experiments by comparing the number of DAPI-stained cells that had remained attached to the wells until fixation, and were therefore assumed living cells, to the number of DAPI-stained cells in the negative control, which had not been electroporated, and was therefore set to 100% viability.

2.4 Screening for positive clones

Many methods are available to evaluate transfected cells for successful introduction of genetic modifications. In this study, it was attempted to perform allele-specific polymerase chain reaction (PCR) to identify clones harboring correctly targeted alleles. This PCR method involves designing one of the primers so that it binds directly to the mutated sequence. Hence, a PCR product would only be obtained if the mutation was introduced correctly. FwAl and RevA primers were designed for this first PCR run, whereby FwAl primer was complementary to the mutated sequence at the specific *EGFR* locus. Subsequently, a second PCR run was planned to amplify this specific gene locus from genomic DNA (gDNA) of expanded positive colonies. Therefore, FwA primer was designed to be used together with RevA primer. Finally, these samples would have been sent to the Duke sequencing co-facility (together with the FwS primer required for sequencing itself) to confirm the correct insertion of the mutation in each positive clone. The set-up of the designed PCR analyses is depicted in Figure 11. However, due to very low transfection efficiencies obtained, and obstacles in culturing BCs at low densities, which would be a prerequisite in order to select distinct colonies that developed from single cells, this part of the project could not be executed.

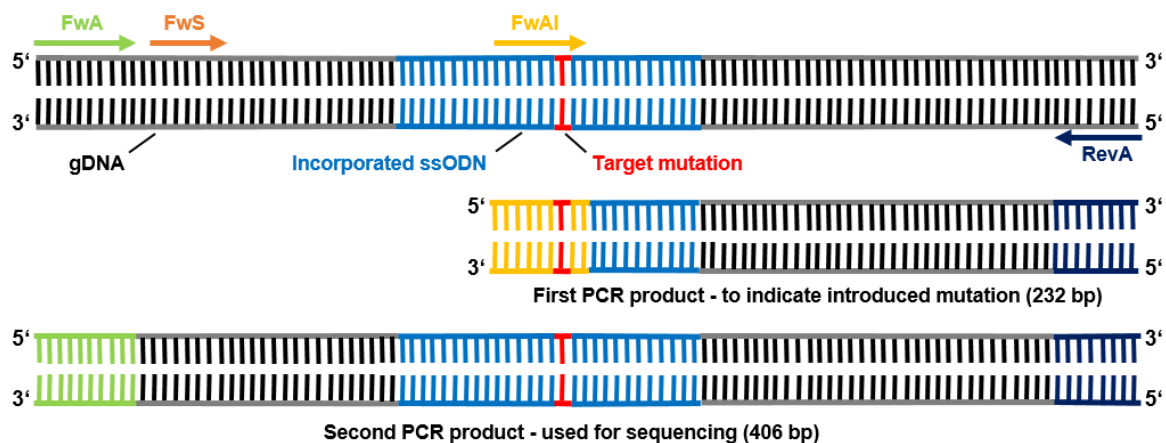


Figure 11: Design of primers for two subsequent PCR analyses. FwAl and RevA primers were designed for the first (allele-specific) PCR run, in order to indicate whether the mutation was successfully introduced at the specific *EGFR* locus. Subsequently, FwA and RevA primers were to be used during the second PCR run, to amplify this specific gene locus from gDNA of positive clones, and samples would have been sent to the Duke sequencing co-facility (together with the FwS primer required for sequencing). Expected product lengths are indicated for T790M mutation.

2.4.1 Single cell culture

Table 7: Materials and reagents used for single cell culture. Company names and order numbers/models are provided for materials and reagents used for single cell culture.

Material/Reagent	Company	Order number/Model
CO ₂ Incubator	Thermo Fisher Scientific	HERAcell VIOS 160i
Laminar flow hood	Labconco	Purifier Class II Biosafety Cabinet
Waterbath	Intertek	WB10
1x Phosphate buffered saline (PBS)	Sigma-Aldrich	D8537-500ML
1x Trypsin/EDTA 0.25% (T/E)	Gibco (Life Technologies)	25200-072
1x DMEM	Corning	10-013-CV
Fetal bovine serum (FBS)	Gibco (Life Technologies)	16141-079
Sterile syringe filters, 0.22 µm	Olympus plastics	25-244
Centrifuge	Thermo Scientific	Heraeus Megafuge 8R
Ward's Economy Improved Neubauer Hemocytometer	VWR	470019-796
Trypan blue	Sigma Life Science	T8154-100ML
SAGM plus	-	-
10 cm Petri dishes	Denville Scientific	T1110
24-well-plates	Denville Scientific	T1024
24-well 0.4 µm transwell inserts	Corning	353095
Light microscope	VWR	89404-462
Fluorescence microscope (used for imaging)	Carl Zeiss	Axiovert 200 Camera: AxioCam MRm

A prerequisite for screening for positive clones was to grow cells at very low densities, or as single cells, in order to enable selection of descendants of a single cell harboring a specific mutation. Therefore, several methods have been tested, including seeding cells in Petri dishes at low densities, culturing them in 96-wells as single cells, including supplementing the media with supernatants of other BCs or MRC5 cells, and culturing single BCs on transwell membranes, with other BCs seeded on the bottom of the well, or directly on the lower side of the membrane.

Specifically, cells were initially grown at densities of 1×10^4 , 2×10^4 and 3×10^4 cells per Petri dish, or as single cells in 96-wells. Due to high mortality rates, single cells were finally placed on transwells with 5,000 BCs grown on the bottom of each well coated with 804G, or 5,000 BCs grown on the lower side of the membrane. This was achieved by first inverting the transwell inserts, coating them with 804G for at least 5 h, discarding the coating medium, and seeding 5,000 BCs on each inverted insert. After incubation for 30 min at 37°C, in order to let the cells attach to the membrane, the inserts were placed in a 24-well-plate and a single BC was seeded on top. The growth behavior of the single cells was closely monitored for up to 24 days in order to determine cell survival rates.

2.5 Culturing organoids

Table 8: Materials and reagents used for organoid culture. Company names and order numbers/models are provided for materials and reagents used in organoid culture.

Material/Reagent	Company	Order number/Model
CO ₂ Incubator	Thermo Fisher Scientific	HERAcell VIOS 160i
Laminar flow hood	Labconco	Purifier Class II Biosafety Cabinet
Waterbath	Intertek	WB10
1x Phosphate buffered saline (PBS)	Sigma-Aldrich	D8537-500ML
1x Trypsin/EDTA 0.25% (T/E)	Gibco (Life Technologies)	25200-072
1x DMEM	Corning	10-013-CV
Fetal bovine serum (FBS)	Gibco (Life Technologies)	16141-079
Sterile syringe filters, 0.22 µm	Olympus plastics	25-244
Centrifuge	Thermo Scientific	Heraeus Megafuge 8R
Ward's Economy Improved Neubauer Hemocytometer	VWR	470019-796
Trypan blue	Sigma Life Science	T8154-100ML
Matrigel	Corning	354230
SAGM plus	-	-
MTEC basic	-	-
MTEC plus	-	-
1x DMEM-F12	Thermo Fisher Scientific	11330-032
ROCK inhibitor Y27632	Selleck Chemicals	S1049
Pen/strep	Gibco (Life Technologies)	15070-063
Multiwell plates <ul style="list-style-type: none"> • 24-well-plates • 6-well-plates 	Denville Scientific Denville Scientific	T1024 T1006
24-well 0.4 µm transwell inserts	Corning	353095
Fluorescence microscope	Carl Zeiss	Axiovert 200 Camera: AxioCam MRm
Imaging software	National Institutes of Health	Fiji Win64 version

The first step was to produce healthy murine lung organoids from airway BCs. Therefore, BCs were mixed with murine MLGs in matrigel, and organoids were established in 6-wells as well as in transwell inserts. In addition, murine trachea epithelia were dissociated and the obtained cell mixture, consisting mainly of BCs, was used to set up healthy organoids without the addition of fibroblasts. Moreover, fluorescence-activated cell sorting (FACS) was used to collect SFTPC⁺ murine lung cells, presumably mainly AEC2s, which were then mixed with human MRC5 fibroblasts to set up organoid cultures, in droplets as well as on transwells. Furthermore, lung lobes were isolated from a LSL-*KRAS*^{G12D} mouse, dissociated, and half of the cells was activated with adeno-cre-GFP virus, in order to activate *KRAS*^{G12D} mutation. Organoids were established from both, *KRAS*-mutated cell mixtures, as well as healthy (not cre-activated) cells. Finally, healthy human lung tissue (obtained from a cadaver lung) was dissociated and enriched for BCs. These BCs were then either grown in healthy control

organoids, or subjected to CRISPR/Cas9-based genome editing via electroporation, in order to introduce specific *EGFR* mutations (T790M, L858R, or Δ E746-A750) for lung tumor organoid culture. In addition, the human lung adenocarcinoma cell line NCI-H23 was used to set up *KRAS*^{G12D} *p53*^{L246M} cancer organoids.

In co-cultures, generally 6,000 lung stem cells were mixed with 50,000 fibroblasts in 20 μ l total volume, and then quickly, but thoroughly mixed with 20 μ l refrigerated matrigel to generate one droplet of 40 μ l total volume. Three droplets were usually placed in a 6-well per experiment. In transwells, 90 μ l total volume were applied, keeping the same cell numbers and a 1:1 ratio of cell suspension to matrigel. For organoids established from cultures without fibroblasts, 50,000 cells were used in total. The organoids generated from murine trachea epithelial cells were cultured in full SAGM plus medium, initially including pen/strep to avoid contamination. All other organoids were grown in MTEC basic or MTEC plus medium, in order to provide the required nutrients and growth factors for all cell types applied. Initially, MTEC media were supplemented with ROCK inhibitor at a concentration of 10 μ M, from day 3 on, concentration was reduced to 3.3 μ M. An overview of all the different organoids established, as well as the culture media used, is given in Table 9.

Table 9: Overview of cultured organoids. Several types of organoids were established in different culture media, both, from murine and human cells, cell mixtures or specific cell types co-cultured with fibroblasts.

Organoid-forming cell type	Co-culture cells	Culture medium
Murine BCs	MLg murine fibroblasts	MTEC basic, ROCK inhibitor
Murine trachea epithelial cells (mainly BCs)	-	SAGM plus, initially pen/strep
SFTPC ⁺ murine lung cells (mainly AEC2s)	MRC5 human fibroblasts	MTEC plus, ROCK inhibitor
Murine lung lobe cell mixtures (mainly AEC2s)	-	MTEC plus, ROCK inhibitor
<i>KRAS</i> ^{G12D} -mutant murine lung lobe cell mixtures (mainly AEC2s)	-	MTEC plus, ROCK inhibitor
Healthy human lung BCs	MRC5 human fibroblasts	MTEC plus, ROCK inhibitor
<i>EGFR</i> -mutant (T790M, L858R, or Δ E746-A750) human lung BCs	MRC5 human fibroblasts	MTEC plus, ROCK inhibitor
Human lung adenocarcinoma cell line NCI-H23 (<i>KRAS</i> ^{G12D} , <i>p53</i> ^{L246M})	-	MTEC plus, ROCK inhibitor

As the cells expanded, they self-assembled and developed into 3-dimensional organoids. Depending on the respective cell type, organoids of various sizes and morphologies formed, as observed at different time points. By monitoring growth kinetics as well as staining for distinct histological markers, the characteristics of human and murine, healthy primary cells and mutated/tumor cells could be compared.

2.5.1 Comparative studies

It was initially planned to transfect hBCs with each of the plasmids created, to identify clones harboring the correct mutations, and to select and expand those to model tumorigenesis. However, since electroporation of hBCs showed a very limited success rate, this part of the project could not be carried out. However, the different types of organoids generated from both, human and murine cells, were investigated on a histological basis. Therefore, the harvested organoids were fixed, embedded in O.C.P. compound, cryosectioned and stained for cell type-specific immunofluorescent markers. Visualization was achieved using confocal fluorescence microscopy. In addition, organoid growth was measured for two weeks at several time points in order to map differential growth kinetics. Finally, the obtained results were directly compared to evaluate similarities and differences between human and murine, healthy and tumorigenic organoids.

2.5.1.1 Cryosectioning

Table 10: Materials and reagents used for preparing cryosections. Company names and order numbers/models are provided for materials and reagents used for cryosectioning.

Material/Reagent	Company	Order number/Model
Waterbath	Thermo Scientific	Precision GP 15D
Histogel	Thermo Fisher Scientific	R904012
Cryomolds <ul style="list-style-type: none"> • 15 x 15 x 5 mm • 25 x 20 x 5 mm 	Sakura TissueTek Sakura TissueTek	REF 4566 REF 4557
Flat blade cell lifter	Celltreat Scientific Products	229305
Paraformaldehyde (PFA)	Santa Cruz Biotechnology	sc-281692
5 ml tubes	Bio Basic Canada	BT693-SN
Fume hood	Fisher Hamilton	373A 107650
Rotating stands	Denville Scientific	R4040
	Denville Scientific	R4045
10x Phosphate buffered saline (PBS)	Bio Basic Canada	PD8117
Sucrose	Sigma Life Science	S0389-5KG
Vacuum filtration system	Millipore Sigma	SCGPU05RE
O.C.T. compound	Fisher HealthCare	4585
Superfrost Plus microscope slides	Fisher Scientific	12-550-15
Cryostat device	Leica Biosystems	CM3050S

In order to embed the organoids, histogel was first dissolved in the waterbath at 66°C for approximately 30 min. Then the medium was removed from the wells containing organoid droplets, and the droplets were detached with a cell scraper. In case of organoids grown on transwells, the matrigel was first detached from the edge of the transwell using a P200 tip, and the membrane was slit on the edge with thin forceps. Then the matrigel was scraped off gently using flat forceps. Next, 300 µl histogel were transferred to a medium-size cryomold, and after approximately 1-2 min of solidification, the organoids were transferred to the middle

of the cryomold using a P1000. Then 700 µl histogel were added at the edges of the cryomold, to avoid spreading of the organoids all over the surface. The mold was then kept on ice until the histogel was fully solid. The sample was removed from the mold and as much gel as possible was cut off from the edges. Then it was transferred to a 5 ml Falcon with approximately 2.5 ml 4% PFA, and fixed at RT for 2 h on a rotating stand. Thereafter, it was washed 3x with 1x PBS, transferred to 30% sucrose in PBS, and kept for at least 2 h at 4°C on a rotating stand. Then, half of the sucrose was discarded, 1.5 ml O.C.T. were added and the sample was kept for another hour at 4°C on a rotating stand. Finally, O.C.T. was added to a large cryomold, the sucrose/O.C.T. solution was removed with a P1000 and the sample was gently dragged through the O.C.T. several times with flat tweezers to remove the sucrose. Then, O.C.T. was added to a medium-size mold, and the sample was transferred to this mold, moved to one side and pushed down to the bottom, to make sure the organoids were in one plane for sectioning. The mold was transferred to a metal plate resting evenly on dry ice. After complete polymerization, the mold was labeled and stored at -80°C.

For cryosectioning, stored samples were first let to acclimatize at -20°C for approximately 30 min. Then, a drop of O.C.T. was applied to a mount within the cryostat, the sample block was put on top, and the block was again let to acclimatize for about 15 min under a weight. Then the sample was mounted within the cryostat and 5-7 µm sections were cut at -23°C. The prepared slides were finally stored at -20°C until staining.

2.5.1.2 Staining of organoid cryosections

Table 11: Materials and reagents used for staining of cryosections. Company names and order numbers/models are provided for materials and reagents used for staining of cryosections.

Material/Reagent	Company	Order number/Model
10x Phosphate buffered saline (PBS)	Bio Basic Canada Inc.	PD8117
Waterbath	Thermo Scientific	Precision GP 15D
Pressure cooker	Aptum Biologics	2100 Antigen Retriever
10x Citrate buffer (CB)	Sigma Life Science	C9999-1000ML
Milli-Q type 1 ultrapure deionized water	Millipore	-
Primary antibodies and dilutions <ul style="list-style-type: none"> • KRT5-Rb, 1:500 • KRT8-Rt, 1:50 • acT-Ms, 1:1000 • SOX9-Gt, 1:500 • EpCAM-Rt, 1:50 • CK20-Rb, 1:300 • SFTPC-Rb, 1:500 • PDPN-Gp, 1:50 • ZO-1-Rt, 1:50 	Abcam DSHB Proteintech R&D DSHB Neobiolab Millipore DSHB DSHB	ab53121 Troma-1-s 66200-1-Ig AF3075 G8.8-s A0248 ab3786 8.1.1-s R26.4C-s
Secondary antibodies (1:500 dilutions) <ul style="list-style-type: none"> • Alexa Fluor Gt-anti-Rb IgG 488 • Alexa Fluor Gt-anti-Rt IgG 594 	Invitrogen Life technologies	A11008 A11007

<ul style="list-style-type: none"> • Alexa Fluor Gt-anti-Ms IgG 647 • Alexa Fluor Dk-anti-Gt IgG 488 • Alexa Fluor Dk-anti-Rt IgG 594 • Alexa Fluor Dk-anti-Rb IgG 647 • Alexa Fluor Gt-anti-Rb IgG 488 • Alexa Fluor Gt-anti-Gp IgG 594 • Alexa Fluor Gt-anti-Rt IgG 647 	<ul style="list-style-type: none"> Life technologies Life technologies Life technologies Life technologies Invitrogen Abcam Invitrogen 	<ul style="list-style-type: none"> A21235 A11055 A21209 A31573 A11008 ab150188 A21247
Triton	Sigma Life Science	X100-1L
Bovine serum albumin (BSA)	Sigma-Aldrich	A7906-500G
Fluoromount DAPI solution	Thermo Fisher Scientific	00-4959-52
Microscope cover glasses 24 x 60 mm	VWR	16004-312
Confocal microscope	Olympus	Fluoview FV3000

First, the slides were washed 3x with 1x PBS to wash off the O.C.T. compound. Then antigen retrieval was performed, depending on the requirements of the specific antibodies used. In particular, the slides stained for SFTPC, PDPN and ZO-1 were kept for 9 min in 1x citrate buffer (CB; diluted in Milli-Q water) at 95°C in the waterbath, after preheating the CB to 95°C for 10 min. For all other antibodies, antigen retrieval was performed for 20 min in 1x CB at 121°C in a pressure cooker. Thereafter, the slide box containing the slides and CB was let cool down to RT for 1 h before removing the slides from the box. Meanwhile, primary antibody solutions were prepared in PBS containing 1% bovine serum albumin (BSA) and 0.1% Triton 100 (1% BSA/PBST). 100 µl solution were prepared per slide (each slide containing 3-5 sections), in varying dilutions depending on antibody strength (see Table 11). Next, the 1x CB was discarded and the slides were labelled with cell type(s), days in culture, and antibodies used. Slides were laid on a tip box containing water to prevent drying out during the staining procedure. Then, slides were washed carefully 3x with 1x PBS using a P1000. A circle was drawn around the samples with super pap pen (a liquid-repellent slide marker pen for staining procedures) to confine the solutions. Then, the samples were washed 1x with PBST for 5 min, and 1x with 1% BSA/PBST for 5 min. 100 µl primary antibody solution were applied per slide, and incubated at RT for 1.5 h within the tip box filled with water underneath. Meanwhile, secondary antibodies were diluted in PBST. Again 100 µl were prepared per slide, each antibody diluted 1:500. After incubation with primary antibodies, slides were washed 3x with PBST for 5 min each, secondary antibodies were added and incubated at RT for 45 min. Then, slides were washed again 3x with PBST for 5 min each. Finally, samples were fixed with Fluoromount DAPI solution, and a cover glass was added gently. Slides were dried at RT in the dark o/n in a tip box without water, and stored at 4°C as of the next day, until imaging via confocal microscopy.

3 Results

3.1 Electroporation

Initially, primary murine BCs (mBCs) were used to optimize electroporation settings. Various electroporation parameter sets were tested with the NEPA21 transfection system, as suggested by the supplier. Apart from the voltage and poring pulse length, all parameters were kept constant, as visible in Table 12. In the first trial, one million mBCs (*SFTPC*-SIG – tam; p12) were transfected with 10 µg Nepa Gene's plasmid at each condition. Whereby, *SFTPC*-*SOX2*-IRES-GFP (SIG) –tam means that the mice had been genetically modified to enable tamoxifen-induced expression of *SOX2*-GFP under *SFTPC* promoter, but tamoxifen was not administered. Therefore, these cells were considered as physiologically normal mBCs. Before electroporation, cells were washed once with Opti-MEM. Directly after electroporation, each sample was mixed with 400 µl SAGM plus. 5 days later, cells were fixed, stained with DAPI and analyzed by fluorescence microscopy.

Table 12: Parameter sets tested with NEPA21 transfection system. 10 different parameter sets were used, with voltages ranging from 110 to 275 V, and poring pulse lengths of 1, 2.5 or 5 ms. All other parameters were kept constant, as suggested by the supplier.

#	Set Parameters											
	Poring Pulse						Transfer Pulse					
	V	Length [ms]	Interval [ms]	No.	D. Rate [%]	Polarity	V	Length [ms]	Interval [ms]	No.	D. Rate [%]	Polarity
1	110	5	50	2	10	+	20	50	50	5	40	+/-
2	125	2.5	50	2	10	+	20	50	50	5	40	+/-
3	125	5	50	2	10	+	20	50	50	5	40	+/-
4	150	5	50	2	10	+	20	50	50	5	40	+/-
5	175	5	50	2	10	+	20	50	50	5	40	+/-
6	200	5	50	2	10	+	20	50	50	5	40	+/-
7	225	2.5	50	2	10	+	20	50	50	5	40	+/-
8	250	2.5	50	2	10	+	20	50	50	5	40	+/-
9	275	1	50	2	10	+	20	50	50	5	40	+/-
10	275	2.5	50	2	10	+	20	50	50	5	40	+/-

The results clearly showed the highest transfection efficiencies at voltages between 150 and 250 V. In particular, the best values were achieved at 175-250 V, whereas the least favorable transfection rates were obtained at 110, 125 and 275 V (see Figure 12 and Figure 13). Moreover, comparison between samples that were electroporated at two different poring pulse lengths, but at the same voltage, showed a moderately better efficiency with the longer poring pulse.

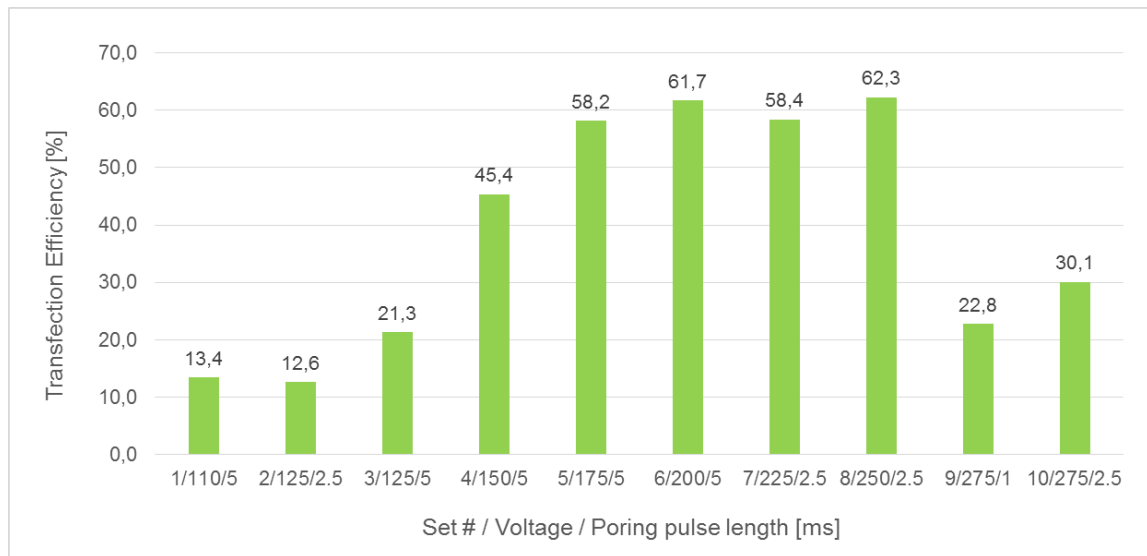


Figure 12: Testing 10 different parameter sets with the NEPA21 transfection system. Initially, 10 different parameter sets were evaluated, ranging from 110-275 V, and poring pulses between 1 and 5 ms. The highest transfection efficiencies were obtained at 175-250 V, the lowest at 110, 125 and 275 V. Longer poring pulses showed slightly higher transfection rates.

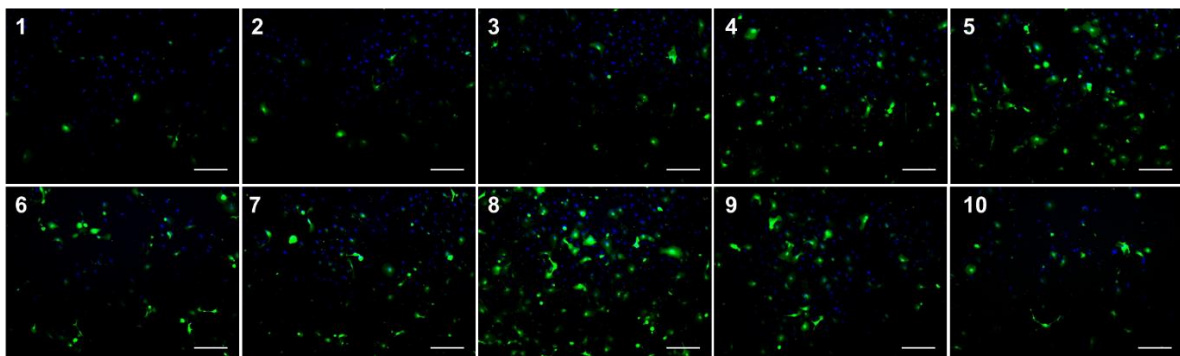


Figure 13: Fluorescence microscopy images of mBCs transfected at 10 different parameter sets tested with NEPA21. The highest numbers of GFP⁺ cells in relation to DAPI-stained nuclei were found in parameter sets 5-8. Numbers indicate the respective parameter sets; Scale bars: 200 μ m

In the next trial, the plasmid px458 was used for electroporation, without sgRNA insertion, at a concentration of 9.8 μ g per sample. Moreover, cells were transfected at two different concentrations, 1×10^6 and 5×10^5 cells, to evaluate differences in transfection efficiency when using lower cell numbers. Therefore, mBCs (*SFTPC-SIG* –tam, p12) were washed once in Opti-MEM, and then resuspended in the appropriate amount of Opti-MEM to achieve the correct cell concentrations. The five most promising parameter sets from the previous trial were applied, and one parameter set was applied twice, once with a new cuvette, and once with a cuvette that was already used before and cleaned with EtOH and PBS. This was to test whether re-using cuvettes would affect electroporation. The samples were evaluated already one day after transfection. In addition to transfection efficiency, also viability was determined, by comparing the number of DAPI-stained nuclei in the electroporated samples,

to the number of DAPI⁺ cells in the negative control, which had not been electroporated, and was therefore set to 100% viability.

As visible in Figure 14, transfection efficiency was overall relatively low, ranging from 1.8 to 9.7%. In general, samples with 5×10^5 cells resulted in better rates, except for parameter set 4, which overall showed the lowest values at both cell concentrations. The highest efficiencies were obtained at 175 V with the lower cell number. Unexpectedly, the samples in the re-used cuvettes achieved even higher success rates at both cell concentrations.

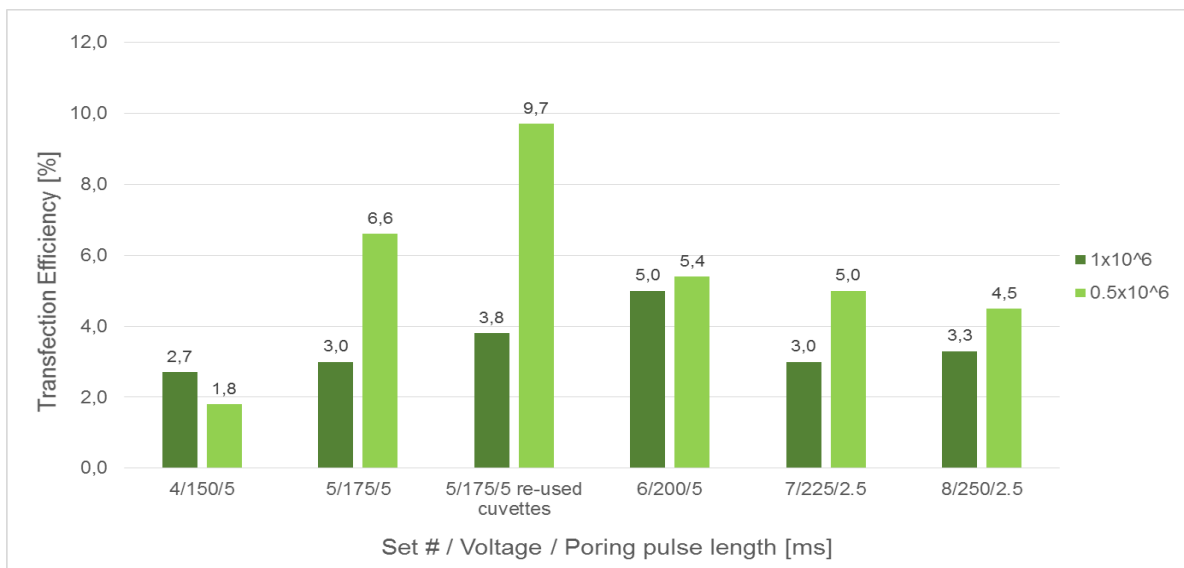


Figure 14: Transfection efficiency of electroporation with different cell numbers and re-used cuvettes. Samples with the lower cell number achieved higher success rates, except for parameter set 4, which overall showed the lowest values. The highest transfection rates were obtained with set 5, whereby samples in re-used cuvettes unexpectedly resulted in the highest values of all.

The determined cell viability values are depicted in Figure 15, which shows a large variability among samples at different voltages. The highest viability rates were obtained at 225 and 250 V, followed by 150 and 200 V. Interestingly, the least viable cells were found in the samples at parameter set 5, which had the highest transfection efficiencies. It seems that the different cell numbers per sample had no influence on viability. Only minor differences were found, and showed an inconsistent pattern, as viability was partly higher and partly lower with each of the cell numbers tested. Representative fluorescence microscopy images of mBCs transfected in this trial are shown in Figure 16.

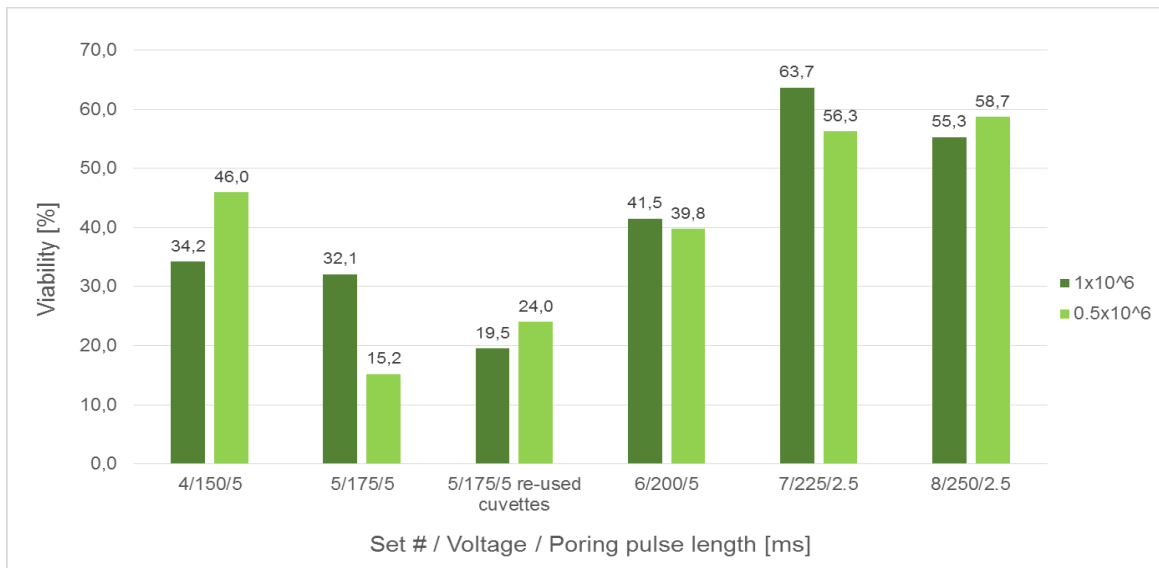


Figure 15: Viability of cells after transfection. A large variability was found among samples at different voltages. The highest viability rates were determined at 225 and 250 V, followed by 150 and 200 V. The least viable cells were found in the samples at parameter set 5. Different cell numbers had only a minor influence on viability, which was inconsistently changing among the different samples.

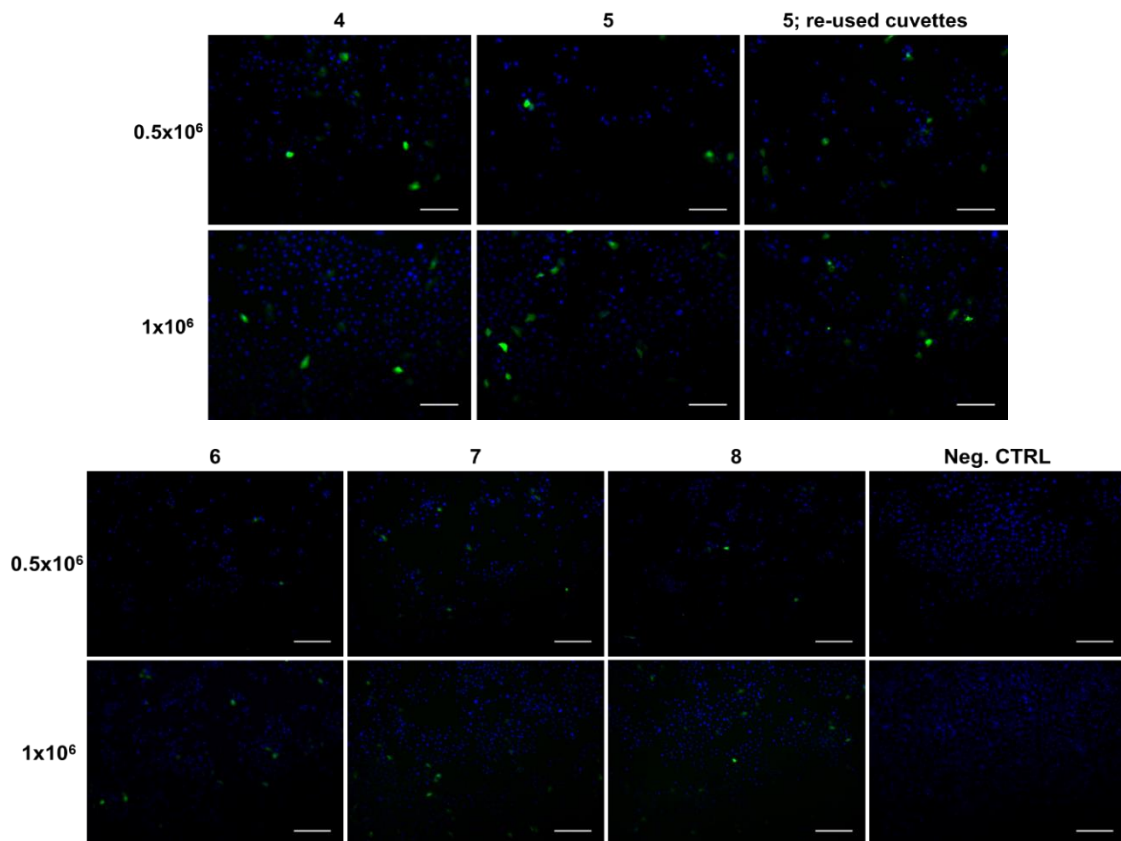


Figure 16: Fluorescence microscopy images of mBCs transfected at different cell numbers, and in re-used cuvettes. Lower cell numbers achieved higher transfection rates, except for parameter set 4, which had the lowest values. The highest numbers of GFP⁺ cells in relation to DAPI-stained nuclei were obtained with set 5, whereby samples in re-used cuvettes resulted in the highest values of all. The negative control was not electroporated, and was used as a reference to determine viability. Numbers indicate the respective parameter sets; Scale bars: 200 μm

Because transfection efficiency was very low in the previous trial, two washing steps in Opti-MEM were performed from this point onwards, in order to completely remove any serum from the medium, which possibly reduced transfection efficiency. Moreover, as depicted in Figure 14, lower cell numbers did not decrease transfection efficiency. Therefore, 0.5×10^6 mBCs (SOX2-CreER/SIG –tam, p8) were transfected with 9.8 μg px458, without sgRNA insertion, per sample. Hereby, SOX2-CreER/SIG –tam describes that mice had been genetically modified to enable tamoxifen-induced expression of SOX2-GFP, but tamoxifen was not administered. Therefore, also these cells were considered as physiologically normal mBCs. Due to low efficiencies with parameter set 4 in the previous trial, only sets 5-8 were used this time. In addition, electroporation was tested using the Amaxa 4D-Nucleofector. In this case, two different incubation strategies after electroporation were evaluated, one according to the aforementioned protocol, the other one according to Lonza's general protocol for nucleofection of adherent cell lines. While one sample was kept inside the cuvette for 10 min after transfection, the other sample was immediately mixed with 500 μl pre-warmed SAGM plus and transferred to an Eppendorf tube for this incubation period. Moreover, to test the influence of DMSO on transfection efficiency, cells for two samples transfected with NEPA21, and one sample transfected with Amaxa, were cultured 24 h before and after electroporation in SAGM plus supplemented with 1.25% or 0.625% DMSO, respectively. Three days after electroporation, cells were fixed, stained with DAPI and evaluated under the fluorescence microscope.

As visible in Figure 17 and Figure 18, transfection efficiencies were overall low again. The highest values were obtained with parameter sets 6 and 8 of NEPA21-transfected cells, while Amaxa electroporation resulted in substantially lower values. The addition of DMSO to the culture medium had a negative effect on NEPA21-transfected cells, but a positive effect on the cells transfected with Amaxa, whereby the higher concentration of DMSO increased the efficiency considerably. Comparison of the two different incubation strategies after Amaxa electroporation also showed no clear results. When comparing the samples cultured in SAGM plus only, the sample immediately transferred to SAGM plus after transfection achieved a slightly higher efficiency. However, the cells cultured in presence of DMSO and incubated within the cuvette showed even better results.



Figure 17: Transfection efficiency of mBCs electroporated with NEPA21 or Amaxa 4D-Nucleofector. Transfection efficiencies were overall relatively low, but slightly higher with NEPA21, whereby the best results were obtained with parameter sets 6 and 8. DMSO had a negative effect on NEPA21-transfected cells, but a positive effect on Amaxa-transfected cells. Comparison of the different incubation strategies after Amaxa electroporation did not show a clear trend.

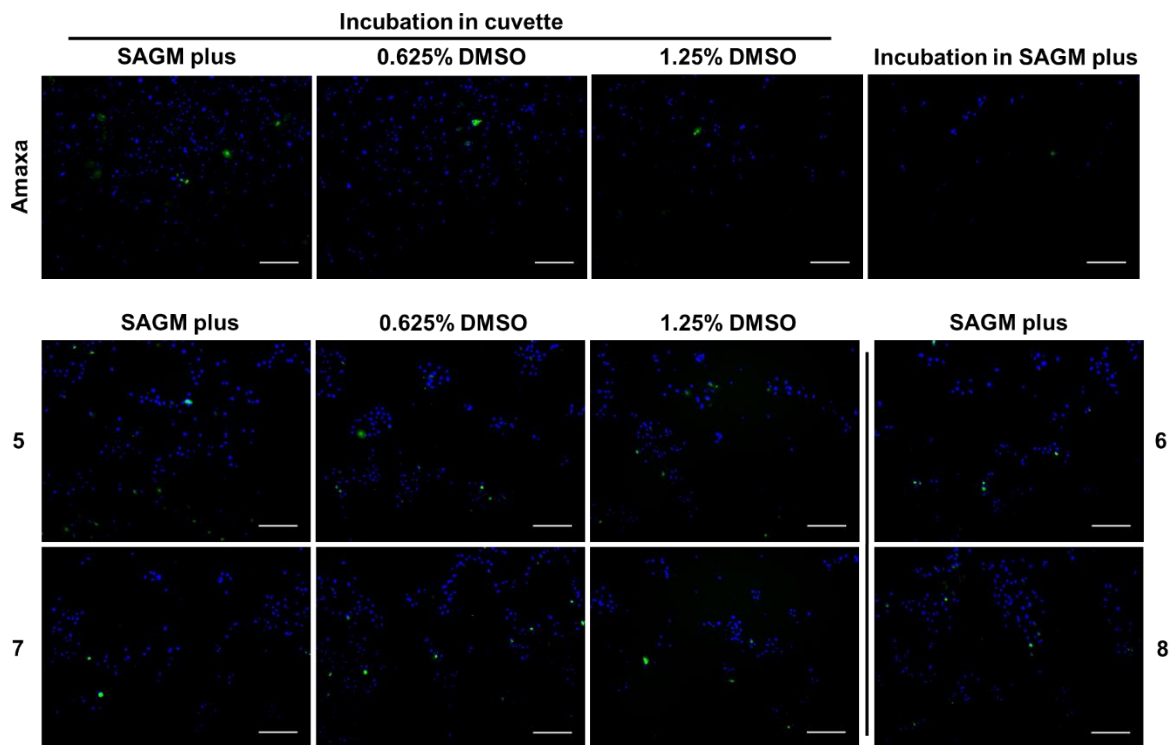


Figure 18: Fluorescence microscopy images of mBCs electroporated with NEPA21 or Amaxa 4D-Nucleofector. Upper panel shows Amaxa-transfected samples, lower panels indicate NEPA21-electroporated cells, with numbers indicating the respective parameter sets. Transfection efficiencies were overall relatively low, but moderately higher with NEPA21. Addition of DMSO did not tremendously influence transfection efficiency. According to the images, incubation within the cuvette after Amaxa electroporation seems to be beneficial for cell viability. Scale bars: 200 μ m

Due to the generally low efficiencies obtained with px458 plasmid compared to Nepa Gene's plasmid, it was then evaluated whether the fact that px458 plasmid had not been purified with endotoxin-free solutions was responsible for this inferiority. Therefore, endotoxin-free C29-52 ITPKA mCherry plasmid was used as a reference for comparison with Nepa Gene's plasmid. Both plasmids were used either alone or combined, at a total concentration of 10 µg DNA per sample, together with 0.5×10^6 mBCs (SOX2-CreER/SIG –tam; p8). Again two washing steps in Opti-MEM were performed to ensure removal of serum. Electroporation was carried out using NEPA21, due to the better results compared to Amaxa in the previous trial. Only parameter set 6 was used, and cells were analyzed two days after transfection.

Both endotoxin-free plasmids were taken up at very high levels, as depicted in Figure 19. When cells were transfected with one plasmid only, both samples showed efficiencies of more than 70%. In contrast, the sample of cells electroporated in the presence of both plasmids resulted in a much lower value of 41.5%. However, 94.7% of the cells that were successfully transfected, had taken up both plasmids at the same time. This is also visible in Figure 20, indicating that multiple plasmids can be introduced simultaneously, which may be applied in the future to induce several mutations at the same time, or to insert a specific fluorescence reporter along with a mutation.

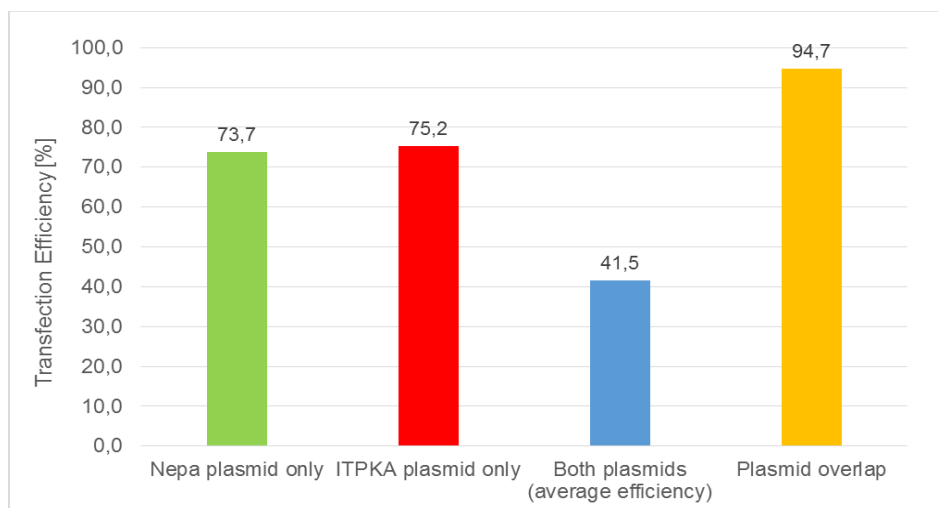


Figure 19: Transfection efficiencies of endotoxin-free plasmids. Both plasmids alone were taken up at very high rates of more than 70%. The cells electroporated in the presence of both plasmids showed only 41.5% efficiency, but 94.7% of these cells had taken up both plasmids at the same time.

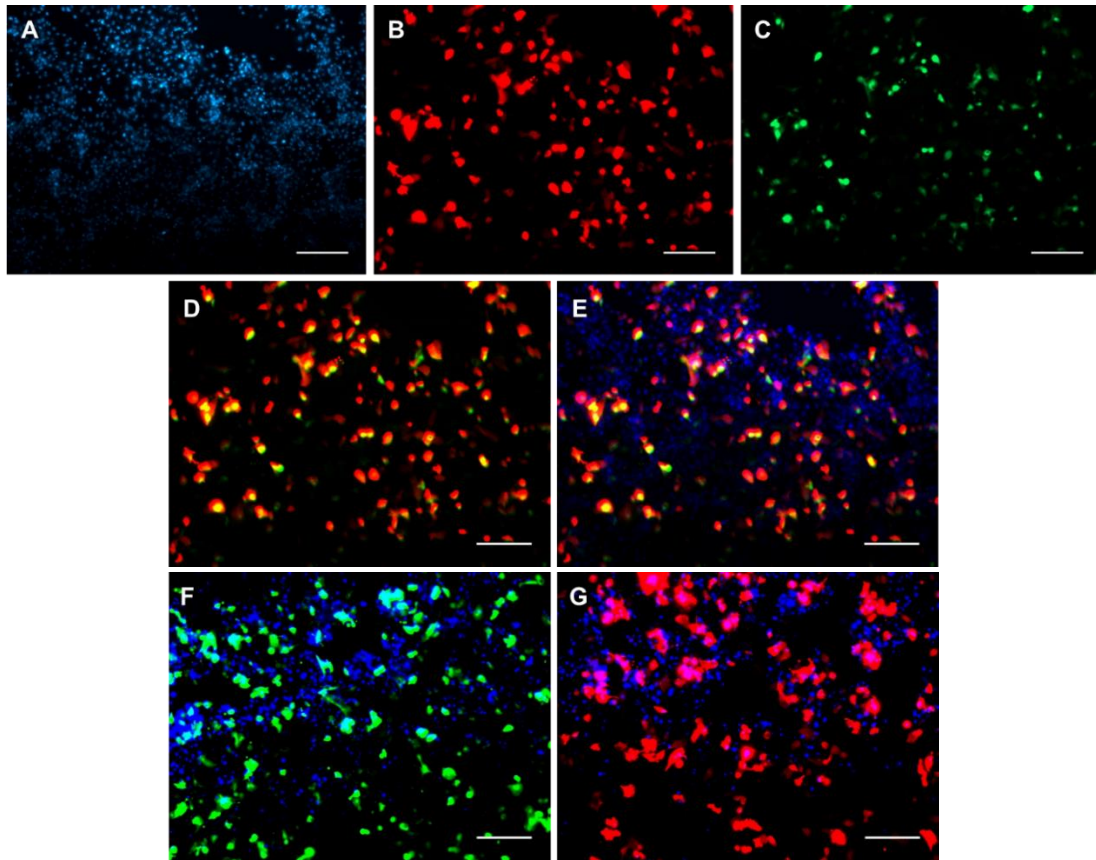


Figure 20: Fluorescence microscopy images of mBCs transfected with endotoxin-free plasmids. A-E) Images of the sample electroporated in presence of both plasmids; A) DAPI, B) mCherry, C) GFP, D) red and green channels merged, E) all channels merged; F) cells transfected with Nepa plasmid only, G) cells transfected with ITPKA mCherry plasmid only. Both plasmids alone were taken up at very high rates. The cells electroporated in the presence of both plasmids showed a lower efficiency, but most of these cells had taken up both plasmids at the same time. Scale bars: 200 μm

3.1.1 Electroporation of human BCs

Meanwhile, cloning and purification of px458 plasmids harboring sgRNA sequences, to target one of the three *hEGFR* mutation sites described previously (T790M, L858R, and $\Delta\text{E746-A750}$), had been completed. However, according to the results of the previous trial, indicating that endotoxin-free generation of plasmids is a prerequisite to achieve adequate electroporation results, purification of px458 plasmid was repeated with E.Z.N.A. endo-free plasmid DNA maxi kit. Simultaneously, primary hBCs could be obtained from Duke Hospital. After dissociation from the tissue and expansion for several passages in SAGM plus medium supplemented with pen/strep to remove contaminating bacteria, cells were ready for transfection. However, due to slow proliferation of hBCs, only low cell numbers could be harvested. Therefore, 0.5×10^6 and 0.1×10^6 hBCs (p7) were transfected with 10 μg endotoxin-free px458^{*hEGFR_T790M*} at parameter set 6 (200 V, 5 ms). In addition, a negative control was used to test the effect of the plasmid DNA on cell viability, with 0.5×10^6 hBCs, electroporated at the same parameters, but without plasmid. Because no fluorescence could be detected within the first days after transfection, cells were only analyzed six days later.

Unexpectedly, as visible in Figure 21, no successful transfection could be observed in either sample. Moreover, cell mortality rates were extremely high, even in the negative control, suggesting that these hBCs were highly sensitive to electroporation. Apparently, the plasmid itself had no additional negative influence on cell viability.

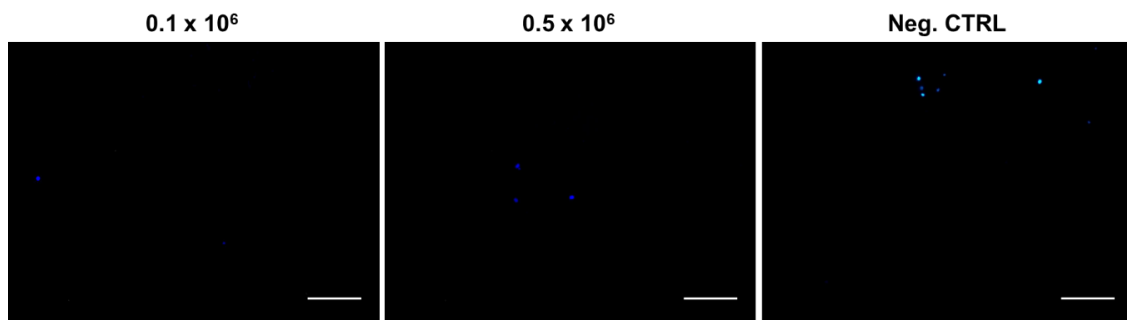


Figure 21: Fluorescence microscopy images of hBCs transfected with px458^{hEGFR_T790M} at 200 V. Both samples, 0.5×10^6 and 0.1×10^6 hBCs, electroporated at parameter set 6 (200 V, 5 ms), did not emit any green fluorescence signal. In both samples, as well as in the negative control, cell mortality rates were extremely high. Scale bars: 200 μ m

Due to these results, the next transfection was performed at lower voltages. According to parameter sets suggested for more vulnerable cells, electroporation was performed at 125 V (5 ms), 150 V (5 ms), 175 V (2.5 ms), and 200 V (2.5 ms). All harvested hBCs (p7) were equally distributed to test these four different voltages, resulting in 222,500 cells per sample. The same endotoxin-free px458^{hEGFR_T790M} plasmid was used again at a concentration of 10 μ g, and cells were analyzed at day 3.

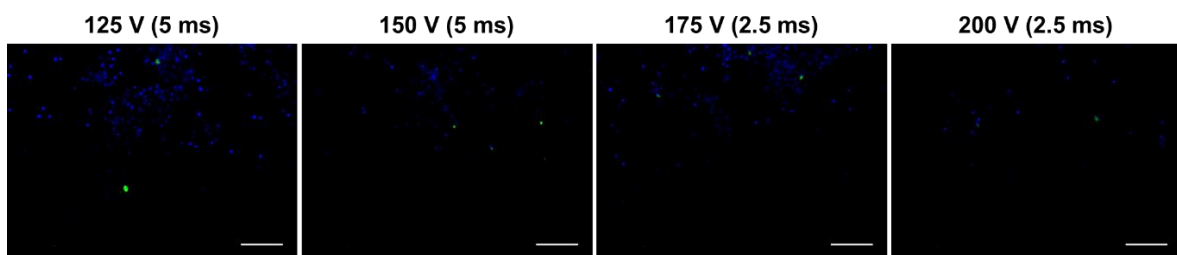


Figure 22: Fluorescence microscopy images of hBCs transfected with px458^{hEGFR_T790M} at 125-200 V. Lower voltages did not tremendously increase transfection efficiency. However, lower voltages clearly have a positive effect on cell viability. Scale bars: 200 μ m

Unfortunately, as visible in Figure 22, lower voltages did not result in substantially better transfection efficiencies. Although some cells emitted a green fluorescence signal, the rate of successful transfections was very low. However, a clear trend regarding improved cell viability at lower voltages could be observed. Therefore, the next trial was performed at 125 V, and the poring pulse length was additionally decreased to 2.5 ms, in an attempt to further increase viability. To test whether the low transfection efficiency was due to px458 plasmid itself, for instance because of its relatively large size, it was directly compared to Nepa Gene's plasmid. Therefore, 1×10^5 hBCs (p5) were electroporated together with one

of the generated endotoxin-free px458 plasmids (harboring either *hEGFR*^{T790M}, *hEGFR*^{L858R}, or *hEGFR*^{ΔE746-A750} sgRNA), or Nepa plasmid, each at a concentration of 10 μg per sample. In addition, Nepa plasmid was applied to one sample transfected at 110 V and 5 ms poring pulse length, to test whether even lower voltages would be beneficial. Cells were again fixed and analyzed three days after transfection.

Unfortunately, transfection efficiency was even lower in this trial compared to the last one. Among all samples, only one transfected cell could be observed in the sample electroporated with Nepa plasmid at 110 V and 5 ms poring pulse length (see Figure 23). Viability was again relatively high at both voltages. However, no significant difference could be observed between the two voltages tested with Nepa plasmid.

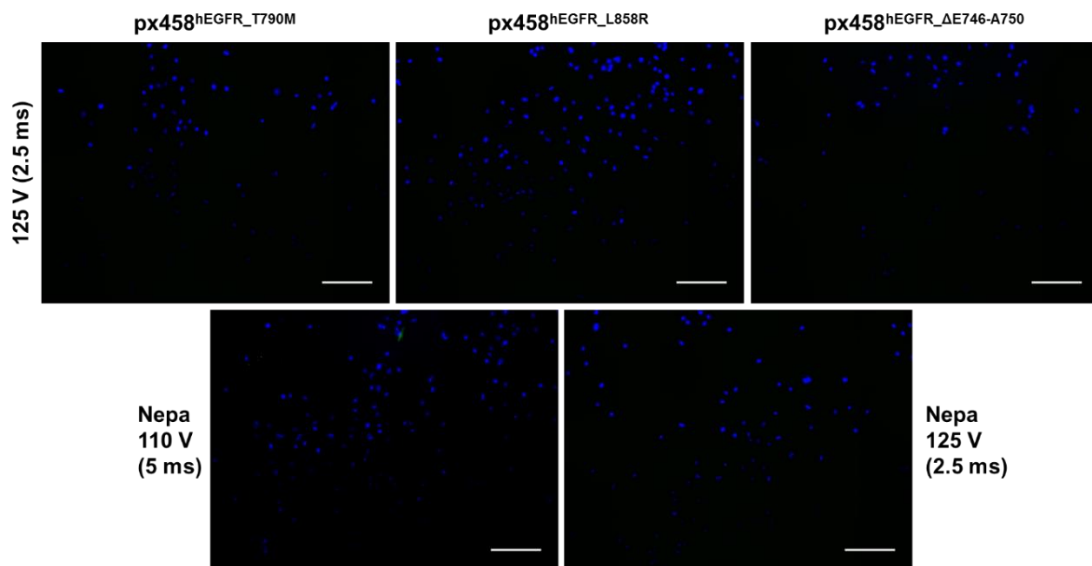


Figure 23: Fluorescence microscopy images of hBCs transfected with px458 or Nepa Gene's plasmid. Among all samples, only one transfected cell could be observed in the sample electroporated with Nepa plasmid at 110 V. Viability was again relatively high at these low voltages. Scale bars: 200 μm

In a last attempt to successfully transfect hBCs, the poring pulse length was increased to 7.5 ms at 150 V. Again, all three px458 plasmids were tested against the Nepa Gene's plasmid, at a concentration of 10 μg. Due to the low number of cells available, only 7×10^4 hBCs (p7) could be transfected per sample. Three days after transfection, cells were stained for DAPI and analyzed using fluorescence microscopy. However, as visible in Figure 24, increasing the poring pulse length did not improve efficiency. Only the sample transfected with Nepa plasmid showed some GFP⁺ cells. In addition, presumably due to the higher voltage and poring pulse length applied, cell viability was again much lower than in the previous trials, even when considering the lower cell number plated per area.

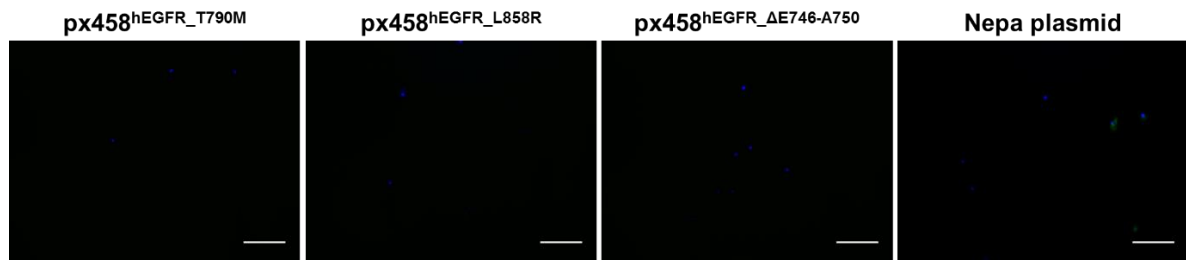


Figure 24: Fluorescence microscopy images of hBCs transfected with px458 or Nepa Gene's plasmid at 150 V and 7.5 ms poring pulse length. Only the sample electroporated with Nepa plasmid showed some GFP⁺ cells. Viability was much lower than in the previous trials, presumably due to higher voltage and poring pulse length. Scale bars: 200 μ m

3.2 Single cell culture

A prerequisite for the selection of successfully transfected clones was to grow cells at very low densities, or as single cells. The first method tested was seeding cells in Petri dishes at low densities. Initially, mBCs were simply diluted to certain concentrations and transferred to 10-cm dishes. However, as many cells usually die after electroporation, the strategy was adapted to immediately plating transfected cells at specific concentrations, in order to determine the optimal cell density despite cell death of a considerable percentage of cells. Therefore, hBCs electroporated with endotoxin-free px458^{hEGFR_T790M} at 175 V, 2.5 ms, were seeded at concentrations of 1×10^4 , 2×10^4 and 3×10^4 in 10-cm dishes. As visible in Figure 25, the most appropriate cell density to prevent different colonies from mixing, was 1×10^4 cells per dish. However, because hBCs were not expanding as dense colonies, but rather as single cells, this method was deemed unsuitable to select positive clones.

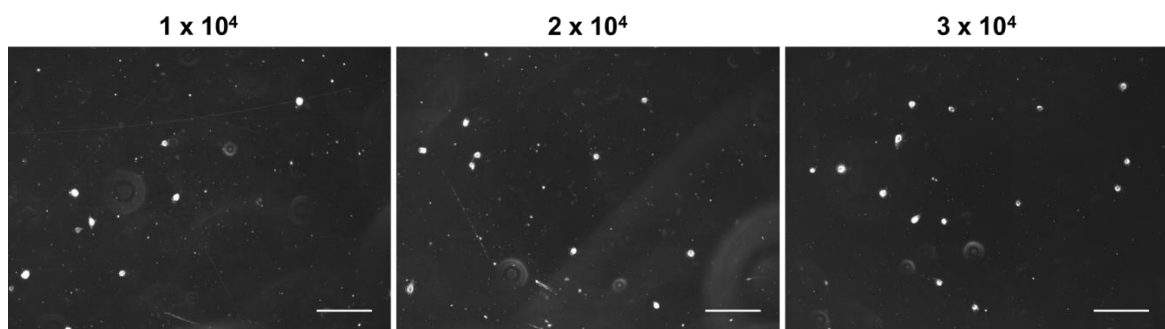


Figure 25: Electroporated hBCs seeded at densities of 1×10^4 , 2×10^4 and 3×10^4 in 10-cm dishes. The most appropriate cell density to prevent different colonies from mixing, seemed to be 1×10^4 cells per dish. However, hBCs were not expanding as dense colonies, but rather as single cells. Scale bars: 200 μ m

In order to avoid the problem of dispersed and intermixing cells from different clones, in the next step single mBCs were seeded in a 96-well-plate, and closely monitored for 15 days. A representative portion of the 96 wells is depicted in Figure 26, which shows that the cells in most wells died within 11 days. From 12 wells indicated in this image, only the cells in two wells survived and started expanding. In total, from the 96 wells monitored, only the cells of 15 wells survived and started proliferating.

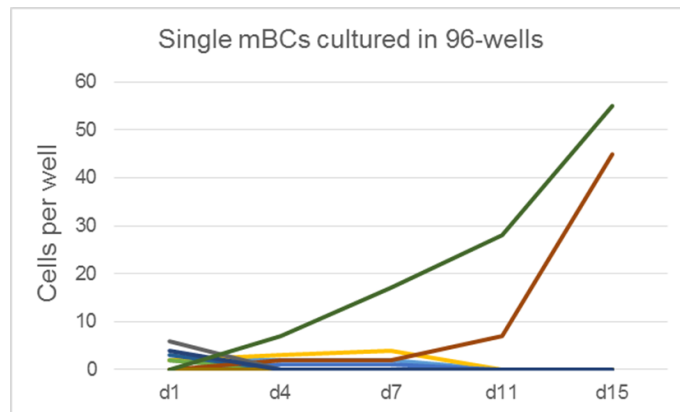


Figure 26: Single mBCs seeded in a 96-well-plate and monitored for 15 days. Each line represents the monitored cell number of one well. Most of the cells died within 11 days of culture. Out of 12 wells, only two cells survived and started proliferating.

When the same experiment was performed with hBCs, even fewer cells survived. More precisely, out of 72 wells, only one cell had generated more than 10 cells after 15 days. Therefore, it was tested if supplementing the growth medium with supernatants of other hBCs or MRC5 cells, or both, could improve cell survival, as cells deprived of signaling cues from other cells usually undergo cell death. In addition, the requirement for freshly collected media was evaluated, by comparing cells that received 'fresh' supernatant every other day, to cells that received supernatant collected several days earlier. Each collected supernatant was sterile-filtered to remove contaminating cells and debris, and mixed 1:1 with fresh SAGM plus medium before application. Unfortunately, as visible in Figure 27, almost all of the cells died within three days of culture. In total, out of 72 wells, only six cells survived for 14 days, but none of them started proliferating. Hence, this method was also deemed unsuitable to expand single transfected cells.

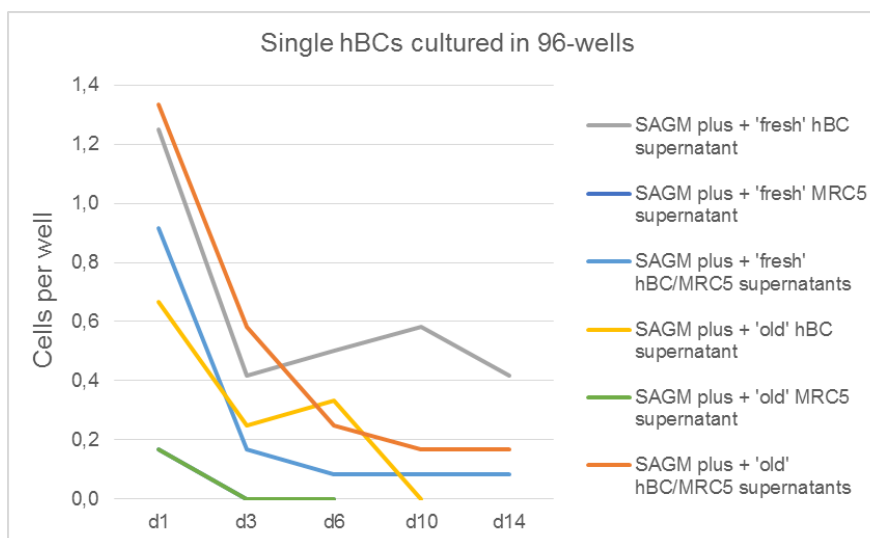


Figure 27: Single hBCs cultured in a 96-well-plate in media supplemented with supernatants of other cells. Almost all of the cells died within 3 days of culture. Out of 72 wells, only six cells survived, but none of them started proliferating. Each data point represents the mean of 12 wells.

Eventually, hBCs were seeded on transwell membranes, with 5,000 other hBCs either seeded on the bottom of the well, or directly on the lower side of the membrane. As visible in the upper panel of Figure 28, when the supporting hBCs are grown on the bottom of the wells, they can easily be distinguished from the single cells seeded on top of the membrane. By contrast, the major drawback of growing cells on the lower side of the membrane, is the difficulty to distinguish between these cells and the cells seeded on top. Especially when only a single cell is seeded on the membrane, it is almost impossible to monitor this cell from the beginning of the culture. However, the transwell method with growing supporting cells on the bottom of the wells was the most promising approach tested. Although transwell inserts are relatively expensive, this method should at least be evaluated for a prolonged period of time in order to make a qualified decision whether these costs would be justified.

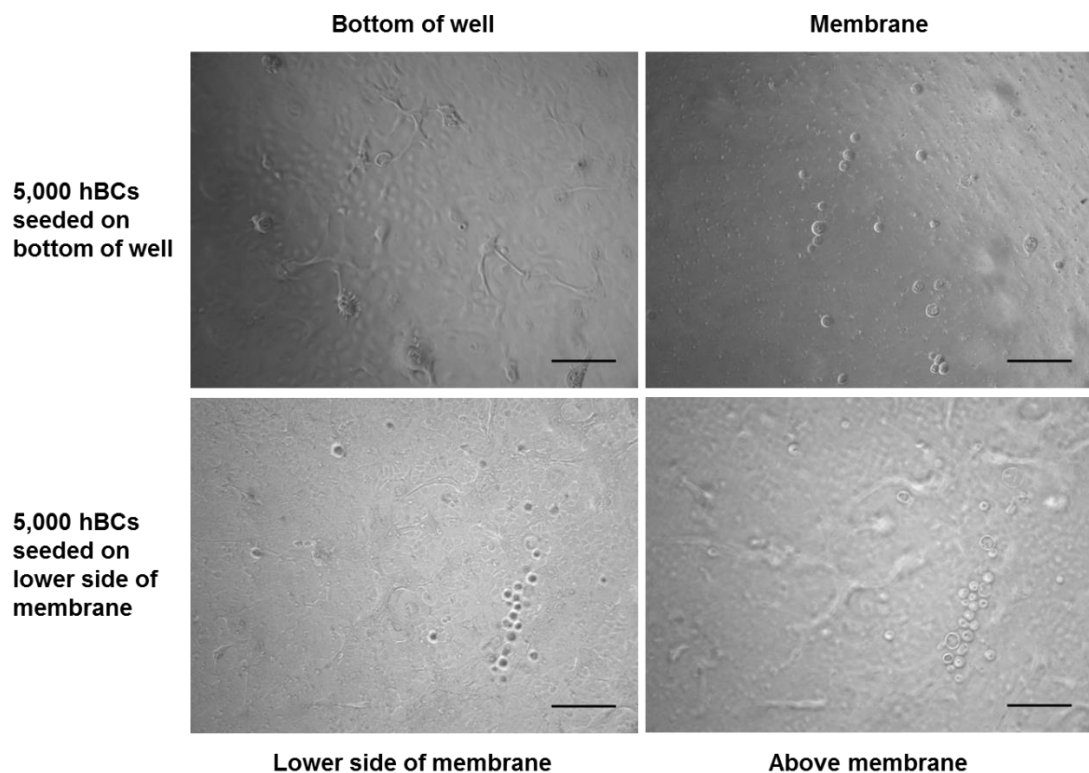


Figure 28: Single hBCs cultured in transwell inserts, with 5,000 hBCs either on the bottom of the well or on the lower side of the membrane. Supporting hBCs grown on the bottom of the wells can easily be distinguished from the single cells seeded on top. By contrast, it is very difficult to distinguish between cells attached to the lower side of the membrane and cells on the upper side. Images were taken on day 4 after seeding. Scale bars: 200 μ m

3.3 Organoid culture

As described in 2.5, organoids were established from several different cell types. The first organoids were generated from healthy mBCs mixed with murine MLGs, grown in 6-well-plates. Organoids were cultured for up to five weeks in MTEC basic supplemented with ROCK inhibitor. As visible in Figure 29, the organoids steadily increased their diameters and

remained stable for this five-week period. Thereafter, organoids were harvested and embedded in O.C.T. compound for cryosectioning and staining.

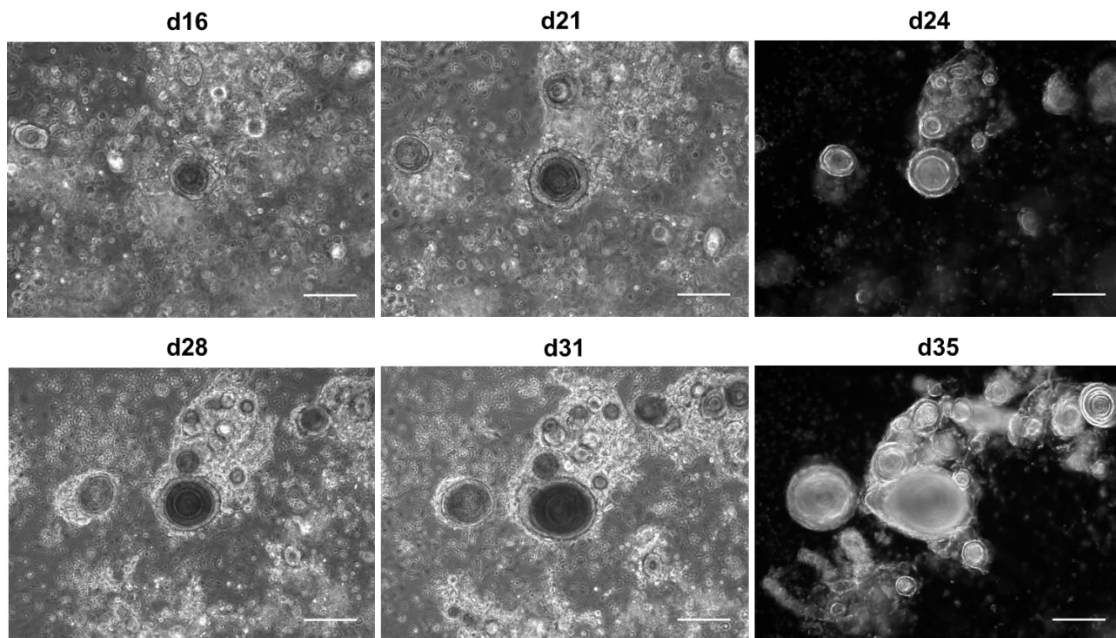


Figure 29: Organoids established from healthy mBCs and murine MLgs cultured for five weeks. Images were taken at six different time points. Many organoids had already formed after two weeks in culture, and their diameters kept on increasing to more than 200 μm in some cases after five weeks. On days 24 and 35, images were unintentionally taken with inverted phase contrast settings. Scale bars: 200 μm

Two different stainings were performed, on the one hand, BC organoids were stained to demonstrate their differentiation into cells that are characteristic for pseudostratified epithelium in the lung airways. Therefore, the BC marker KRT5, the luminal cell marker KRT8, and ciliated cell-specific acetylated tubulin (acT) were stained in one experiment. On the other hand, BC organoids were compared to *NKX2-1* organoids, which were derived from BCs, but have lost their lung lineage identity and differentiate towards intestinal cell types in a process termed cellular plasticity, which allows cells to convert into other cell types [118]. Therefore, both organoid types were stained for the aforementioned lung-specific markers, and on the other hand for the intestinal markers SOX9, which is found among all intestinal cells, and KRT20, which is found in most differentiated intestinal cells. In addition, both organoids were stained for EpCAM, which is found in all epithelial cells of the body.

As visible in Figure 30, staining for KRT5 clearly showed that organoids were mainly consisting of BCs. In contrast, not many acT⁺ ciliated cells could be observed, which may be explained by the fact that the organoids were maintained for five weeks, and it has been shown that they lose their cilia after long times in culture. Unfortunately, staining for KRT8⁺ luminal cells did not show the expected results. No staining could be observed whatsoever, suggesting that the antibody did not bind at all, either due to a defect of the antibody itself, or due to an error that occurred during implementation.

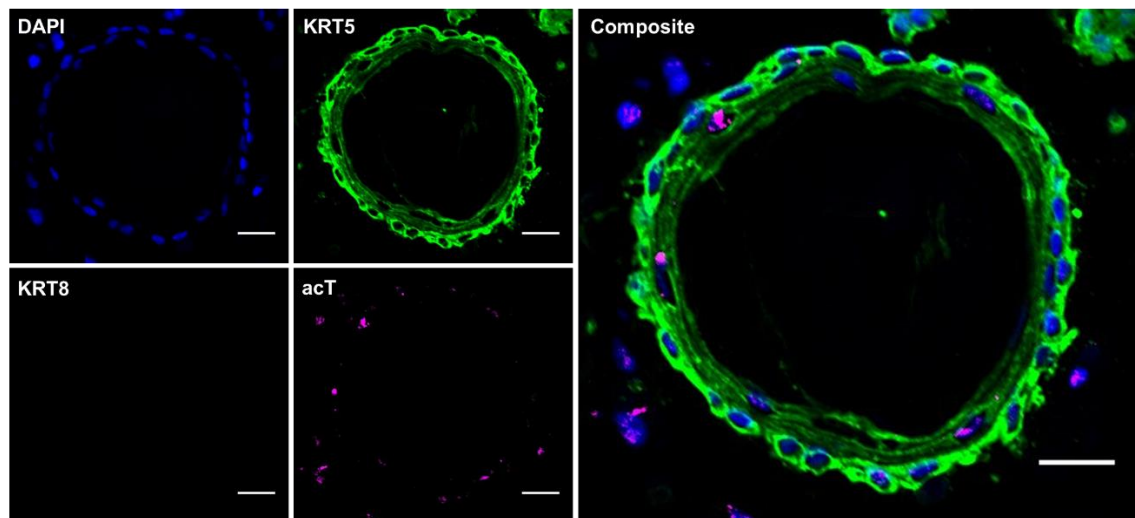


Figure 30: Organoids established from healthy mBCs and murine MLGs cultured for five weeks and stained for lung epithelial markers. Confocal fluorescence images showing DAPI in blue, KRT5 in green, KRT8 in red and acT in magenta. Organoids were mainly consisting of KRT5⁺ BCs, not many ciliated cells (acT) could be observed, and staining for KRT8⁺ luminal cells failed. Scale bars: 20 μ m

Confocal fluorescence images showing the staining for intestinal cell-specific markers can be seen in Figure 31. Organoids were mainly consisting of EpCAM⁺ epithelial cells, as already indicated by staining for KRT5, which showed that the organoids were mainly formed by BCs. No SOX9⁺ intestinal cells could be observed. The two small dots visible are presumably dust particles, as SOX9 is a transcription factor and should be found in the nuclei, which can clearly be seen in Figure 33. Surprisingly, staining for KRT20 to indicate differentiated intestinal cells resulted in a very faint signal at the outer edge of the organoid.

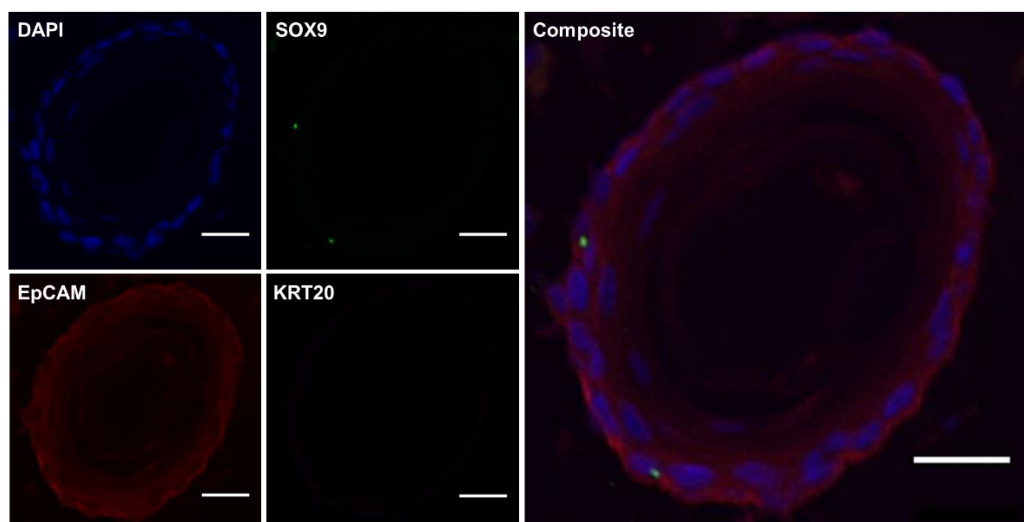


Figure 31: Organoids established from healthy mBCs and murine MLGs cultured for five weeks and stained for intestinal cell markers. Confocal fluorescence images showing DAPI in blue, SOX9 in green, EpCAM in red and KRT20 in magenta. Organoids were mainly consisting of EpCAM⁺ epithelial cells, no SOX9⁺ intestinal cells could be observed, and staining for KRT20⁺ differentiated intestinal cells resulted in a very light signal at the outer edge of the organoid. Scale bars: 20 μ m

As mentioned before, BC-derived *NKX2-1*⁻ organoids, which lose their lung lineage identity and differentiate towards an intestinal fate, were used as a comparison (cryosections were kindly provided by Dr. Tata). Sections were stained for lung-specific markers KRT5, KRT8 and acT, for the intestinal markers SOX9 and KRT20, and for EpCAM, which is found in all epithelial cells. As visible in Figure 32, *NKX2-1*⁻ organoids were negative for KRT8 luminal cell marker and acT ciliated cell marker. In contrast, KRT5 was clearly expressed in these organoids, indicating that BCs had maintained at least some of their characteristics after 12 days in culture. However, it is known that they lose their BC-specific markers with time, suggesting that KRT5 levels would further decrease during prolonged culture.

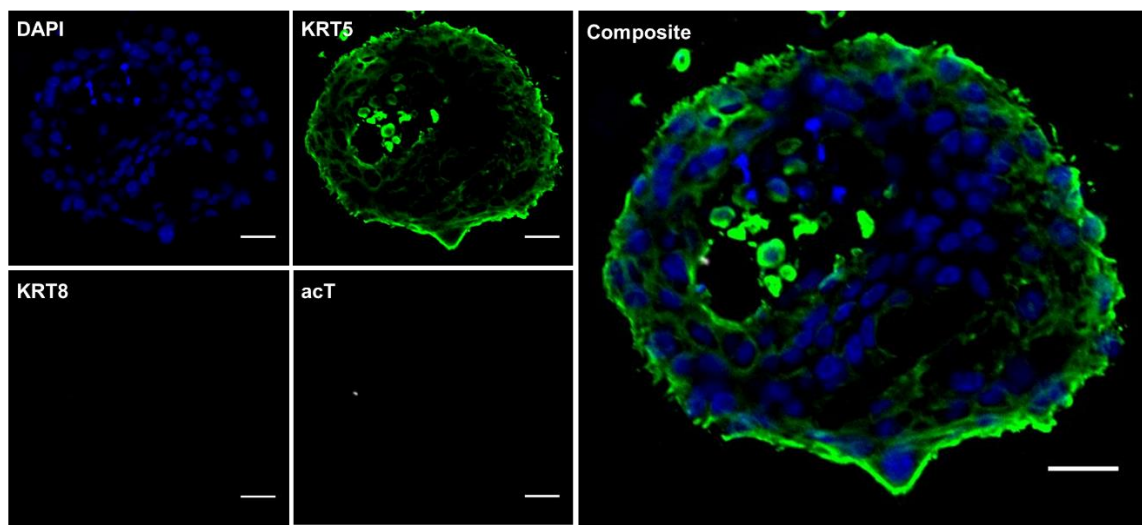


Figure 32: Organoids established from *NKX2-1*⁻ lung cells cultured for 12 days and stained for lung epithelial markers. Confocal fluorescence images showing DAPI in blue, KRT5 in green, KRT8 in red and acT in gray. *NKX2-1*⁻ organoids were negative for KRT8 luminal cell marker and acT ciliated cell marker. In contrast, KRT5 was clearly expressed, indicating preserved BC-characteristics. Scale bars: 20 μ m

Staining *NKX2-1*⁻ organoids for intestinal markers clearly showed differentiation towards an intestinal fate. Significant expression of both intestinal markers, SOX9 and KRT20, can clearly be seen among the majority of cells depicted in Figure 33. Moreover, the differential distribution of these markers is visible very well, with SOX9 located in the nuclei, and KRT20 dispersed throughout the cytoplasm. Similarly, the epithelial cell marker EpCAM was found to be both, abundant and distributed across the entire cell bodies. Together these results suggest that despite *NKX2-1*⁻ cells differentiate towards the intestinal lineage, their epithelial identity remains.

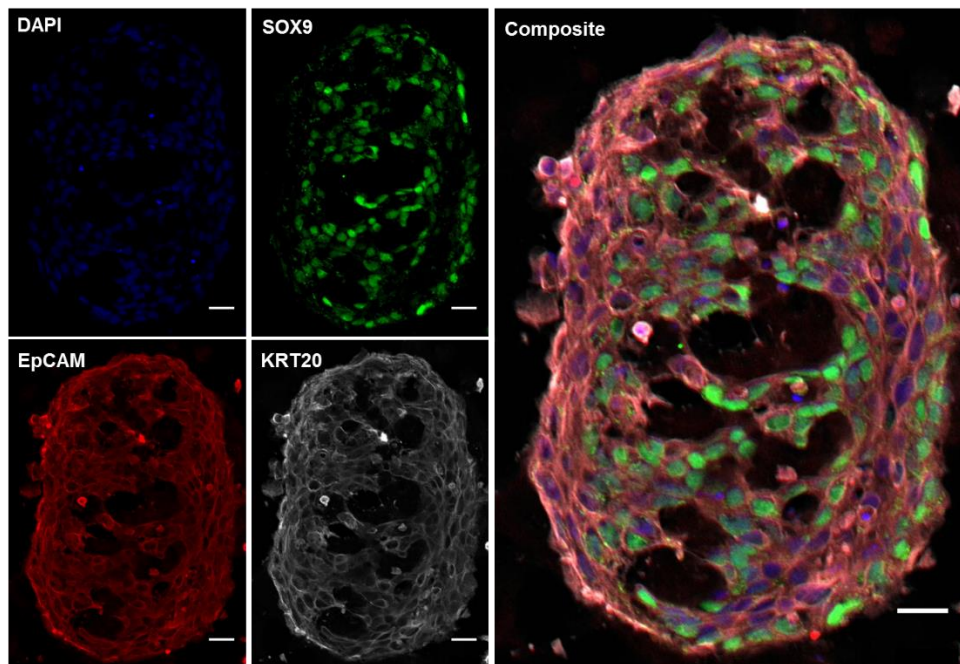


Figure 33: Organoids established from *NKX2-1* lung cells cultured for 12 days and stained for intestinal markers. Confocal fluorescence images showing DAPI in blue, SOX9 in green, EpCAM in red and KRT20 in gray. *NKX2-1* organoids were highly positive for all markers, intestinal markers SOX9 and KRT20, as well as EpCAM, suggesting that *NKX2-1* cells differentiate towards an intestinal fate, but keep their epithelial characteristics. While SOX9 was found in the nuclei, KRT20 and EpCAM were distributed throughout the cytoplasm. Scale bars: 20 μm

Furthermore, alveolar-like organoids were generated from two different sources. First, lung lobes were isolated from a *LSL-KRAS^{G12D}* mouse, dissociated, and half of the cells was activated with adeno-cre-GFP virus, in order to activate *KRAS^{G12D}* mutation. Then, organoids were established from both, *KRAS*-mutated cell mixtures, as well as healthy (not cre-activated) cells. As a comparison, the human lung adenocarcinoma cell line NCI-H23 was used to set up *KRAS^{G12D} p53^{L246M}* cancer organoids. Both types of organoids were cultured for 14 days, and then stained for SFTPC as AEC2 marker, PDPN as AEC1 marker, and ZO-1 to indicate cell polarity, as it is only found at tight junctions, and therefore almost exclusively at apicolateral cell-cell contacts.

Images of organoids that developed from murine lung lobe cell mixtures are depicted in Figure 34. Both, cells that were not activated with adeno-cre-GFP virus, as well as cells with activated *KRAS^{G12D}* mutation generated a high number of organoids. However, *KRAS*-mutant cells formed substantially larger structures of up to 700 μm diameter. Moreover, different organoid shapes were observed. While most organoids appeared similar to the spherical organoids established from BCs, some organoids had very dense, more irregular shapes (indicated by asterisks). These organoids were rather resembling alveolar architectures, and had therefore presumably developed from AEC2s. Furthermore, as visible, the matrigel droplets had already started to detach from the 6-well-plate on day 14, suggesting that cultures should be terminated on day 14 at the latest.

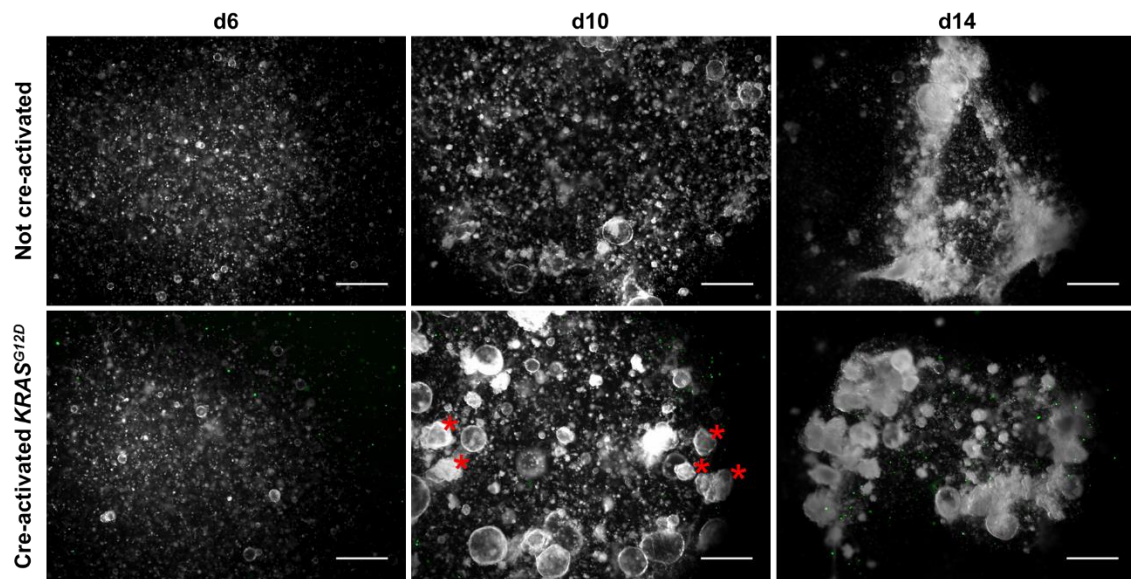


Figure 34: Organoids established from murine lung lobe cell mixtures cultured for 14 days. The upper panel shows organoids of cells that were not activated with adeno-cre-GFP virus, the lower panel indicates organoids established from cells with activated $KRAS^{G12D}$ mutation; green fluorescence indicates cells that were successfully infected by adeno-cre-GFP virus. Many organoids formed in both cases, but $KRAS$ -mutant cells formed substantially larger structures of up to 700 μm diameter. Most organoids appeared spherical, while some were very dense and irregular, resembling alveolar architectures (asterisks). Scale bars: 800 μm

Unfortunately, no sections could be obtained showing cre-activated $KRAS^{G12D}$ organoids, hence only non-cre-activated organoids were stained. The structure captured in Figure 35 consisted mainly of SFTPC⁺ cells, which were therefore considered AEC2s. Moreover, many SFTPC-filled granules within the cytoplasm of these cells could clearly be seen. ZO-1 staining was rather weak, and did not allow clear determination of cell polarity. Whereby, the captured structure did not show a very well defined organoid, which additionally hampered this endeavor. Interestingly, no PDPN⁺ AEC1s could be observed at all, despite the fact that alveolar-like organoids usually contain both cell types, as the cells attempt to form structures similar to natural alveoli.

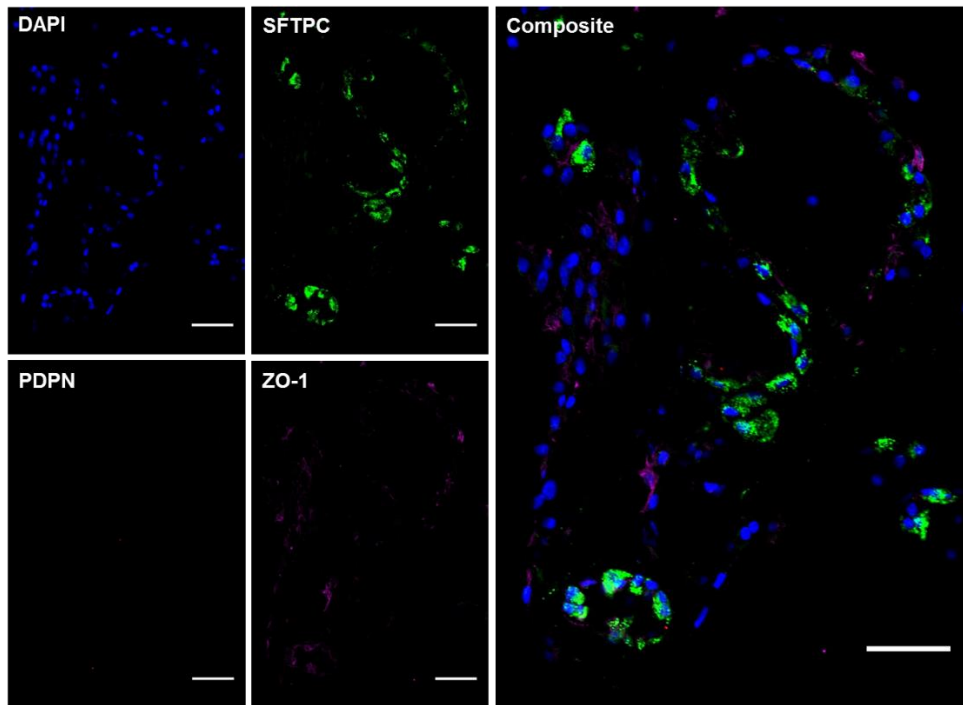


Figure 35: Staining of AEC2-dominated organoids established from non-cre-activated murine lung cells cultured for 14 days. Confocal fluorescence images showing DAPI in blue, SFTPC in green, PDPN in red and ZO-1 in magenta. The captured structure consisted mainly of SFTPC⁺ cells, and many SFTPC-filled granules within the cytoplasm of these cells could be seen. ZO-1 staining was rather weak, and did not allow clear determination of cell polarity. No PDPN⁺ AEC1s could be observed at all, despite the fact that alveolar-like organoids usually contain both cell types. Scale bars: 50 μ m

By contrast, the second structure captured on the same slide harbored many cells positive for PDPN, as shown in Figure 36. Apparently, most of these cells were surrounding SFTPC⁺ AEC2s, which were also distributed throughout most of the structure. Another interpretation may be that cells were double positive, indicating either precursor cells that have the potential to give rise to both cell types, or AEC2s that were captured in a transition state of differentiating into AEC1s. Only very few cells could be observed that were clearly SFTPC⁺ only. In contrast to the previous figure, ZO-1 was found distributed almost everywhere, very similar to areas positive for PDPN, suggesting that cells were connected by abundant tight junctions. However, due to this abundance, cell polarity could not be evaluated for these cells either.

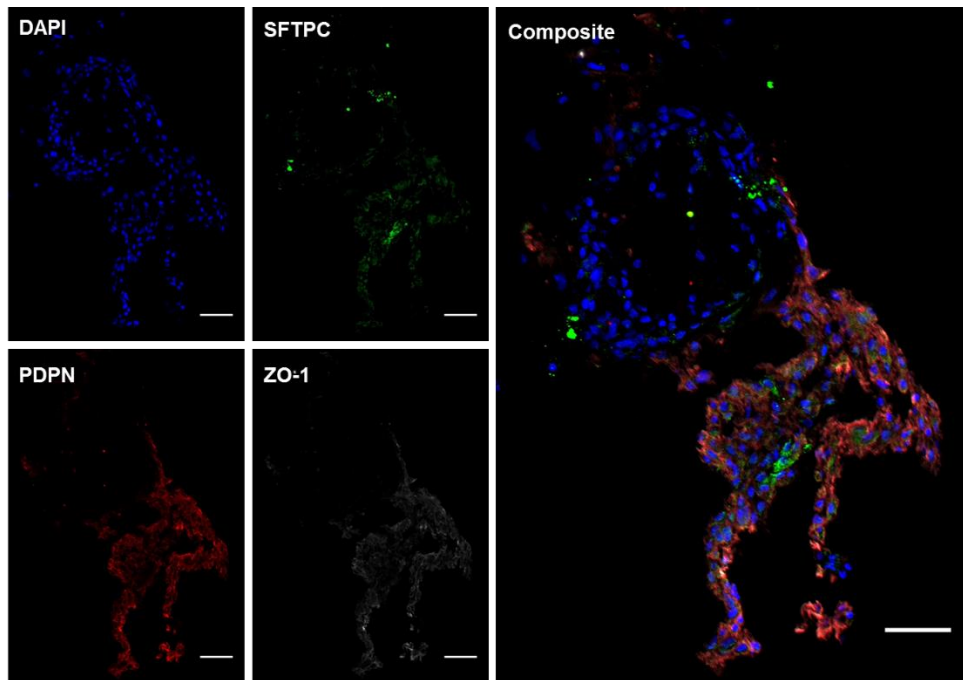


Figure 36: Staining of alveolar-like organoids established from non-cre-activated murine lung cells cultured for 14 days. Confocal fluorescence images showing DAPI in blue, SFTPC in green, PDPN in red and ZO-1 in gray. The captured structure harbored many PDPN⁺ cells, which were either surrounding SFTPC⁺ cells, or cells were double positive for both markers. Only very few cells were clearly SFTPC⁺ only. ZO-1 was found distributed almost everywhere, suggesting abundant tight junctions. Scale bars: 50 μ m

In order to compare the alveolar-like organoids described in the previous image to cancerous alveolar spheres, the human lung adenocarcinoma cell line NCI-H23 was used. As visible in Figure 37, these cells generated many organoids within two weeks. However, the majority remained very small, with diameters of approximately 20 μ m.

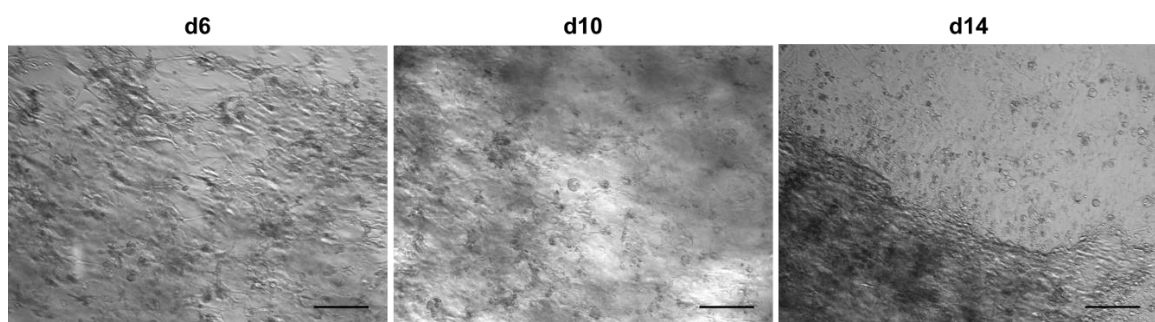


Figure 37: Organoids established from lung adenocarcinoma cell line NCI-H23 cultured for 14 days. Many organoids formed within two weeks, but the majority remained very small, with diameters of approximately 20 μ m. Scale bars: 200 μ m

As depicted in Figure 38, staining revealed that the majority of cells was SFTPC-positive. Also many PDPN⁺ cells could be observed, although the signal was considerably weaker. Both cell types were dispersed throughout the entire cluster of cells. Also, the overall shape of the captured structure is not very well defined, and does not resemble a natural alveolus.

Moreover, no ZO-1 could be detected, presumably due to the fact that tumor cells lose their polarity, which further underscores the tumorous identity of these cells.

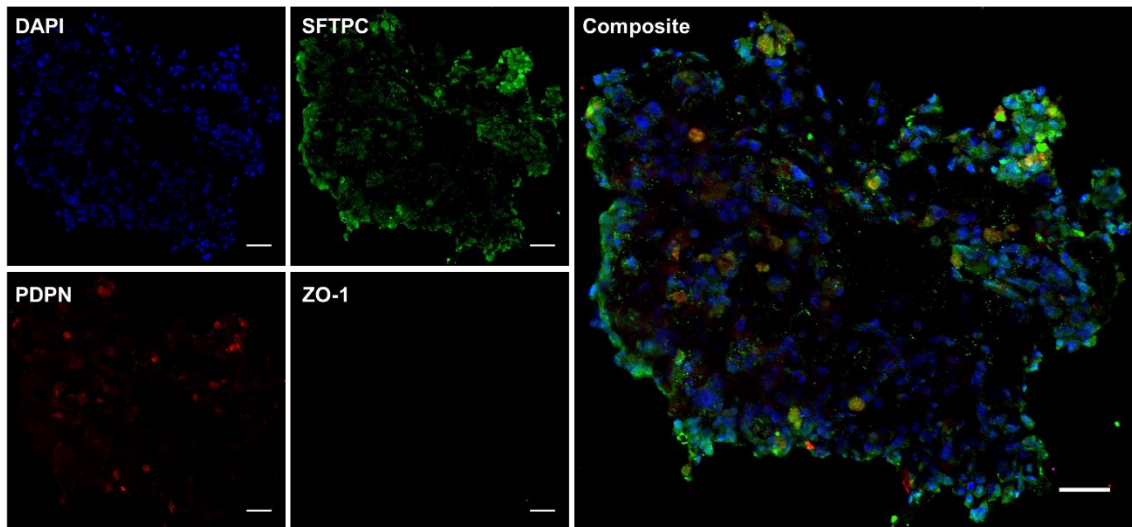


Figure 38: Staining of organoids established from human lung adenocarcinoma cell line NCI-H23 cultured for 14 days. Confocal fluorescence images showing DAPI in blue, SFTPC in green, PDPN in red and ZO-1 in magenta. Many SFTPC-positive as well as PDPN-positive cells could be observed, both dispersed throughout the entire cluster of cells. The overall shape of the captured structure does not resemble a natural alveolus. In addition, no ZO-1 could be detected, presumably because tumor cells lose their polarity. Scale bars: 50 μ m

3.3.1 Growth kinetics

In addition to staining the different organoids for distinct histological markers, their growth kinetics were monitored, in order to compare characteristics of human and murine, healthy and tumorigenic cells. An overview of all the different organoids established is given in Table 9. Briefly, apart from healthy mBC organoids, organoids were established from murine trachea epithelial cells, SFTPC⁺ murine lung cells, and murine lung lobe cell mixtures, whereby one portion was infected with adeno-cre-GFP virus, in order to activate *KRAS*^{G12D} mutation. Finally, healthy hBCs were grown as control organoids, or subjected to CRISPR/Cas9-based genome editing, in order to introduce specific *EGFR* mutations (T790M, L858R, or Δ E746-A750) to create lung tumor organoids. In addition, the human lung adenocarcinoma cell line NCI-H23 was used to set up *KRAS*^{G12D} *p53*^{L246M} cancer organoids. Most organoids were cultured and closely monitored for two weeks. However, the organoids generated from murine trachea epithelial cells were cultured for 6 days only, as it has been observed that they usually collapse around day 7. Moreover, no growth kinetics data from healthy mBC organoids were available for comparison, as images were only taken from day 16 on. Unfortunately, in case of hBCs, cultures had to be terminated on day 9, as the droplets had already partly detached from the culture plate. Representative images of the different established organoids, taken on day 6, are shown in Figure 39.

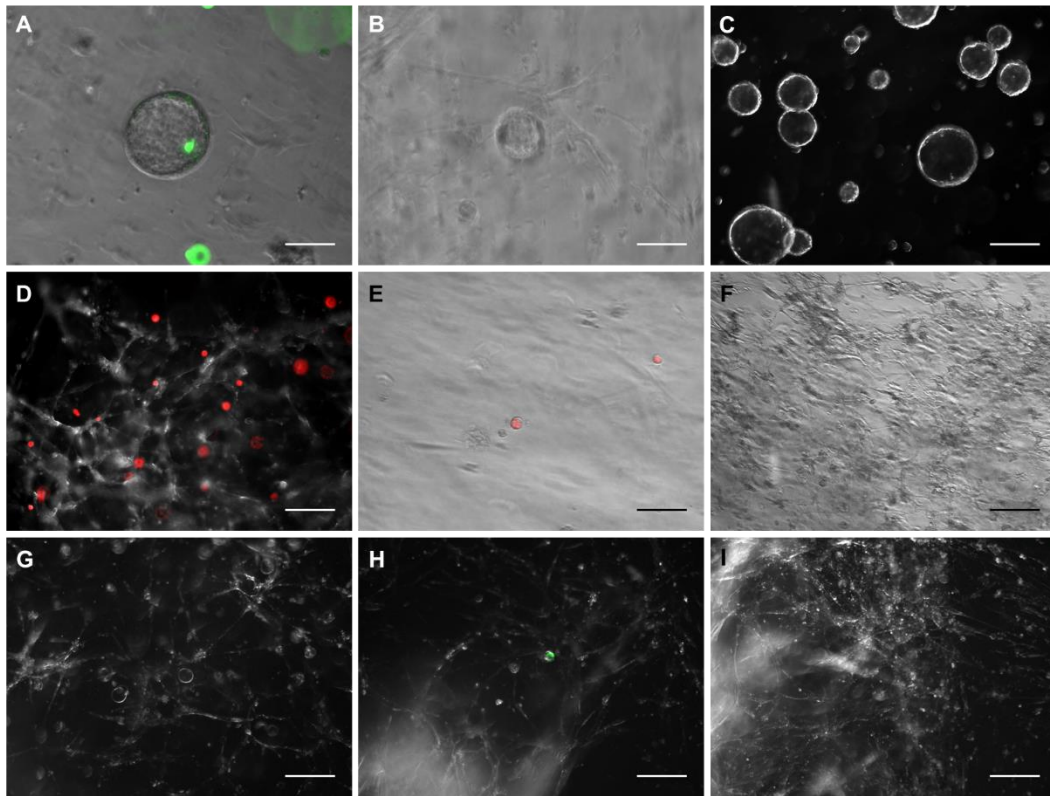


Figure 39: Comparison of the various organoids established from different cell types. A) Murine cre-activated $KRAS^{G12D}$ cells; green fluorescence indicates adeno-cre-GFP virus infection; B) non-cre-activated murine lung cells; C) murine trachea epithelial cells; D) murine tm-labeled SFTPC⁺ cells cultured together with MRC5 cells in a 6-well; E) murine tm-labeled SFTPC⁺ cells cultured together with MRC5 cells in a transwell; F) NCI-H23 human lung adenocarcinoma cell line; G) hBCs cultured with MRC5 cells; H) Nepa plasmid-transfected hBCs cultured with MRC5 cells; fluorescence indicates successful transfection; I) px458^{hEGFR_T790M}-transfected hBCs cultured with MRC5 cells. Images were taken on day 6. Scale bars: 100 μm (A and B), 200 μm (C-I)

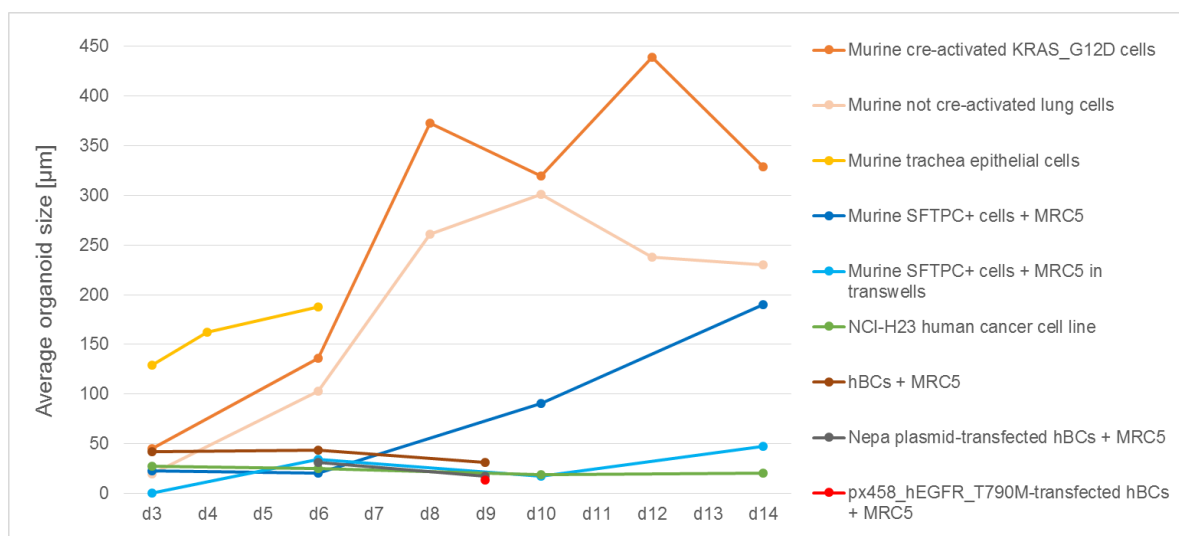


Figure 40: Comparison of growth kinetics data obtained from different organoid cultures. The largest organoids were obtained from murine $KRAS^{G12D}$ -mutant lung cells, followed by non-cre-activated cells. Also murine trachea epithelial cells and SFTPC⁺ murine lung cells reached considerably large diameters. SFTPC⁺ cells cultured in transwell inserts remained substantially smaller. Cultures established from human cells did not show much growth at all. Even the cancer cell line NCI-H23 produced only little organoids. Moreover, no substantial differences were observed regarding healthy hBC cultures and transfected hBCs.

As shown in Figure 40, most organoids increased in diameter over the 14 days monitored. The largest organoids were obtained from murine lung lobe cell mixtures, whereby the portion with activated *KRAS*^{G12D} mutation grew significantly bigger compared to not re-activated cells (329 µm compared to 230 µm on average, respectively). Also murine trachea epithelial cells and SFTPC⁺ murine lung cells reached considerably large diameters (188 µm and 190 µm, respectively). Interestingly, SFTPC⁺ murine lung cells cultured in transwell inserts remained substantially smaller (47 µm on average). Organoids generated from mBCs that had been in culture for many passages already, reached an average diameter of 124 µm after 16 days (see Figure 29).

By stark contrast to murine cell-derived organoids, cultures made of human cells did not show much growth at all. Even the cancer cell line NCI-H23 produced only little organoids during the two week period (21 µm on average). Moreover, no substantial differences could be determined regarding healthy hBC cultures and hBCs transfected with Nepa plasmid or px458 plasmid. Healthy hBCs generated organoids of 31 µm average size, whereas hBC-organoids electroporated with Nepa plasmid reached 17 µm, and cells transfected with px458^{hEGFR_T790M} 14 µm on average. Very similar results were obtained for cells electroporated with px458 plasmid inducing one of the other two mutations (data not shown). However, not a single one of the organoids established from px458-transfected cells was GFP-positive, indicating that none of them originated from a successfully transfected cell. Moreover, due to their slow expansion, organoids could only be observed from day 6 on in case of cells transfected with Nepa plasmid, and not before day 9 for px458-transfected cells.

4 Discussion

4.1 Availability and other limitations of cells

The main obstacle in this project was the limited availability of human tissue samples. Therefore, mBCs had to be used for establishing electroporation parameters. However, these cells do not only exert distinct growth kinetics, they also respond differently to electroporation. Therefore, the parameter sets that had been determined to achieve best efficiencies with mBCs were not appropriate for hBCs. Moreover, once hBCs were obtained, they proliferated at a very low level and showed a high tendency to elongate and differentiate when seeded in low densities, so that they could only be split 1:2 for expansion. As visible in Figure 41, when split at a ratio of 1:3, the cells reached confluency only after 14 days in a 6-cm dish, which tremendously delayed all intended experiments. Also the organoids established from hBCs grew very slowly and remained substantially smaller than organoids generated from other cell types.

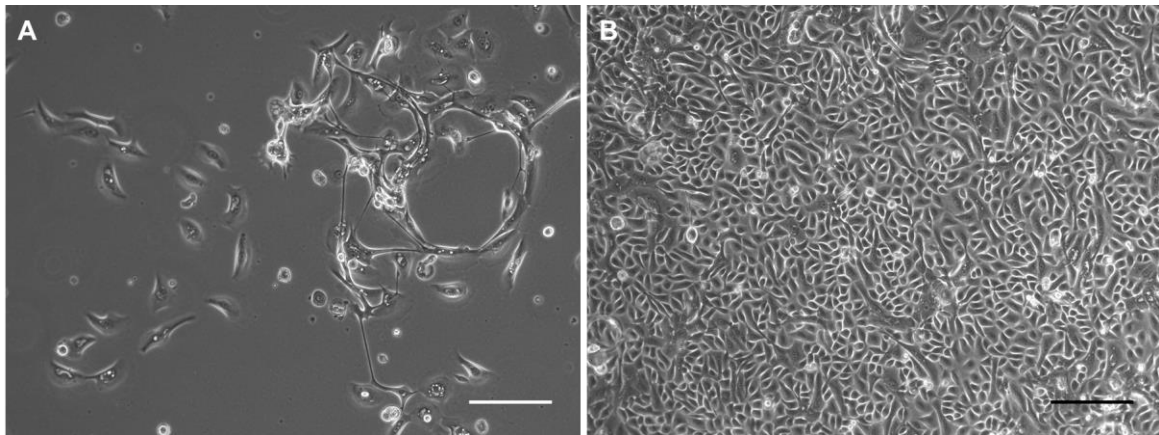


Figure 41: Morphology and growth behavior of primary hBCs cultured *in vitro*. hBCs proliferated at a very low level and showed a high tendency to differentiate when sub-cultured at low densities. A) hBCs (p5) split at a 1:3 ratio and cultured for 8 days were far from reaching confluency. In addition, most of the cells were elongated or differentiated. B) hBCs (p7) cultured for 14 days finally reached confluency in a 6-cm dish. Scale bars: 200 μ m

This growth behavior was maybe due to the advanced age of the patient, from whom the cells were obtained. Therefore, in prospective studies, it will be advantageous to use cells from a younger patient. However, the actual target for establishing lung tumor organoids are AEC2s. Unfortunately, these cells require a 3-dimensional environment to grow, and the opportunity of maintaining them for prolonged periods is currently limited. Thus, a suitable culture system has yet to be designed, in order to enable long-term expansion, transfection and selection of positive clones, so that tumor organoids can eventually be established from AEC2s. Currently, possible culture conditions are evaluated involving the use of other biomaterials as alternative to matrigel. One of the advantages of these systems would be that these biomaterials can be designed and modified according to the specific requirements of AEC2s, which will hopefully allow for successful cultivation in the near future.

4.2 Electroporation with px458 plasmid

In general, electroporation efficiencies for cells transfected with px458 plasmid were very low in all trials. Therefore, further experiments are definitely required to substantially improve electroporation results. As described in 3.1, electroporation was much more efficient using Nepa Gene's plasmid when compared to transfection with px458. This may be due to the different plasmid sizes, as Nepa Gene's plasmid consists of approximately 5.5 kilo bases (kb), while px458 is almost twice as large with 9.3 kb. Therefore, it is possible that efficient uptake is hampered due to size. Moreover, when using the same amount of plasmid, such as 10 μ g, the actual copy number of plasmids administered is smaller when the plasmid is bigger, and therefore heavier. Thus, a higher concentration of plasmid per sample may be beneficial. However, because high concentrations of at least 1 μ g/ μ l are required by the protocol for NEPA21 electroporation, and the volume added per sample should not exceed 10 μ l, the amount of DNA used cannot be increased limitless. Therefore, it would be necessary to generate a higher concentrated stock, by eluting the plasmids in a very small

volume after purification, or by resuspending them in a lower volume after precipitation. Unfortunately, the former is restricted by a certain amount of elution buffer that is needed to fully cover the filter surface, and the latter may reduce solubility. Therefore, the volume cannot be reduced beyond a certain limit. However, since transfection efficiencies for cells transfected with px458 plasmid were very low in all trials, the use of a different plasmid should definitely be considered in prospective experiments.

Moreover, slightly better results were obtained with mBCs compared to hBCs. This was possibly due to the age of the patient from whom the hBCs were obtained, resulting in more susceptible and less resilient cells. Therefore, further trials should preferably be performed with hBCs obtained from a younger patient. If cells can be obtained that show higher proliferation rates, cell numbers per sample may be raised again as well. Furthermore, if the handling of samples during preparation for electroporation can be further improved and accelerated, cell viability may be increased. However, in case that none of these strategies leads to better results, other transfection methods need to be considered. Since hBCs have not been electroporated with Amaxa so far, this device could be tested as an alternative. Eventually, if electroporation is not suitable for hBCs under any conditions, lentiviral transduction may be applied. Fortunately, the requirements for working with viruses under biosafety level 2 classification are already met at the host laboratory.

4.3 Single cell culture

Another major obstacle for the goal of this project was that hBCs could not be grown at low densities, which would be necessary to obtain clones of single cells harboring a specific mutation. When cells were grown at very low concentrations, unfortunately almost all cells died after some time, probably as a result of lacking survival signals from other cells. According to Fujii *et al.*, the limited capacity to recover single cells is mainly due to anoikis [105], which is a type of programmed cell death induced when anchorage-dependent cells detach from their surrounding ECM. The reason for this is thought to be the absence of essential growth factors and survival signals provided by neighboring cells and the ECM. However, several methods have been tested, including seeding cells in Petri dishes at low densities, culturing them in 96-wells as single cells, supplementing the media with supernatants of other hBCs or MRC5 cells, or both, and culturing single hBCs on transwell membranes, with other hBCs seeded on the bottom of the wells, or directly on the lower side of the membranes. Unfortunately, most of the methods did not achieve a sufficient rate of surviving cells. The only method that seemed promising, was the transwell culture, which would imply a relatively high economic burden, even when growing only fifty clones for each mutation to be introduced. However, this method should at least be evaluated for a prolonged period of time in order to make a qualified decision whether these costs would be justified.

4.4 Characteristics of organoid cultures

Unfortunately, not all intended parts of the project could be performed eventually. It was initially planned to transfect hBCs with each of the plasmids created, to identify clones harboring the correct mutations, and to select and expand those to model tumorigenesis. However, since establishing the methods was relatively time-consuming, and electroporation of hBCs eventually showed a very limited success rate, this part of the project could not be carried out. It would be necessary to generate at least several hundred cells harboring a specific mutation, in order to have sufficient positive clones available that can be expanded to generate tumor organoids. Therefore, it was not possible to grow lung organoids harboring one of the *EGFR* mutations, and to compare them to other types of organoids that were established. Hence, also categorization of tumorigenic spheres on a molecular basis could not be performed. Moreover, no primary tumors could be obtained from human patients, forfeiting the chance to evaluate similarities and differences between designed tumor organoids and primary lung tumors.

However, as described in 3.3, many organoids could be established from other cell sources, which showed distinct expression of specific markers. BC-derived organoids mainly harbored KRT5⁺ EpCAM⁺ BCs, however, not many ciliated cells (acT⁺) could be observed, and staining for KRT8⁺ luminal cells failed. As expected, no SOX9⁺ intestinal cells could be observed, but surprisingly, staining for KRT20 resulted in a very faint signal at the outer edge of the organoid, which usually indicates differentiated intestinal cells. Since no evidence has been found in literature that airway BCs differentiate towards intestinal cells under normal conditions, this outcome was possibly due to insufficient washing steps or unspecific binding.

In contrast, it could be shown that BC-derived *NKX2-1*⁻ organoids indeed lose their lung lineage identity and differentiate towards an intestinal fate. Thus, *NKX2-1*⁻ organoids were negative for KRT8 luminal cell marker and acT ciliated cell marker. Moreover, significant expression of both intestinal markers, SOX9 and KRT20, could clearly be seen among the majority of cells. However, KRT5 was also expressed in these organoids, indicating that BCs had maintained at least some of their characteristics after 12 days in culture. EpCAM was found abundantly distributed across most cells, suggesting that despite *NKX2-1*⁻ cells differentiate towards the intestinal lineage, their epithelial cell identity remains.

Alveolar-like organoids were generated from dissociated murine lung lobes. Interestingly, one captured structure consisted mainly of SFTPC⁺ cells, which were therefore considered AEC2s, and no PDPN⁺ AEC1s, despite the fact that alveolar-like organoids usually contain both cell types. By contrast, the second observed structure harbored many PDPN⁺ cells that seemed to be surrounding SFTPC⁺ AEC2s. Another interpretation may be that cells were double positive, indicating either precursor cells that have the potential to give rise to both cell types, or AEC2s that were captured in a transition state of differentiating into AEC1s. In

contrast to the aforementioned structure, ZO-1 was found distributed almost everywhere in this case. This finding suggests that cells were connected by abundant tight junctions, which may be an indicator for AEC1 identity, as they need to form robust alveolar boundaries.

As a comparison, the human lung adenocarcinoma cell line NCI-H23 was used to generate cancerous alveolar spheres. Staining revealed that the majority of cells was SFTPC-positive. Also many PDPN⁺ cells could be observed, although the signal was considerably weaker. Both cell types were dispersed throughout the entire cluster of cells. The overall shape of the captured structure was not very well defined, and did not resemble a natural alveolus. Moreover, no ZO-1 could be detected, presumably due to the fact that tumor cells lose their polarity, which further underscores the tumorous identity of these cells.

4.4.1 Growth kinetics of organoid cultures

Analysis of growth kinetics showed that most organoids increased in diameter over time. The largest organoids were obtained from murine lung lobe cell mixtures, followed by murine trachea epithelial cells and SFTPC⁺ murine lung cells. These observations were presumably due to the fact that these cells were obtained from relatively young mice (4-8 weeks). Interestingly, SFTPC⁺ murine lung cells cultured in transwell inserts remained substantially smaller. Organoids generated from mBCs that had been in culture for long periods already, were in the middle. These findings indicate that primary cells have a higher potential for proliferation and differentiation compared to cell lines, especially when obtained from young individuals.

By contrast, cultures established from human cells did not show much growth at all. Even the cancer cell line NCI-H23 produced only little organoids. Moreover, no substantial differences could be determined regarding healthy and transfected hBC cultures. Unfortunately, not a single one of the organoids established from px458-transfected cells was GFP-positive, indicating that none of them originated from a successfully transfected cell. Moreover, only few organoids could be observed, which expanded very slowly, additionally suggesting that the transfection procedure had negative effects on cell growth and differentiation.

4.5 Outlook

Once transfection of hBCs, or AEC2s respectively, will show sufficient success rates, and the issue of expanding single cells can be solved, knock-in reporters will be applied to the system in prospective studies, in order to facilitate the identification of specific tumor types. Therefore, distinct reporters will be introduced to promoter regions of genes that are specifically expressed in adenocarcinomas or squamous cell carcinomas. For instance, cDNA expressing GFP will be introduced to the SOX9 promoter of AEC2s using

CRISPR/Cas9. It has been shown that the *SOX9* gene is expressed in developing embryonic lung tissues, but not in adult AEC2s. However, preliminary data from Dr. Tata's laboratory have demonstrated that *SOX9* expression is reactivated in lung adenocarcinomas. Therefore, using this system will enable the identification of mutations that cause adenocarcinoma-like phenotypes in lung organoids. The expression of a fluorescent reporter can easily be visualized by fluorescence microscopy. Moreover, the application of different reporters may be used to indicate the presence of distinct tumor types in different organoids. For example, GFP could be introduced in the *SOX9* gene locus indicating adenocarcinomas, whereas RFP may be introduced in the *SOX2* gene of squamous cell carcinomas. Therefore, this system will enable the distinction of different types of tumors easily, as the reporter cells would give a green signal when adenocarcinomas develop, and a red signal when squamous cell carcinomas are generated.

The overarching goal of the project was to pave the way for using the 'lung-on-a-chip' model to screen for small molecules as potential drugs to treat lung cancer. Therefore, once the generated organoids sufficiently emulate specific physiological tumor types, they will be combined with the chip technology, and single-cell RNA sequencing will be applied to investigate the cellular response of lung tumors to certain chemicals. The Duke University has a library of about 300,000 different chemicals that may be used for this purpose. Distinct forms of cancer will be treated with promising chemicals to investigate their effects, as well as to monitor the emergence of resistances. Ultimately, clinically-relevant substances will be tested for their efficiency to treat specific cancer types, assessed by single-cell RNA sequencing at certain stages of tumor growth. With this method, potential therapeutic substances will hopefully be discovered, in order to create novel, tailored treatment options for patients suffering from lung cancer.

Bibliography

- [1] E. A. Collisson *et al.*, “Comprehensive molecular profiling of lung adenocarcinoma,” *Nature*, vol. 511, no. 7511, pp. 543–550, 2014.
- [2] P. S. Hammerman *et al.*, “Comprehensive genomic characterization of squamous cell lung cancers,” *Nature*, vol. 489, no. 7417, pp. 519–525, 2012.
- [3] J. G. Paez *et al.*, “EGFR mutations in lung cancer: Correlation with clinical response to Gefitinib therapy,” *Science (80-.)*, vol. 304, no. 5676, pp. 1497–1500, 2004.
- [4] H. S. Shim *et al.*, “Unique genetic and survival characteristics of invasive mucinous adenocarcinoma of the lung,” *J. Thorac. Oncol.*, vol. 10, no. 8, pp. 1156–1162, 2015.
- [5] S. V. Sharma, D. W. Bell, J. Settleman, and D. A. Haber, “Epidermal growth factor receptor mutations in lung cancer,” *Nat. Rev. Cancer*, vol. 7, pp. 169–181, 2007.
- [6] M.-Y. Park *et al.*, “Generation of lung cancer cell lines harboring EGFR T790M mutation by CRISPR/Cas9-mediated genome editing,” *Oncotarget*, pp. 1–8, 2017.
- [7] E. L. Kwak *et al.*, “Anaplastic lymphoma kinase inhibition in non-small-cell lung cancer,” *N. Engl. J. Med.*, vol. 363, no. 18, pp. 1693–1703, 2010.
- [8] K. Bergethon *et al.*, “ROS1 rearrangements define a unique molecular class of lung cancers,” *J. Clin. Oncol.*, vol. 30, no. 8, pp. 863–870, 2012.
- [9] A. Drilon *et al.*, “Response to cabozantinib in patients with RET fusion-positive lung adenocarcinomas,” *Cancer Discov.*, vol. 3, pp. 630–635, 2013.
- [10] E. Manchado *et al.*, “A combinatorial strategy for treating KRAS-mutant lung cancer,” *Nature*, vol. 534, pp. 647–651, 2016.
- [11] T. Takahashi *et al.*, “p53: A frequent target for genetic abnormalities in lung cancer,” *Science (80-.)*, vol. 246, pp. 491–494, 1989.
- [12] M. Sanchez-Cespedes *et al.*, “Inactivation of LKB1/STK11 is a common event in adenocarcinomas of the lung,” *Cancer Res.*, vol. 62, pp. 3659–3662, 2002.
- [13] G. I. Shapiro *et al.*, “Reciprocal Rb inactivation and p16 INK4 expression in primary lung cancers and cell lines,” *Cancer Res.*, vol. 55, pp. 505–509, 1995.
- [14] A. Singh *et al.*, “Dysfunctional KEAP1-NRF2 interaction in non-small-cell lung cancer,” *PLoS Med.*, vol. 3, no. 10, pp. 1865–1876, 2006.
- [15] P. P. Medina *et al.*, “Frequent BRG1/SMARCA4-inactivating mutations in human lung cancer cell lines,” *Hum. Mutat.*, vol. 29, no. 5, pp. 617–622, 2008.
- [16] J. W. Scannell, A. Blanckley, H. Boldon, and B. Warrington, “Diagnosing the decline in pharmaceutical R&D efficiency,” *Nat. Rev. Drug Discov.*, vol. 11, pp. 191–200, 2012.
- [17] P. Perel *et al.*, “Comparison of treatment effects between animal experiments and clinical trials: systematic review,” *BMJ*, vol. 334, pp. 197–202, 2007.
- [18] A. Knight, J. Bailey, and J. Balcombe, “Which drugs cause cancer? For and against: Cancer bioassays,” *BMJ*, vol. 331, 2005.
- [19] P. Pound and M. B. Bracken, “Is animal research sufficiently evidence based to be a cornerstone of biomedical research?,” *BMJ*, vol. 348, 2014.
- [20] C. Kilkeny *et al.*, “Survey of the quality of experimental design, statistical analysis

and reporting of research using animals,” *PLoS One*, vol. 4, no. 11, 2009.

- [21] U. Marx *et al.*, “Biology-inspired microphysiological system approaches to solve the prediction dilemma of substance testing,” *ALTEX*, vol. 33, no. 3, pp. 272–321, 2016.
- [22] H. Ledford, “Translational research: 4 ways to fix the clinical trial,” *Nature*, vol. 477, pp. 526–528, 2011.
- [23] A. R. Perestrelo, A. C. P. Águas, A. Rainer, and G. Forte, “Microfluidic organ/body-on-a-chip devices at the convergence of biology and microengineering,” *Sensors*, vol. 15, pp. 31142–31170, 2015.
- [24] M. L. McCain, S. P. Sheehy, A. Grosberg, J. A. Goss, and K. K. Parker, “Recapitulating maladaptive, multiscale remodeling of failing myocardium on a chip,” *Proc. Natl. Acad. Sci. U. S. A.*, vol. 110, no. 24, pp. 9770–9775, 2013.
- [25] A. Grosberg, P. W. Alford, M. L. McCain, and K. K. Parker, “Ensembles of engineered cardiac tissues for physiological and pharmacological study: Heart on a chip,” *Lab Chip*, vol. 11, no. 24, pp. 4165–73, 2011.
- [26] G. A. Giridharan *et al.*, “Microfluidic cardiac cell culture model (μ CCEM),” *Anal. Chem.*, vol. 82, pp. 7581–7587, 2010.
- [27] M. A. Lancaster *et al.*, “Cerebral organoids model human brain development and microcephaly,” *Nature*, vol. 501, no. 7467, 2013.
- [28] D. Huh, B. D. Matthews, A. Mammoto, M. Montoya-Zavala, H. Y. Hsin, and D. E. Ingber, “Reconstituting organ-level lung functions on a chip,” *Science (80-.)*, vol. 328, no. 5986, pp. 1662–1668, 2010.
- [29] P. R. Tata *et al.*, “Dedifferentiation of committed epithelial cells into stem cells in vivo,” *Nature*, vol. 503, pp. 218–223, 2013.
- [30] F. Zhang, Y. Wen, and X. Guo, “CRISPR/Cas9 for genome editing: Progress, implications and challenges,” *Hum. Mol. Genet.*, vol. 23, no. R1, pp. R40–R46, 2014.
- [31] J. D. Sander and J. K. Joung, “CRISPR-Cas systems for genome editing, regulation and targeting,” *Nat. Biotechnol.*, vol. 32, no. 4, pp. 347–355, 2014.
- [32] Y. G. Kim, J. Cha, and S. Chandrasegaran, “Hybrid restriction enzymes: zinc finger fusions to Fok I cleavage domain,” *Proc. Natl. Acad. Sci.*, vol. 93, pp. 1156–1160, 1996.
- [33] G. Silva *et al.*, “Meganucleases and other tools for targeted genome engineering: perspectives and challenges for gene therapy,” *Curr. Gene Ther.*, vol. 11, pp. 11–27, 2011.
- [34] J. Smith *et al.*, “A combinatorial approach to create artificial homing endonucleases cleaving chosen sequences,” *Nucleic Acids Res.*, vol. 34, no. 22, pp. 1–12, 2006.
- [35] F. D. Urnov, E. J. Rebar, M. C. Holmes, H. S. Zhang, and P. D. Gregory, “Genome editing with engineered zinc finger nucleases,” *Nat. Rev. Genet.*, vol. 11, pp. 636–646, 2010.
- [36] S. A. Wolfe, L. Nekudova, and C. O. Pabo, “DNA recognition by cys2his2 zinc finger proteins,” *Annu. Rev. Biophys.*, vol. 3, pp. 183–212, 1999.
- [37] J. D. Sander *et al.*, “Selection-free zinc-finger-nuclease engineering by context-dependent assembly (CoDA),” *Nat. Methods*, vol. 8, no. 1, pp. 67–69, 2011.
- [38] M. L. Maeder *et al.*, “Rapid ‘open-source’ engineering of customized zinc-finger nucleases for highly efficient gene modification,” *Mol. Cell*, vol. 31, pp. 294–301, 2008.

- [39] A. Gupta, R. G. Christensen, A. L. Rayla, A. Lakshmanan, G. D. Stormo, and S. A. Wolfe, "An optimized two-finger archive for ZFN-mediated gene targeting," *Nat. Methods*, vol. 9, no. 6, pp. 588–590, 2012.
- [40] B. Gonzalez, L. J. Schwimmer, R. P. Fuller, Y. Ye, L. Asawapornmongkol, and C. F. Barbas, "Modular system for the construction of zinc-finger libraries and proteins," *Nat. Protoc.*, vol. 5, no. 4, pp. 791–810, 2010.
- [41] D. Reyon, S. Q. Tsai, C. Khayter, J. A. Foden, J. D. Sander, and J. K. Joung, "FLASH assembly of TALENs enables high-throughput genome editing," *Nat. Biotechnol.*, vol. 30, no. 5, pp. 460–465, 2012.
- [42] M. Holkers *et al.*, "Differential integrity of TALE nuclease genes following adenoviral and lentiviral vector gene transfer into human cells," *Nucleic Acids Res.*, vol. 41, no. 5, 2013.
- [43] E. Pennisi, "The CRISPR Craze," *Science (80-.)*, vol. 341, pp. 833–836, 2013.
- [44] M. Jinek, K. Chylinski, I. Fonfara, M. Hauer, J. A. Doudna, and E. Charpentier, "A programmable dual-RNA-guided DNA endonuclease in adaptive bacterial immunity," *Science (80-.)*, vol. 337, pp. 816–821, 2012.
- [45] B. Wiedenheft, S. H. Sternberg, and J. A. Doudna, "RNA-guided genetic silencing systems in bacteria and archaea," *Nature*, vol. 482, pp. 331–338, 2012.
- [46] P. Horvath and R. Barrangou, "CRISPR/Cas, the immune system of bacteria and archaea," *Science (80-.)*, vol. 327, pp. 167–170, 2010.
- [47] P. C. Fineran and E. Charpentier, "Memory of viral infections by CRISPR-Cas adaptive immune systems: Acquisition of new information," *Virology*, vol. 434, pp. 202–209, 2012.
- [48] E. Deltcheva *et al.*, "CRISPR RNA maturation by trans-encoded small RNA and host factor RNase III," *Nature*, vol. 471, pp. 602–607, 2011.
- [49] K. S. Makarova *et al.*, "Evolution and classification of the CRISPR-Cas systems," *Nat. Rev. Microbiol.*, vol. 9, pp. 467–477, 2011.
- [50] J.-H. Zhang, P. Adikaram, M. Pandey, A. Genis, and W. F. Simonds, "Optimization of genome editing through CRISPR-Cas9 engineering," *Bioengineered*, vol. 7, no. 3, pp. 166–174, 2016.
- [51] W. Y. Hwang *et al.*, "Efficient genome editing in zebrafish using a CRISPR-Cas system," *Nat. Biotechnol.*, vol. 31, no. 3, pp. 227–229, 2013.
- [52] P. Mali *et al.*, "RNA-guided human genome engineering via Cas9," *Science (80-.)*, vol. 339, pp. 823–826, 2013.
- [53] L. Cong *et al.*, "Multiplex genome engineering using CRISPR/Cas systems," *Science (80-.)*, vol. 339, pp. 819–823, 2013.
- [54] A. Wenginger, A. M. Hatzl, C. Schmid, T. Vogl, and A. Glieder, "Combinatorial optimization of CRISPR/Cas9 expression enables precision genome engineering in the methylotrophic yeast *Pichia pastoris*," *J. Biotechnol.*, 2016.
- [55] B. E. Housden, S. Lin, and N. Perrimon, *Cas9-based genome editing in Drosophila*, 1st ed., vol. 546. Elsevier Inc., 2014.
- [56] R. Maresch *et al.*, "Multiplexed pancreatic genome engineering and cancer induction by transfection-based CRISPR/Cas9 delivery in mice," *Nat. Commun.*, vol. 7, no. 10770, 2016.

- [57] Y. Kang *et al.*, “CRISPR/Cas9-mediated Dax1 knockout in the monkey recapitulates human AHC-HH,” *Hum. Mol. Genet.*, vol. 24, pp. 7255–7264, 2015.
- [58] X. Hu, C. Wang, Y. Fu, Q. Liu, X. Jiao, and K. Wang, “Expanding the range of CRISPR/Cas9 genome editing in rice,” *Mol. Plant*, vol. 267, 2016.
- [59] J. Calarco and A. Friedland, “Creating genome modifications in *C. elegans* using the CRISPR/Cas9 system,” *Methods Mol. Biol.*, vol. 1327, pp. 59–74, 2015.
- [60] A. Vojta *et al.*, “Repurposing the CRISPR-Cas9 system for targeted DNA methylation,” *Nucleic Acids Res.*, 2016.
- [61] A. A. Dominguez, W. A. Lim, and L. S. Qi, “Beyond editing: repurposing CRISPR-Cas9 for precision genome regulation and interrogation,” *Nat. Rev. Mol. Cell Biol.*, vol. 17, pp. 5–15, 2015.
- [62] H. Y. Xue, L. J. Ji, A. M. Gao, P. Liu, J. D. He, and X. J. Lu, “CRISPR-Cas9 for medical genetic screens: applications and future perspectives,” *J. Med. Genet.*, vol. 0, pp. 1–7, 2015.
- [63] R. Vassena *et al.*, “Genome engineering through CRISPR/Cas9 technology in the human germline and pluripotent stem cells,” *Hum. Reprod. Update*, 2016.
- [64] N. Savic and G. Schwank, “Advances in therapeutic CRISPR/Cas9 genome editing,” *Transl. Res.*, no. 967, 2015.
- [65] M. Müller *et al.*, “*Streptococcus thermophilus* CRISPR-Cas9 systems enable specific editing of the human genome,” *Mol. Ther.*, 2015.
- [66] D. Wojtal *et al.*, “Spell checking nature: Versatility of CRISPR/Cas9 for developing treatments for inherited disorders,” *Am. J. Hum. Genet.*, vol. 98, pp. 1–12, 2016.
- [67] M. K. White and K. Khalili, “CRISPR/Cas9 and cancer targets: future possibilities and present challenges,” *Oncotarget*, vol. 7, no. 11, pp. 12305–12317, 2016.
- [68] A. S. L. Wong *et al.*, “Multiplexed barcoded CRISPR-Cas9 screening enabled by CombiGEM,” *Proc. Natl. Acad. Sci. U. S. A.*, vol. 113, pp. 2544–2549, 2016.
- [69] J. G. Doench *et al.*, “Optimized sgRNA design to maximize activity and minimize off-target effects of CRISPR-Cas9,” *Nat. Biotechnol.*, vol. 34, pp. 184–191, 2016.
- [70] H. Chen and S. Bailey, “Cas9, poised for DNA cleavage,” *Science (80-.)*, vol. 351, no. 6275, pp. 811–812, 2016.
- [71] I. M. Slaymaker, L. Gao, B. Zetsche, D. A. Scott, W. X. Yan, and F. Zhang, “Rationally engineered Cas9 nucleases with improved specificity,” *Science (80-.)*, 2015.
- [72] C. E. Nelson and C. A. Gersbach, “Cas9 loosens its grip on off-target sites,” *Nat. Biotechnol.*, vol. 34, no. 3, pp. 298–299, 2016.
- [73] V. A. Brazelton *et al.*, “A quick guide to CRISPR sgRNA design tools,” *GM Crops Food*, vol. 6, pp. 266–276, 2015.
- [74] F. A. Ran *et al.*, “In vivo genome editing using *Staphylococcus aureus* Cas9,” *Nature*, vol. 520, no. 7546, pp. 186–191, 2015.
- [75] V. Pattanayak, S. Lin, J. P. Guilinger, E. Ma, J. A. Doudna, and D. R. Liu, “High-throughput profiling of off-target DNA cleavage reveals RNA-programmed Cas9 nuclease specificity,” *Nat. Biotechnol.*, vol. 31, pp. 839–843, 2013.
- [76] J. A. Gagnon *et al.*, “Efficient mutagenesis by Cas9 protein-mediated oligonucleotide insertion and large-scale assessment of single-guide RNAs,” *PLoS One*, vol. 9, no. 5, p. e98186, 2014.

- [77] B. P. Kleinstiver *et al.*, "Broadening the targeting range of *Staphylococcus aureus* CRISPR-Cas9 by modifying PAM recognition," *Nat. Biotechnol.*, vol. 33, pp. 1293–1298, 2015.
- [78] S. Ramakrishna *et al.*, "Surrogate reporter-based enrichment of cells containing RNA-guided Cas9 nuclease-induced mutations," *Nat. Commun.*, vol. 5, no. 3378, 2014.
- [79] L. E. M. Vriend, M. Jasin, and P. M. Krawczyk, *Assaying break and nick-induced homologous recombination in mammalian cells using the DR-GFP reporter and Cas9 nucleases*, 1st ed., vol. 546. Elsevier Inc., 2014.
- [80] J. H. Zhang *et al.*, "Improving the specificity and efficacy of CRISPR/CAS9 and gRNA through target specific DNA reporter," *J. Biotechnol.*, vol. 189, 2014.
- [81] F. A. Ran *et al.*, "Double nicking by RNA-guided CRISPR Cas9 for enhanced genome editing specificity," *Cell*, vol. 154, no. 6, pp. 1380–1389, 2013.
- [82] S. W. Cho *et al.*, "Analysis of off-target effects of CRISPR/Cas-derived RNA-guided endonucleases and nickases," *Genome Res.*, vol. 24, pp. 132–141, 2014.
- [83] Y. Fu, J. D. Sander, D. Reyon, V. M. Cascio, and J. K. Joung, "Improving CRISPR-Cas nuclease specificity using truncated guide RNAs," *Nat. Biotechnol.*, 2014.
- [84] J. R. Rock, S. H. Randell, and B. L. M. Hogan, "Airway basal stem cells: a perspective on their roles in epithelial homeostasis and remodeling," *Dis. Model. Mech.*, vol. 3, pp. 545–556, 2010.
- [85] B. L. M. Hogan *et al.*, "Repair and regeneration of the respiratory system: complexity, plasticity, and mechanisms of lung stem cell function," *Cell Stem Cell*, vol. 15, no. 2, pp. 123–138, 2014.
- [86] C. E. Barkauskas *et al.*, "Type 2 alveolar cells are stem cells in adult lung," *J. Clin. Invest.*, vol. 123, no. 7, pp. 3025–3036, 2013.
- [87] K. A. A. Schilders *et al.*, "Regeneration of the lung: Lung stem cells and the development of lung mimicking devices," *Respir. Res.*, vol. 17, no. 44, 2016.
- [88] T. J. Desai, D. G. Brownfield, and M. A. Krasnow, "Alveolar progenitor and stem cells in lung development, renewal and cancer," *Nature*, vol. 507, pp. 190–194, 2014.
- [89] J. Choi, E. Ilich, and J.-H. Lee, "Organogenesis of adult lung in a dish: Differentiation, disease and therapy," *Dev. Biol.*, vol. 420, no. 2, pp. 278–286, 2016.
- [90] J. E. Boers, A. W. Ambergen, and F. B. J. M. Thunnissen, "Number and proliferation of basal and parabasal cells in normal human airway epithelium," *Am. J. Respir. Crit. Care Med.*, vol. 157, pp. 2000–2006, 1998.
- [91] M. J. Evans and P. C. Moller, "Mini-Review Biology of Airway Basal Cells," *Exp. Lung Res.*, vol. 17, pp. 513–531, 1991.
- [92] M. Nakajima *et al.*, "Immunohistochemical and ultrastructural studies of basal cells, Clara cells and bronchiolar cuboidal cells in normal human airways," *Pathol. Int.*, vol. 48, pp. 944–953, 1998.
- [93] J. R. Rock *et al.*, "Basal cells as stem cells of the mouse trachea and human airway epithelium," *Proc. Natl. Acad. Sci.*, vol. 106, no. 31, pp. 12771–12775, 2009.
- [94] J. Stingl *et al.*, "Purification and unique properties of mammary epithelial stem cells," *Nature*, vol. 439, pp. 993–997, 2006.
- [95] T. Tumber *et al.*, "Defining the epithelial stem cell niche in skin," *Science (80-.)*, vol. 303, pp. 359–363, 2004.

- [96] Y. Daniely *et al.*, “Critical role of p63 in the development of a normal esophageal and tracheobronchial epithelium,” *Am. J. Physiol. Cell Physiol.*, vol. 287, pp. C171–C181, 2004.
- [97] K. U. Hong, S. D. Reynolds, S. Watkins, E. Fuchs, and B. R. Stripp, “In vivo differentiation potential of tracheal basal cells: evidence for multipotent and unipotent subpopulations,” *Am. J. Physiol. Lung Cell. Mol. Physiol.*, vol. 286, pp. L643–L649, 2004.
- [98] K. U. Hong, S. D. Reynolds, S. Watkins, E. Fuchs, and B. R. Stripp, “Basal cells are a multipotent progenitor capable of renewing the bronchial epithelium,” *Am. J. Pathol.*, vol. 164, pp. 577–588, 2004.
- [99] J. G. Rheinwald and H. Green, “Serial cultivation of strains of human epidermal keratinocytes: the formation of keratinizing colonies from single cells,” *Cell*, vol. 6, pp. 331–344, 1975.
- [100] H. Mou *et al.*, “Dual SMAD Signaling Inhibition Enables Long-Term Expansion of Diverse Epithelial Basal Cells,” *Cell Stem Cell*, vol. 19, pp. 217–231, 2016.
- [101] D. A. Lawson, L. Xin, R. U. Lukacs, D. Cheng, and O. N. Witte, “Isolation and functional characterization of murine prostate stem cells,” *Proc. Natl. Acad. Sci. U. S. A.*, vol. 104, no. 1, pp. 181–186, 2007.
- [102] X. Yin, H. F. Farin, J. H. van Es, H. Clevers, R. Langer, and J. M. Karp, “Niche-independent high-purity cultures of Lgr5+ intestinal stem cells and their progeny,” *Nat. Methods*, vol. 11, pp. 106–112, 2014.
- [103] T. Sato *et al.*, “Single Lgr5 stem cells build crypt-villus structures in vitro without a mesenchymal niche,” *Nature*, vol. 459, pp. 262–265, 2009.
- [104] X. Liu *et al.*, “ROCK inhibitor and feeder cells induce the conditional reprogramming of epithelial cells,” *Am. J. Pathol.*, vol. 180, no. 2, pp. 599–607, 2012.
- [105] M. Fujii, M. Matano, K. Nanki, and T. Sato, “Efficient genetic engineering of human intestinal organoids using electroporation,” *Nat. Protoc.*, vol. 10, no. 10, pp. 1474–1485, 2015.
- [106] J. R. Rock *et al.*, “Multiple stromal populations contribute to pulmonary fibrosis without evidence for epithelial to mesenchymal transition,” *Proc. Natl. Acad. Sci. U. S. A.*, vol. 108, no. 52, pp. E1475–1483, 2011.
- [107] W. Yu *et al.*, “Formation of cysts by alveolar type II cells in three-dimensional culture reveals a novel mechanism for epithelial morphogenesis,” *Mol. Biol. Cell*, vol. 18, pp. 1693–1700, 2007.
- [108] R. Bals, C. Beisswenger, S. Blouquit, and T. Chinet, “Isolation and air-liquid interface culture of human large airway and bronchiolar epithelial cells,” *J. Cyst. Fibros.*, vol. 3, pp. 49–51, 2004.
- [109] W. Zuo *et al.*, “p63(+)Krt5(+) distal airway stem cells are essential for lung regeneration,” *Nature*, vol. 517, no. 7536, pp. 616–620, 2014.
- [110] C. F. Bender Kim *et al.*, “Identification of bronchioalveolar stem cells in normal lung and lung cancer,” *Cell*, vol. 121, pp. 823–835, 2005.
- [111] K. BéruBé, Z. Prytherch, C. Job, and T. Hughes, “Human primary bronchial lung cell constructs: The new respiratory models,” *Toxicology*, vol. 278, pp. 311–318, 2010.
- [112] A. P. Wong *et al.*, “Directed differentiation of human pluripotent stem cells into mature airway epithelia expressing functional CFTR protein,” *Nat. Biotechnol.*, vol. 30, pp.

876–882, 2012.

- [113] R. Peerani and P. W. Zandstra, “Enabling stem cell therapies through synthetic stem cell-niche engineering,” *J. Clin. Invest.*, vol. 120, no. 1, pp. 60–70, 2010.
- [114] G. Benton, I. Arnaoutova, J. George, H. K. Kleinman, and J. Koblinski, “Matrigel: From discovery and ECM mimicry to assays and models for cancer research,” *Adv. Drug Deliv. Rev.*, vol. 79, pp. 3–18, 2014.
- [115] H. Chen *et al.*, “Airway epithelial progenitors are region specific and show differential responses to bleomycin-induced lung injury,” *Stem Cells*, vol. 30, pp. 1948–1960, 2012.
- [116] M. Langhofer, S. B. Hopkinson, and J. C. Jones, “The matrix secreted by 804G cells contains laminin-related components that participate in hemidesmosome assembly in vitro,” *J. Cell Sci.*, vol. 105 (Pt 3), no. July, pp. 753–764, 1993.
- [117] T. K. Kim and J. H. Eberwine, “Mammalian cell transfection: The present and the future,” *Anal. Bioanal. Chem.*, vol. 397, pp. 3173–3178, 2010.
- [118] P. R. Tata and J. Rajagopal, “Cellular plasticity: 1712 to the present day,” *Curr. Opin. Cell Biol.*, vol. 43, pp. 46–54, 2016.

List of Figures

Figure 1: Scheme depicting the generation of <i>ex vivo</i> organoids to recapitulate <i>in vivo</i> tumor phenotypes	6
Figure 2: Most frequent mutations in the <i>EGFR</i> gene	7
Figure 3: Different biology-inspired microphysiological <i>in vitro</i> systems used to simulate the human biology	9
Figure 4: An example of a cross-sectional view of a murine lung organoid generated in <i>ex vivo</i> cultures	10
Figure 5: Cellular repair mechanisms of CRISPR/Cas9-induced DSBs	12
Figure 6: Structure of pseudostratified epithelia and alveoli in the lung	14
Figure 7: Effects of ROCK inhibitor, TGF β and BMP antagonists on human airway stem cells	17
Figure 8: Culture systems to study the differentiation of lung stem cells	20
Figure 9: Murine tumor-like lung organoids generated by <i>KRAS</i> ^{G12D} and <i>NKX2-1</i> knockout mutations in AEC2s	21
Figure 10: Scheme of the px458 plasmid used for transfection	26
Figure 11: Design of primers for two subsequent PCR analyses	32
Figure 12: Testing 10 different parameter sets with the NEPA21 transfection system	40
Figure 13: Fluorescence microscopy images of mBCs transfected at 10 different parameter sets tested with NEPA21	40
Figure 14: Transfection efficiency of electroporation with different cell numbers and re-used cuvettes	41
Figure 15: Viability of cells after transfection	42
Figure 16: Fluorescence microscopy images of mBCs transfected at different cell numbers, and in re-used cuvettes	42
Figure 17: Transfection efficiency of mBCs electroporated with NEPA21 or Amaxa 4D-Nucleofector	44
Figure 18: Fluorescence microscopy images of mBCs electroporated with NEPA21 or Amaxa 4D-Nucleofector	44
Figure 19: Transfection efficiencies of endotoxin-free plasmids	45
Figure 20: Fluorescence microscopy images of mBCs transfected with endotoxin-free plasmids	46
Figure 21: Fluorescence microscopy images of hBCs transfected with px458 ^{hEGFR_T790M} at 200 V	47
Figure 22: Fluorescence microscopy images of hBCs transfected with px458 ^{hEGFR_T790M} at 125-200 V	47
Figure 23: Fluorescence microscopy images of hBCs transfected with px458 or Nepa Gene's plasmid	48

Figure 24: Fluorescence microscopy images of hBCs transfected with px458 or Nepa Gene's plasmid at 150 V and 7.5 ms poring pulse length	49
Figure 25: Electroporated hBCs seeded at densities of 1×10^4 , 2×10^4 and 3×10^4 in 10-cm dishes	49
Figure 26: Single mBCs seeded in a 96-well-plate and monitored for 15 days.....	50
Figure 27: Single hBCs cultured in a 96-well-plate in media supplemented with supernatants of other cells	50
Figure 28: Single hBCs cultured in transwell inserts, with 5,000 hBCs either on the bottom of the well or on the lower side of the membrane.....	51
Figure 29: Organoids established from healthy mBCs and murine MLgs cultured for five weeks.....	52
Figure 30: Organoids established from healthy mBCs and murine MLgs cultured for five weeks and stained for lung epithelial markers	53
Figure 31: Organoids established from healthy mBCs and murine MLgs cultured for five weeks and stained for intestinal cell markers.....	53
Figure 32: Organoids established from <i>NKX2-1</i> lung cells cultured for 12 days and stained for lung epithelial markers	54
Figure 33: Organoids established from <i>NKX2-1</i> lung cells cultured for 12 days and stained for intestinal markers	55
Figure 34: Organoids established from murine lung lobe cell mixtures cultured for 14 days.....	56
Figure 35: Staining of AEC2-dominated organoids established from non-cre-activated murine lung cells cultured for 14 days	57
Figure 36: Staining of alveolar-like organoids established from non-cre-activated murine lung cells cultured for 14 days	58
Figure 37: Organoids established from lung adenocarcinoma cell line NCI-H23 cultured for 14 days	58
Figure 38: Staining of organoids established from human lung adenocarcinoma cell line NCI-H23 cultured for 14 days	59
Figure 39: Comparison of the various organoids established from different cell types	60
Figure 40: Comparison of growth kinetics data obtained from different organoid cultures.....	60
Figure 41: Morphology and growth behavior of primary hBCs cultured <i>in vitro</i>	62

List of Tables

Table 1: Materials and reagents used for basic cell culture.....	21
Table 2: Components of full SAGM plus medium.....	23
Table 3: Components of MTEC basic and MTEC plus media.....	25
Table 4: Materials and reagents used for cloning of vectors.....	26
Table 5: Materials and reagents used for purification of plasmids.	28
Table 6: Materials and reagents used for electroporation.....	30
Table 7: Materials and reagents used for single cell culture	33
Table 8: Materials and reagents used for organoid culture.	34
Table 9: Overview of cultured organoids.	35
Table 10: Materials and reagents used for preparing cryosections	36
Table 11: Materials and reagents used for staining of cryosections.....	37
Table 12: Parameter sets tested with NEPA21 transfection system.....	39

List of Abbreviations

ADME	Absorption, distribution, metabolism and excretion
AEC1s	Alveolar type 1 epithelial cells
AEC2s	Alveolar type 2 epithelial cells
ALI	Air-liquid interface
AQP5	Aquaporin 5
ATP	Adenosine triphosphate
BCs	Basal cells
bp	Base pair(s)
BPE	Bovine pituitary extract
Cas9	CRISPR-associated protein 9
CB	Citrate buffer
CRISPR	Clustered regularly interspaced short palindromic repeat
crRNA	CRISPR RNA
DAPI	4',6-Diamidino-2-phenylindole, dilactate
dCas9	Dead Cas9
dH ₂ O	Ultrapure distilled water
DMEM	Dulbecco's modified Eagle medium
DMSO	Dimethyl sulfoxide
DSB	Double strand break
EB	Elution buffer
EDTA	Ethylenediaminetetraacetic acid
EGF	Epidermal growth factor
EGFP	Enhanced green fluorescent protein
EGFR	Epidermal growth factor receptor
FACS	Fluorescence-activated cell sorting
FBS	Fetal bovine serum
gDNA	Genomic DNA
GFP	Green fluorescent protein
gRNA	Guide RNA
GSK-3	Glycogen synthase kinase 3
hBCs	Human basal cells
HDR	Homology-directed repair
HOPX	Homeodomain only protein x
indels	Insertion/deletion mutations
kb	Kilo base(s)
KRT5	Cytokeratin 5
KRT14	Cytokeratin 14
mBCs	Murine basal cells

MEM	Minimum essential medium
NaOAc	Sodium acetate
NaOH	Sodium hydroxide
NEAA	Non-essential amino acids
NHEJ	Non-homologous end joining
NSCLC	Non-small-cell lung cancer
nt	Nucleotide(s)
PAM	Protospacer adjacent motif
PBS	Phosphate buffered saline
PBST	0.1% Triton 100 in PBS
PCR	Polymerase chain reaction
PDPN	Podoplanin
Pen/strep	Penicillin/Streptomycin
PFA	Paraformaldehyde
RFP	Red fluorescent protein
ROCK	Rho-associated protein kinase
RPMI	Roswell Park Memorial Institute
RT	Room temperature
SABM	Small Airway Epithelial Cell Basal Medium
SAGM	Small Airway Epithelial Cell Growth Medium
SCLC	Small-cell lung cancer
SFTPC	Surfactant protein C
sgRNA	Single guide RNA
ssODN	Single-stranded oligodeoxynucleotide
TALEN	Transcription activator-like effector nuclease
tracrRNA	Trans-activating crRNA
TRP63	Transformation-related protein 63
T/E	Trypsin/EDTA
ZFN	Zinc finger nuclease
ZO	Zonula occludens